INFORMATION TO USERS

This manuscript has been reproduced from the microfilm master. UMI films the text directly from the original or copy submitted. Thus, some thesis and dissertation copies are in typewriter face, while others may be from any type of computer printer.

The quality of this reproduction is dependent upon the quality of the copy submitted. Broken or indistinct print, colored or poor quality illustrations and photographs, print bleedthrough, substandard margins, and improper alignment can adversely affect reproduction.

In the unlikely event that the author did not send UMI a complete manuscript and there are missing pages, these will be noted. Also, if unauthorized copyright material had to be removed, a note will indicate the deletion.

Oversize materials (e.g., maps, drawings, charts) are reproduced by sectioning the original, beginning at the upper left-hand corner and continuing from left to right in equal sections with small overlaps.

Photographs included in the original manuscript have been reproduced xerographically in this copy. Higher quality 6" x 9" black and white photographic prints are available for any photographs or illustrations appearing in this copy for an additional charge. Contact UMI directly to order.

Bell & Howell Information and Learning
300 North Zeeb Road, Ann Arbor, MI 48106-1346 USA
800-521-0600

Université d'Ottawa · University of Ottawa

NOVEL SIGNAL PROCESSING APPROACHES FOR CHARACTERIZATION OF TRANSIENT TWO-PHASE GAS-LIQUID FLOW

© Deepak Kirpalani

A thesis submitted to the School of Graduate Studies and Research
in partial fulfillment of the requirements for
the degree of
Master of Applied Science
in the Department of Chemical Engineering
University of Ottawa

September 1999

ABSTRACT

The flow pattern generated in pipes for two-phase gas-liquid horizontal flows can significantly affect the efficiency of chemical process equipment. Since the early 1900's, scientists and engineers have investigated various methods for characterizing the flow patterns generated for various two-phase chemical systems. A notable effort was made by Baker to quantify physical fluid properties and correlate them to observed flow patterns in pipe flow.

The primary objective of this research was to develop a flow pattern recognition system, for industrial implementation, that is suitable for characterizing transient two-phase flow patterns. Since the advent of computer and system control equipment, researchers have focused on quantifying flow characteristics by analyzing pressure fluctuation because the natural tendency of multiphase flow is to pulse as the fluid phases mix while moving along the pipe length.

Analysis of the pressure-fluctuation signal has been typically made using Fast Fourier Transform, or similar signal analysis and statistical methods, to report and correlate the pressure fluctuation to observed flow phenomena. These methods have demonstrated usefulness for process systems that are operated in well-defined flow regimes. However, this approach has limited application in the transition zones of the regimes where transients are observed in the flow pattern.

Recent developments in digital signal processing provide new methods for characterizing transient signals. A novel approach using wavelet transform analysis to study pressure fluctuations in two-phase flow systems has been developed in this research. A flow pattern recognition system consisting of a LabVIEW® based pressure data collection system and MATLAB® scripts for processing of recorded pressure fluctuations is developed. Experimental development includes the design of a baseline system and a flow pattern recognition system. A phased approach is adopted for evaluating the novel signal processing method before applying it for flow pattern characterization. Preliminary tests conducted on software generated model data show that this method is capable of identifying intermittencies in a signal. Baseline experiments demonstrate the differences between single and two-phase flows and also validate the

data collection and analysis procedures. As a result of these experiments, Morlet's wavelets with advanced spectral analysis approaches were selected for flow pattern recognition.

Flow pattern recognition experiments have been conducted by selecting operating conditions using Baker's flow map. Pressure fluctuations have been collected for annular, dispersed and slug flow regimes. The analysis of pressure fluctuations for dispersed and annular flow patterns show that flow patterns well within a regime or near its boundary can be identified in real-time using these methods. Further, an intermittency index has been developed for quantifying the transients in the annular and dispersed flow patterns. The intermittency index is found to be significantly higher for annular flow compared to dispersed flow conditions. Recommendations for further characterization are suggested in this work.

RÉSUMÉ

La configuration d'écoulement générée dans les tuyaux par un écoulement à deux phases liquide-gaz peut affecter de façon significative les appareils utilisés dans certains procédés chimiques. Depuis le début des années 1900, scientifiques et ingénieurs ont étudié différentes méthodes pour caractériser les différentes configurations d'écoulement produites dans différents systèmes à deux phases. Un effort remarquable a été fait par Baker dans le but de quantifier les propriétés physiques des fluides et de les mettre en corrélation avec des configurations d'écoulement observées dans des tuyaux.

L'objectif principal de ces travaux de recherche était de développer un système pouvant être implémenté en industrie capable de reconnaître les configurations d'écoulement et approprié pour la charactérisation de configurations d'écoulement transitoires à deux phases. Depuis l'avènement de l'ordinateur et des appareils de contrôle de systèmes, des chercheurs ont axé leurs études sur la quantification des caractéristiques de l'écoulement en examinant la fluctuation des pressions observées, ceci parce que la tendance naturelle de l'écoulement multiphase est de provoquer des pulsations lorsque les phases du fluide se mélangent tout en se déplaçant le long de la longueur du tuyau.

L'analyse du signal relié à la fluctuation de la pression a été réalisée à l'aide de la transformation de Fourier rapide, ou d'un autre type similaire d'analyse de signal combiné à des méthodes statistiques, afin de rapporter et de mettre en corrélation la fluctuation de la pression avec les phénomènes d'écoulement observés. Ces méthodes se sont avérées utiles pour des systèmes fonctionnels qui agissent à des régimes d'écoulement bien définis. Cependant cette approche n'a qu'une application limitée dans les zones de transition des régimes où des espèces transitoires sont observées dans la configuration d'écoulement.

Des développements récents dans le traitement numérique du signal fournissent de nouvelles méthodes pour caractériser les signaux des espèces transitoires. Au cours de ces travaux de recherche, nous avons développé une nouvelle

approche qui fait appel à l'analyse de la transformation d'ondelettes dans le but d'identifier les configurations d'écoulement à deux phases. Nous exposons un système d'identification de configurations d'écoulement comprenant un système de collecte de mesures de pression basé sur LabVIEW® et des scripts MATLAB® pour le traitement des fluctuations des pressions enregistrées. Le développement expérimental comprend la conception d'un système de ligne de base et un système d'identification de configuration d'écoulement. Une approche par introduction graduelle a été choisie pour l'évaluation de la nouvelle méthode de traitement du signal avant de l'appliquer à la caractérisation de la configuration d'écoulement. Des essais préliminaires effectués sur des données obtenues avec un modèle logiciel montrent que cette méthode est capable d'identifier des intermittences dans un signal. Des expériences pour établir une ligne de base démontrent les différences entre les écoulements à phase unique et à phase double et corroborent aussi les procédures d'analyses et de collecte des données. À la suite de ces essais, nous avons choisi des ondelettes de Morlet, accompagnées d'approches d'analyses spectrales, pour caractériser les configurations d'écoulement.

Les expériences d'identification des configurations d'écoulement ont été menées à partir de conditions d'opération sélectionnées selon les représentations conventionelles de Baker. Des mesures de fluctuation de pression ont été faites pour des régimes d'écoulement dispersés, annulaires ainsi que intermittent. L'analyse de la fluctuation de la pression pour des représentations d'écoulement dispersées et annulaires montre que les configurations d'écoulement, bien à l'intérieur d'un régime ou près de ses limites, peuvent être identifiées en faisant appel à ces méthodes. De plus, un index d'intermittence a été développé pour quantifier les espèces transitoires dans les configurations d'écoulement annulaires et dispersées. Nous avons observé que l'index d'intermittence est significativement plus élevé pour les écoulement annulaires comparativement aux conditions d'écoulement dispersées. Nous suggérons des recommandations pour une caractérisation plus élaborée.

ACKNOWLEDGEMENTS

This work was carried out at the Institute for Chemical Process and Environmental Technology (ICPET) at the National Research Council (NRC). I would like to thank my supervisors, Dr. Bryan Sparks and Dr. Graham Neale, for their guidance throughout this research. In addition, I am grateful to Mr. Thomas McCracken, Dr. Zahra Tafreshi and Mr. Adam Bennett at the National Research Council for their interest and support during this work.

NOMENCLATURE

Notation

a	number of scales for wavelet analysis
b	number of translations of the wavelet
c	conversion factor for Y-co-ordinate axis of Baker's chart
C_δ	empirically derived factor (C_δ=0.776 for Morlet's wavelet)
D4	Daubechies basis-4 wavelet analyzing function
f(ϕ(t))	scaling function of a wavelet
g	acceleration due to gravity, m/s^2
G	mass velocity of gas, $\frac{kg}{m^2 s}(\frac{lb}{ft^2 hr})$
i	complex number, $(\sqrt{-1})$
L	mass velocity of liquid, $\frac{kg}{m^2 s}(\frac{lb}{ft^2 hr})$
N	number of samples in time series,
$P'(t)$	time variation of the fluctuation (dynamic pressure fluctuation), kPa (psi)
$P(t)$	time-dependent pressure (static pressure fluctuation), kPa (psi)
$\bar{P}$	time-averaged pressure, kPa (psi)
$R_p'(\tau)$	Auto-correlation function for dynamic pressure fluctuation, P' (t), kPa (psi)
s	number of scales calculated for a wavelet transform
$S_p'(f)$	Power Spectral Density (PSD) for dynamic pressure fluctuation, P' (t), kPa^2 (psi)^2
$\lvert W_n(s)\rvert$	Wavelet coefficients with respect to the number of samples
$\overline{W}^2(s)$	Global wavelet spectrum coefficients

$\overline{W}_n^2$	Scale-averaged wavelet power
$\lvert W_n(s_j)\rvert$	Local scale-averaged wavelet spectral coefficients for scales s_j
X	X-coordinate for Baker's two-phase flow map
Y	Y-coordinate for Baker's two-phase flow map, $\frac{kg}{m^2-hr}$ $(\frac{lb}{ft.^2 hr})$
$\overline{X}(t)$	time series for wavelet analysis
$\overline{X}(a,b)$	Wavelet transform of a time series

Greek Letters

α	gas holdup
δt	time interval between samples, (s)
δ_j	interval between the scales s_1. and s_2
λ	dimensionless number based on fluid properties
η	non-dimensional time parameter for Morlet wavelet
μ_L	viscosity of liquid phase, Pa-s (cP)
ρ_g	density of the gas phase, kg/m^3 (lb_m/ft^3)
ρ_L	density of the liquid phase, kg/m^3 (lb_m/ft^3)
σ	surface tension, N/m (dyne/cm)
ψ	dimensionless number based on fluid properties
$\psi_{a,b}$ (t)	analyzing wavelet function.
ψ (t), ψ_0 (t)	mother wavelet function
τ	auto-correlation time , (s)
τ	number of translations of the wavelet function
ω_0	non-dimensional frequency for Morlet wavelet

CONTENTS

Chapter Three

Experimental Studies in Two-Phase Flow Characterization

Chapter Four

Signal Processing Methods for Flow Pattern Characterization

Chapter Five

Results and Discussion

Appendix B

Appendix C

LIST OF FIGURES AND TABLES

LIST OF FIGURES

LIST OF TABLES

Chapter One

Introduction

1.1 Two-Phase Flow

The prediction of flow patterns in two-phase horizontal gas liquid systems has been recognized as a pivotal issue in two-phase gas-liquid flows in pipes owing to an increased interest in the transportation of flow mixtures. Also, design parameters such as pressure drop and heat and mass transfer for process equipment like heat exchangers and droplet size distribution for spray nozzles are strongly dependent on the flow pattern. As suggested by Hosler (1968), knowledge of the flow pattern in two-phase flow is analogous in a single-phase flow to knowing whether the flow is laminar or turbulent. In two-phase flow systems, it has been observed that although the two phases can distribute in a variety of ways, there are natural patterns or regimes that have been identified. These flow patterns are broadly classified by identifying similar features in the spatial location of the two phases in a system. A conventional approach (Baker, 1958; Govier and Aziz, 1972; Hubbard and Dukler, 1966; Dukler and Taitel, 1986) is to conduct several experiments on a two-phase system over varying operating conditions and to visually observe the flow patterns through a test section of the system. The collected data is then mapped on a two-dimensional map by locating transition boundaries between the patterns and hence identifying different regimes (Baker, 1954; DeGance and Atherton 1970; Govier and Aziz, 1972; Dukler and Taitel, 1986). The conventional approach is suitable only when experimental conditions permit the use of a transparent section of pipe, or channel, in the two-phase flow system. However this approach for characterizing two-phase flow patterns cannot be applied to industrial processes because the piping arrangement may be under high pressure.

The problem in flow pattern detection (Dukler and Taitel, 1986) is further complicated by two factors:

1) Certain flow pattern distributions contain arbitrary elements and different flow patterns can be identified at different locations in the same system.
2) Transition between two flow patterns is a gradual process and it has been found to be

difficult to define the boundary for flow transition.

The need for reliable flow pattern detection devices coupled with a suitable signal processing approach has been the driving force behind a very large research effort in two-phase gas-liquid flow systems for a few decades.

1.2 Two-Phase Flow Patterns

A review of the scientific literature conducted for this thesis includes descriptions of the flow patterns/regimes identifying the different flow patterns observed in two-phase flow through pipes. During horizontal, concurrent gas-liquid flow in circular cross-section pipes, researchers (DeGance and Atherton, 1970) found that a variety of flow regimes existed simultaneously at different locations in the system. Each pattern, or regime, results from the particular manner in which the gas and liquid distribute in the pipe. Researchers (Hubbard and Dukler, 1966; Govier and Aziz, 1972; Dukler and Taitel, 1986) differ in the assignation of names to the different flow patterns; nevertheless six flow regimes have been identified by most researchers (Dukler and Taitel, 1986; Wambsganss, 1991) based on the spatial distribution of the two phases. As discussed earlier, these six flow regimes have been classified on the basis of visual observations:

1) **Stratified smooth flow:** During stratified flow, the liquid is observed to be at the bottom of the pipe and the gas at the top, the interface between them is smooth.

2) **Stratified wavy flow:** The liquid and the gas are separated as in stratified flow, but the interface between them is wavy.

3) **Elongated bubble or plug flow:** Elongated gas bubbles are located in the middle of the tube. The gas bubbles are observed to be separated by sections of continuous liquid.

4) **Slug flow:** Liquid slugs separated by gas pockets move violently downstream. A slug may contain small bubbles at higher gas flows. The differences between elongated bubble and slug flows are not very well defined.

5) **Annular flow:** Annular flow takes place at high gas flow rates. The gas flows at the center of the pipe while the liquid flows in the annulus. Annular flow can be considered to be a development from slug flow when the rate of aeration becomes sufficiently high to form a continuous gas phase. It forms from a stratified liquid when the gas velocity is sufficiently high to spread around the pipe.

6) **Dispersed bubble flow:** For high liquid flow rates, the gas is dispersed as small bubbles within a continuous liquid phase. Normally, the bubble density at the top will be less than that at the bottom of the pipe.

1.3 Previous Research in Flow Pattern Detection

Several workers (Hubbard and Dukler, 1966; Govier and Aziz, 1972; Jones and Zuber; 1975; Barnea, 1980b; Tutu, 1982; Merzkirch, 1987; Hseih et al., 1997; Samways et al., 1997) in the field of two-phase flow research have examined the use of different sensors for the prediction of flow patterns. In this earlier work, statistical analysis and signal processing methods available at that time proved to be only partially satisfactory owing to the unsteady or transient nature of the collected data in some flow regimes. The flow pattern detection methods, adopted by several researchers, using different sensors and data analysis methods are summarized here.

1) Hot wire anemometry for measuring void distribution in two-phase flows.
2) X-ray void measurement systems (Jones and Zuber, 1975) for obtaining statistical measurements in vertical air-water systems in a rectangular channel. The probability density function of the void fraction fluctuations was used as a quantitative flow pattern discriminator for different types of flow. Although, the present research is conducted on a horizontal air-water system in circular pipes, X-ray based void fraction measurements represent a method for quantifyig flow patterns.
3) Pressure gradient measurements (Govier and Aziz, 1972) to discriminate between flow patterns.
4) A further development to the above method was the determination of the spectral distribution of the wall pressure fluctuations. These fluctuations were found to distinguish the flow patterns into separated, intermittent and distributed flows. They

could not discriminate between stratified and annular flows or between dispersed liquid and dispersed gas flow regimes.

5) Conductance probes have been used for boiling flows in horizontal systems. Researchers (Barnea, 1980b) used a single conductivity probe for detecting differences among bubbly, slug and annular flows. Further developments to this method were made to detect flow pattern differences.
6) Flow visualization (Govier and Aziz, 1972; Merzkirch, 1987; Hseih et al., 1991, Mishima et al., 1997) has been the most commonly used method for two-phase flow characterization.

These methods have been applied on a laboratory scale for detecting flow patterns. However, some of the sensors, cannot be industrially implemented owing to high costs or lack of robustness.

1.4 Rationale for Selecting Pressure Transducers for Characterization

In two-phase flow, the pressure at any point in a pipe is caused either by the direct hydrodynamic nature of the two-phase flow or by the vibrations acting upon the system. As reported in recent research (Samways et al., 1997), very few attempts have been made to investigate pressure fluctuations in two-phase flows. Researchers (Hubbard and Dukler, 1966; Tutu, 1982; Samways et al., 1997) have experimented with fast response pressure transducers for sensing the pressure at the conduit wall to detect commonly observed flow regimes. They combined conventional signal processing methods with empirical correlations to discriminate between flow regimes. Other researchers carried out time series analysis on collected pressure fluctuations using statistical correlation methods to identify specific regimes.

Dynamic pressure transducers respond only to fluctuations in pressure and consequently to collect meaningful data this type of transducer was selected for this research.

1.5 Novel Signal Processing Approaches

Conventional methods for characterization of two-phase flows have been found to be lacking in the area of signal processing because some of the flow patterns are irregular

in occurrence. It has been observed that the fluctuations in pressure are transient or intermittent in some flow patterns. Recent advances in signal processing have resulted in the development of new methods for identifying such signals.

A novel signal processing method based on wavelet analysis is proposed for characterization of the transient pressure fluctuations for these flow patterns. The present findings show that the intermittent occurrence of pressure fluctuation peaks can be characterized using the proposed method. The intermittency is further quantified based on a proposed index to characterize the flow pattern within a regime.

1.6 Outline of Thesis

The primary objectives of this research can be summarized as follows:

1) To gain an improved understanding of two-phase flow characterization methods.
2) To develop a flow pattern recognition method capable of identifying and characterizing two-phase flow patterns.
3) To implement the developed method with robust equipment so that the method can be applied industrially.
4) To evaluate the method by a fundamental study of two-phase flow systems.

This thesis primarily focuses on identifying flow patterns by analyzing pressure fluctuations in a horizontal, two-phase flow system using a new signal processing approach for flow pattern characterization. It presents a formal methodology for data collection and analysis of dynamic pressure fluctuations to characterize two-phase flow patterns based on automatic extraction of temporal features from the pressure fluctuations.

A theoretical review of the work carried out by researchers on two-phase flow was required to gain an understanding of the existing methods. Wavelet based signal processing approaches are researched and a novel approach developed for flow pattern characterization. These methods are evaluated on model data and applied to pressure fluctuations from a baseline system and then extended to experimental results from a two-phase flow pattern recognition arrangement. Flow patterns were verified for each experiment by observing the flow through a transparent section of the pipe.

Pressure fluctuations for flows well within the regime boundaries and near the transition zones are analyzed to demonstrate the use of the proposed methods for quantifying the flow patterns. Based on the experimental results, recommendations for future work have been proposed.

1.7 Practical Aspects

Air and water were used in experiments to develop a flow pattern recognition method in this research. Two-phase flow is inherently unsteady (DeGance, 1970), even with constant operating conditions and no fluctuations in feed composition; a long pipeline may take a considerable period of time to achieve steady state. Also, flow regimes are subject to hysteresis effects. This means that the flow regime is a function of the flow conduit as well as the liquid and gas mixing arrangement. In this work, such effects were overcome by locating the pressure transducer far away from the point where the two-phases are initially mixed. Also, an improved mixing arrangement (Kirpalani et al., 1998) was used. The experimental work required a transparent pipe for visualization and photography purposes. Owing to the equipment limitations, such as maximum flow rates of fluids, the experimental conditions were carefully selected in this work.

Chapter Two

Theoretical Aspects of Two-Phase Flow

Transport of fluid mixtures in horizontal or near horizontal pipelines is becoming increasingly common. This is particularly evident in the processing of liquid and gaseous hydrocarbons. In these cases, two-phase flow transport offers economies in the pipeline construction itself and permits the centralization of gas processing and crude oil or condensate stabilization facilities; this usually results in both improved processing economics and conservation. Two-phase flow in horizontal lines is also encountered in the operation of evaporators, chemical reactors, heat exchangers and other types of chemical process equipment. Additional applications of horizontal gas-liquid two-phase flow are found in boilers, condensers and refrigerating equipment. In many of these applications, the rate of transport or the identification of a change in the process may be of prime importance (Govier and Aziz, 1972). The determination of the flow pattern is necessary for optimization of process conditions and calculation of transportation rates.

In gas-liquid flows, the two phases are distributed in a conduit in a variety of patterns not entirely under the control of the experimentalist (DeGance, 1970). Flow patterns are quite often chaotic and even basic classification is subject to a non-uniform approach that has not yet been standardized. The prediction of these patterns in gas-liquid flows is commonly based on visual observation, instrumental measurement of physical properties or empirical models. Typically, data interpretation is based on individual assessment of visual observations or on mathematical models. Physically realistic mechanisms have been proposed for models based on the analytical and numerical predictions of the transition between regimes. Detailed research has been performed to study two-phase gas-liquid flows, however the development of an accepted method for flow pattern classification has eluded researchers.

This chapter summarizes the experimental and modeling methods for flow pattern detection. The different flow regimes introduced in chapter one are discussed with

reference to the instrumentation applied for flow pattern recognition. A procedure for modeling of two-phase flow patterns with reference to Baker's conventional two-phase flow map is also described here. This map was useful in selecting the experimental conditions for this work.

2.1 Classification of Flow Regimes

In chapter 1 of this thesis, a brief description of the different flow patterns encountered in gas-liquid flows was introduced. A detailed description of the three basic horizontal flow regimes; separated, intermittent and dispersed flow regimes and their specific characterization methods are described here. Some researchers (Dukler and Taitel, 1986) have also coupled stratified and annular regimes into a **separated flow** regime. Also, slug and plug flow regimes are considered to be **intermittent flows**. In vertical two-phase flows, similar regimes namely; **slug, bubble, churn and annular** are observed. In this thesis, research experiments are carried out on a horizontal flow pattern recognition system. However, because detection methods are commonly developed independent of the orientation of the two-phase system a brief theoretical description of vertical flow patterns has been included in this work for future research.

2.2 Intermittent Flow Regime

Gas-liquid flow through conduits may take a variety of configurations related to the spatial distribution of the two phases in the pipe. These configurations are generally referred to as flow patterns or regimes. Slug flow is a complex pattern with unsteady characteristics where the liquid in the conduit exists as non-uniformly distributed axial plugs. Alternatively slugs of liquid, filling the pipe, are separated by gas zones which contain a stratified liquid layer flowing at the bottom of the pipe. In vertical slug flow most of the gas is located in large bullet shaped bubbles occupying most of the cross section of the pipe. These bubbles, Taylor bubbles, are separated by liquid slugs containing very small bubbles. The liquid confined between the bubble and the pipe wall flows around the Taylor bubbles in a thin falling film. In horizontal and inclined flows, slugs that fill the entire cross section of the pipe are separated by a stratified zone with an elongated bubble in the upper part of the pipe and a liquid layer at the bottom. The

intermittent flow regime has been further sub-divided into slug and elongated bubble patterns.

Researchers (Dukler and Taitel, 1986) have defined the elongated bubble flow pattern as liquid slugs not accompanied by gas bubbles. Slug flow patterns are considered at high flow rates when the liquid is aerated with gas bubbles. Methods have been proposed for calculating the slug hydrodynamic parameters and approximate models are being formulated to simulate this flow behavior accurately. Complex slugs, which are transient in nature and abnormally long, have not been predicted successfully. Researchers (Dukler and Taitel, 1986; Taitel, 1977b, 1986) emphasized the importance of predicting the conditions at which slug flow occurs. To model this successfully, experimentalists concluded that the slug length was a function of the slug frequency. Further research showed the effect of pressure drop on the slug frequency (Taitel, 1990b).

2.2.1 Mechanism of Slug Flow

The determination of slug frequency proposed by other researchers requires the analysis and understanding of the mechanism of slug formation. Visual observation revealed that slugs are created as a result of unsteady waves formed on a growing stratified flow layer which blocks the gas passage. This physical phenomenon occurs near the entrance to the pipe causing unsteady or transient slugging. In contrast, steady slug flow is observed to be independent of entrance phenomena.

Hubbard and Dukler (1966) used wall pressure fluctuations to classify two-phase flow into three general regimes of separated, intermittent and dispersed flows. He defined the flow transition in the separated flow-intermittent types on the basis of the spectral distributions of the wall pressure fluctuations. He determined that the location of the peak power obtained from the spectral distribution of the wall pressure variations allowed the differentiation of the flow regimes. He concluded that separated flow existed at zero frequency while at any other frequency the wall pressure variations indicated intermittent flow. Hubbard and Dukler (1966) suggested further work to confirm these preliminary test results. They also concluded that distributions of energy based on pressure fluctuations were relatively independent of factors like conduit size and pressure signal intensity.

2.3 Separated Flow Regimes

2.3.1 Stratified Flow Regime

Stratified flow is defined as the flow pattern where there is continuity of both phases in the axial direction. In this flow regime, water flows at the bottom and the air flows at the top of the pipe. This type of regime is studied in connection with the generation of waves at the interface and the transition into intermittent or annular flow. The gas-liquid interface may be smooth or wavy. The approach to transition or instability analysis is further classified into linear vs. non-linear analysis, inviscid vs. viscous analysis and one-dimensional vs. two-dimensional analysis.

Waves, generated at the interface, owing to the interfacial instability, can lead either to a wavy interface or to conditions where they reach the top of the pipe and cause a transition from stratified flow. Researchers (Dukler and Taitel, 1986) have found that the instability, which leads to the growth of short waves, results in a pebbly flow, because short waves saturate quickly and their effect is to roughen the surface and increase the interfacial shear stress rather than cause a transition. On the other hand long-wave instability is associated with the generation of rolling waves which, under certain conditions, may grow and result in the transition from stratified flow to intermittent or annular flow.

2.3.2 Annular Flow Pattern

One of the most important flow patterns, associated with a high gas flow rate, is the annular flow pattern (Barnea, 1989) as it is widely encountered in commercial applications. The annular flow pattern in gas-liquid systems is characterized by an upward moving smooth to wavy film of liquid on the conduit wall. A much more rapidly moving central core of gas contains entrained droplets of liquid with a concentration that vary from high to low. The liquid phase may be in laminar motion or it may be laminar only close to the pipe wall and the gas-liquid interface (Dukler and Taitel, 1986). This flow pattern has been defined as a "small ripple" regime and a "disturbing wave" regime. In the small ripple regime, small waves develop on the liquid surface moving at velocities

in the order of the interface velocities before losing their identity. At higher liquid flow rates, the waves are more intense and they travel faster than the interfacial velocity.

Researchers (Dukler and Taitel, 1986) have considered the annular and mist flow patterns separately. These two regimes have the liquid distributed between the film and the entrained droplets and there is a gradual change in the distribution in both cases. At the extreme conditions of the operating envelope, these conditions differ for the two regimes.

2.3.3 Dispersed Flow Regime

In the dispersed bubble flow regime, the gas phase is distributed as discrete bubbles in an axially continuous liquid phase. The size, shape and distribution of the bubbles depend upon the gas and the liquid rates, the manner in which the two-phases are originally intermixed and the interfacial forces. At very low gas-liquid ratios the bubble shape is that of a distorted sphere, but as the ratio is increased the bubbles become larger both in cross section and length.

The bubble concentration is usually greater in the center of the pipe. However, at lower velocities of the continuous phase, or with high-density contrast, the distribution becomes asymmetric peaking near the top of the pipe. If the continuous phase velocity is reduced to the point where there is no turbulence, or insufficient turbulence exists to offset the rising tendency of the bubbles, and when coalescence among the bubbles becomes significant, elongated bubbles that ride high in the tube are formed. These elongated bubbles are analogous to the Taylor bubbles discussed earlier. Further reduction in the velocity of the continuous phase results in complete coalescence of the elongated bubbles to form the stratified flow pattern. Increase in the gas velocity at constant liquid velocity results in the enlargement and elongation of the bubbles and the flow is transformed into the slug flow pattern.

2.3.4 Churn Flow Regime (Vertical Two-Phase Flow)

Churn flow is somewhat similar to slug flow. It is, however, more chaotic, frothy and disordered. In this type of flow pattern, the Taylor bubble becomes narrow and its shape is distorted. The continuity of the slug in the liquid between successive Taylor

bubbles is repeatedly destroyed by a high local gas concentration in the slug. This causes the falling liquid to form a bridge that is subsequently lifted by gas. Churn flow is observed to oscillate or alternate its direction of flow.

2.4 Flow Pattern Detection

Flow pattern detection has been complicated by two factors: (a) Some of the flow patterns described above contain arbitrary elements and (b) transition between flow pattern pairs is a gradual process. This has made it difficult to define the boundary for regime transition. Moreover researchers (DeGance and Atherton, 1970) have found that there are a range of flow conditions in a pipe where more than one pattern exists. A description of the flow pattern determination methods, pertinent to this thesis, has been reported here.

2.4.1 Visual methods

Visual methods are the simplest approach for the detection of flow patterns (Sato and Segokchi, 1975). However, modern methods like particle image velocimetry (PIV) have replaced standard video recording or high-speed film recording. The instrumental limitations in image processing (Clarke, 1996) have been significantly overcome. The structure of the liquid flow has been revealed by repeated analysis of Lagrangian scans on a small section of the pipe by some researchers for low flow rates (Dukler and Taitel, 1986). An alternative approach for recording flow pattern structures using high speed flash photography was applied in the present work and is described in section 3.6. However, it was found to be very difficult to distinguish the transition boundaries.

2.4.2 Instrument Methods

2.4.2.1 Methods Based on Pressure Measurement

Preliminary efforts to characterize two-phase flow with reference to pressure measurements were based on the observation that systematic changes in gas or liquid flow rate caused a concomitant change in the slope of the time-averaged pressure curve. However, these results were not conclusive in characterization of the flow pattern as the method relied only on visual observation for detecting flow pattern transitions

Some researchers (Hubard and Dukler, 1966) first proposed a method based on the spectral analysis of wall pressure fluctuations. They found that the fluctuations in wall pressure were reflections of liquid and gas velocities and the manner in which they were distributed in the pipe.

The time trace of the static pressure ($P(t)$) at the wall of the conduit is further analyzed to obtain the power spectral density $S_p'(f)$. These terms can be defined by the following set of statistical equations:

$$P'(t) = P(t) - \overline{P} \tag{2.1}$$

$$R'_p(\tau) = \lim_{t\to\infty} \frac{1}{t} \int_{-\infty}^{\infty} P'(t)P'(t+\tau)dt \tag{2.2}$$

$$S'_p(f) = \int_{-\infty}^{\infty} R'_p(\tau) e^{i2\pi f\tau} d\tau \tag{2.3}$$

$P'(t)$ = Time variation of the fluctuation (dynamic pressure fluctuation), (kPa.)

$P(t)$ = Time-dependent pressure (static pressure fluctuation), (kPa.)

$\overline{P}$ = Time-averaged pressure

$R'_p(\tau)$ = Auto-correlation function for dynamic pressure fluctuation, P' (t). (kPa.)

$S'_p(f)$ = Power Spectral Density (PSD) for dynamic pressure fluctuation, P' (t). $(\text{kPa.})^2$

τ = auto-correlation time (s)

Although a wide variety of apparent phase distributions are observed, it was concluded that only three basic spectra existed and these spectra could serve as fingerprints for flow pattern determination.

a) **Type A**, separated flow patterns such as stratified or annular flow where the spectra peaked at f=0 with decay at increasing f. These regimes exhibit low entrainment rates because the phases of the fluids can be considered to be axially continuous; the spectra were found to be similar to turbulent flow (Dukler and Taitel, 1986).

b) **Type B**, intermittent flow patterns, such as those of slug flow and elongated bubble were classified under this category. Peak spectra in this case, were found to be

displaced from zero frequency on the power spectral density plot and represented the frequency of the slug passage.

c) **Type C**, represents dispersed or distributed flow patterns, such as bubbles in liquid and drops in gas. PSD plots for this type of flow revealed spectra similar to band-limited white noise. The fluctuations in this type of flow were controlled by the passage of successive elements of the dispersion. The generation of a white noise-like plot was concluded by calculating the auto-correlation coefficient. The coefficient was expected to approach a delta function as the successive fluctuations were expected to be small. The Fourier transform of the delta function is a white noise.

Thus, classification of distinct flow patterns was achieved based on the PSD of the pressure fluctuations measured by previous workers (Dukler and Taitel, 1986).

In practical situations, the superposition of these spectra is observed owing to flow transitions existent throughout the pipe. In annular-dispersed flow transitions, where the presence of low frequency annular flow and high frequency, pseudo-white noise spectra co-exist, determination by this method is rather difficult. Similarly, in the case of wavy-annular flow, the spectra appeared as a superposition of annular and slug flow. An attempt to characterize the transitional flow patterns was made by introducing amplitude analysis into the characterization (Dukler and Taitel., 1986). The suggested method identified specific criteria on the amplitude and frequency. These numbers were found to be characteristic of a specific system. A further attempt based on vertical flows was carried out by Tutu (1982) to determine the pressure gradient variations. The pressure gradient is strongly dominated by the hydrostatic gradients or the void fractions.

Hence, for gas-liquid flows located in the bubbly flow regime, the pressure gradient will fluctuate about $\rho_L (1-\alpha) g$, while for those in annular flow, it will center about $\rho_g g$, where:

ρ_g = Density of the gas phase (kg/m^3),

ρ_L = Density of the liquid phase (kg/m^3),

g = Acceleration due to gravity (m/s^2),

α = Gas holdup.

Because the two fluids are usually found to be significantly different in density, this can be used as a diagnostic tool. Oscillations in pressure gradient during bubbly flow reflect the variations in the voids with time between the two metering stations resulting from a few bubbles entering or leaving the volume between the two stations. Similarly, in annular flow the pressure drop fluctuations result from the variation of a few droplets in the core, again a small number. However, in slug flow, the pressure gradient oscillates between a maximum of that for bubble flow, where the liquid slug occupies the space between the detectors, to near zero where a Taylor bubble passes between the detectors. A distinction between the three patterns was then obtained (Hubbard and Dukler, 1966) by plotting probability density functions (PDF) for each time trace. This was considered to be one of the first methods for spatial and time representation of the distribution of phases in a conduit or pipe.

2.4.2.2 Additional Instrumentation Methods

Researchers (Jones and Zuber, 1976; Merzkirch, 1987; Mishima et al., 1997) attempted other classification methods based on the photon attenuation for calculation of void fraction using X-ray and gamma-ray attenuation approaches. These methods were also based on the characteristic PDF curves of the different flow patterns. But these methods were of limited use largely owing to high installation and operational costs. Methods, based on hot film anemometry and electrical conductivity have also been conducted with limited success.

2.5 Modeling Flow Pattern Transitions

2.5.1 General Concepts

The prediction of flow pattern transitions is typically carried out based on experimental results at different flow rates, fluid properties and pipe sizes. The results from flow visualization are then used to map the collected data in a two-dimensional plot by locating transitional boundaries between the regimes.

The axes for the plot are selected based on the co-ordination of the data rather than a predictive correlation and the results depend strongly on the particular data being used to predict the map. Several researchers (DeGance and Atherton, 1970; Dukler and

Taitel, 1986) have concluded that an extension to other conditions of pipe sizes, fluid properties or flow rates is unreliable.

Investigators (Baker, 1958, Al-Shiekh et al., 1970; Mandhane et al., 1974; Govier and Aziz, 1972; Dukler and Taitel, 1986) have selected various co-ordinates for the axes. The oldest and most reliable of these maps is the Baker's chart. The use of dimensionless groups in the development of such charts depends on the selection of the groups available. This choice is made by dimensional analysis. Dimensionless coordinates for maps have been suggested because the experimentally based transitions might be valid at other conditions of pipe size and fluid properties.

Physical properties, like superficial velocities, densities and surface tension for the gas and liquid, along with the acceleration due to gravity, have been found to have a significant influence on the transition process. Similarly, geometrical parameters like diameter of the pipe, the pipe inclination (Barnea, 1980a, 1980c) and the pipe roughness (Taitel, 1977a) are also found to influence the flow transition.

The selection of the dimensionless numbers for the different flow maps is made by judiciously guessing the most important numbers. However, there is no certainty that any single set of the selected groups will characterize all flow pattern transitions.

2.5.2 Modeling with Baker's Flow Pattern Map

Baker (1954) proposed a flow pattern map that is widely used in the oil and gas industry. The map is based upon the co-ordinates of G/λ and $L\psi\lambda/G$ which are proportional to the mass velocity of the gas and the ratio of mass velocity of the liquid to the gas respectively. Because Baker's flow map was developed in the British system of units, a conversion factor is provided to accommodate the fluid properties and flow rates in the SI system.

The co-ordinates on the flow pattern map shown in **Figure 2.1** are based on the following fluid properties:

G = Mass velocity of gas $\frac{kg}{m^2 s}$ or, $\frac{lb}{ft^2 hr}$,

L = Mass velocity of liquid $\frac{kg}{m^2 s}$ or $\frac{lb}{ft^2 hr}$,

λ, ψ = Dimensionless numbers

c = 737.0984, conversion factor for plotting fluid conditions in SI system.

The quantities λ and ψ are defined in the SI system as follows:

$$\lambda = \left(\frac{\rho_g \quad \rho_L}{(1.202) \quad (1000)}\right)^{\frac{1}{2}} \tag{2.3}$$

$$\psi = \frac{0.073}{\sigma}\left[\frac{\mu_L}{0.001} \quad \left(\frac{1000}{\rho_L}\right)^2\right]^{\frac{1}{3}} \tag{2.4}$$

The quantities λ and ψ in the FPS system are defined as

$$\lambda = \left(\frac{\rho_g \quad \rho_L}{(0.075) \quad (62.4)}\right)^{\frac{1}{2}} \tag{2.5}$$

$$\psi = \frac{73}{\sigma}\left[\frac{\mu_L}{1} \quad \left(\frac{62.3}{\rho_L}\right)^2\right]^{\frac{1}{3}} \tag{2.6}$$

ρ_g = Density of the gas phase (kg/m^3 or lb$_m$/ft^3),

ρ_L = Density of the liquid phase (kg/m^3 or lb$_m$/ft^3),

μ_L = Viscosity of liquid phase (Pa-s or cP.),

σ = Surface tension (dyne/cm or N/m).

The coordinates for the map are given by;

$$X = \frac{L\lambda}{G\psi} \tag{2.7}$$

$$Y = \frac{G}{\lambda} \tag{2.8}$$

In the SI system of units;

$$Y = \frac{cG}{\lambda} \tag{2.9}$$

λ and ψ are wholly empirical devices designed to bring the transition lines for systems other than air and water into co-incidence with the air-water system on which this flow pattern map was based.

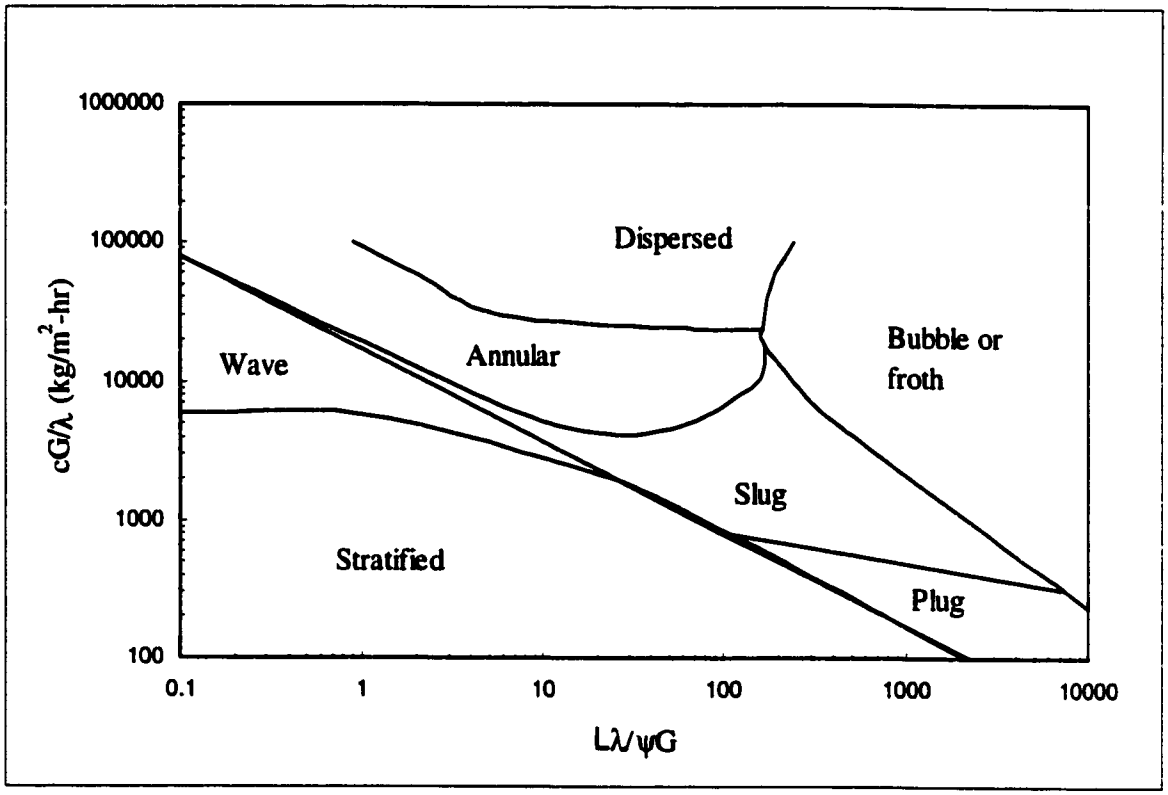

Figure 2.1: Baker's flow pattern map for modeling horizontal two-phase flows.

The linear relationship between the co-ordinates is one of the major disadvantages of the Baker's chart. Owing to this factor, the modeling of fluids, other than air-water, is inaccurate. This chart uses dimensionless co-ordinates which clearly limit the conditions near those of the experiments used to locate the transition boundaries.

Despite these restrictions, Baker's chart has been selected for the determination of experimental conditions for this work because:

1) As air-water mixtures are used in the experimental work, the problem of extending the flow pattern map to other fluids was avoided,
2) It has been traditionally used in the oil and gas industry for flow pattern modeling,
3) The limitations of this flow pattern map are well known,

4) The map is only required to provide a basis for selecting flow conditions for experimental tests and not for detailed characterization work.

2.5.2.1 Modeling Efforts by Other Researchers

Based on visual observations for different types of flow systems, many different flow pattern maps that satisfy a given flow condition have been suggested.

Dukler and Taitel (1986) presented a generalized flow pattern map for horizontal two-phase flow based on the gas and liquid flow rates, physical properties, tube size and inclination angle. The pipe roughness was not specifically considered in the development of their map. However, these researchers suggested that the pressure gradients could be calculated using known roughness parameters to determine whether the flow transition boundaries applied (Taitel, 1977a).

DeGance and Atherton (1970) suggested that fluids do not exhibit one flow regime, but a succession of regimes whose transition should be predicted by the co-ordinate axes. Knowles flow pattern map takes into account these parameters but is inconsistent with Dukler's chart for dimensional similarity.

2.6 Discussion

Two-phase flow is inherently unsteady. Past research has concluded that the flow regimes are subject to a hysteresis effect that is a function of both the physical conditions at a given location in the flow and the particular conduit geometry through which it flows. Researchers have also reported that the equipment used to initially mix the two phases can have a significant effect on the flow regime. Owing to these factors, flow pattern maps are system-specific and are limited in applicability to other systems. Baker's flow pattern map was chosen in this work to provide a guideline for flow pattern selection only.

Based on a review of available instrument methods, a dynamic pressure transducer was found to be a robust and economical unit for flow pattern characterization. Different methods for processing pressure variations have demonstrated the requirement for a novel approach that recognizes the pattern of variation of the two-phases in time.

Chapter Three

Experimental Studies in Two-Phase Flow Characterization

This chapter describes the experimental arrangement and the data collection system used for characterizing two-phase flows. The two-phase flow system for this research is designed to be flexible in configuration to allow for a wide range of experimental tests to be carried out.

Changes in mechanical arrangements and pressure signal digitization are easy to configure in the system. The experimental tests are carried out using air and water as the gas and liquid system for two-phase characterization. Air and water were selected for these studies for the following reasons:

1) The physical properties of these media are very well known.
2) Other researchers (Baker, 1954; DeGance and Atherton, 1970; Govier and Aziz, 1972) have developed flow regime maps for air-water mixtures. Other liquid-gas systems can be modeled with respect to water systems because most flow pattern maps use dimensionless parameters for fluid properties.
3) Ease of availability of the media and low comparative costs.
4) Operational safety.

This chapter includes a description of the mechanical arrangement, sensor configuration and the associated data acquisition system. Experimental conditions for collecting pressure fluctuations are selected from the Baker's flow pattern map described in chapter two.

3.1 Mechanical Arrangement for Two-Phase Flow System

Two different mechanical arrangements were selected to perform a series of experiments for this research. These arrangements are primarily classified on the basis of the pulsation pattern, aperiodic or periodic achieved. A small-scale pulsating flow system, referred to as a "**Baseline System**", with a regular pulse of liquid flow, was designed for evaluating the proposed signal analysis methodology and to demonstrate the

complexity resulting from the introduction of a second compressible phase (air) into the system. The experimental techniques and data processing methods from the reference system were then applied to a "**Two-phase flow pattern recognition arrangement**".

3.1.1 Air and Water Delivery System

Compressed air for the experiments is supplied at 1.2 MPa (160 psig) by a 5.6 kW(75HP) electric powered screw compressor (CompAir® Model: 6000C) with a capacity of $1836*10^3$ m^3/s. at a pressure of 1.2 MPa.

A high-pressure centrifugal pump (Max. pressure 1.26 MPa.) provides a maximum water flow rate of 11.35 m^3/h (50 US gallons/min.). The centrifugal pump draws water from a water storage tank WST-1 (tank capacity: 500 L.). The system is operated at the required water flow rate by partially re-circulating the water and operating a pneumatic control valve. Airflow to the system is controlled manually. Owing to high requirements for liquid and gas flow rates, the two-phase flow system is designed as a loop to recycle the water through the system. Water, from the two-phase flow system, is collected in a re-circulation water storage tank (WST-2) and transferred back to WST-1 by an auxiliary low-pressure re-circulation pump. Reinforced, flexible hosepipes (0.0254 m ID) supply water to the baseline system and the two-phase arrangement. Air flow rate is monitored on a mass velocity meter (Eldridge Model: 8712) that reports it at standard temperature and the water flow rate is monitored on a magnetic flow meter (Yokogawa Model: YEWMAG) during the experiments.

3.1.2 Water Collection Tower

To collect the water into WST-2, the outlets for the two arrangements are located near a water collection tower. The tower is provided with blowers to control the direction of exiting water from the two-phase system as shown in **Figure 3.1**.

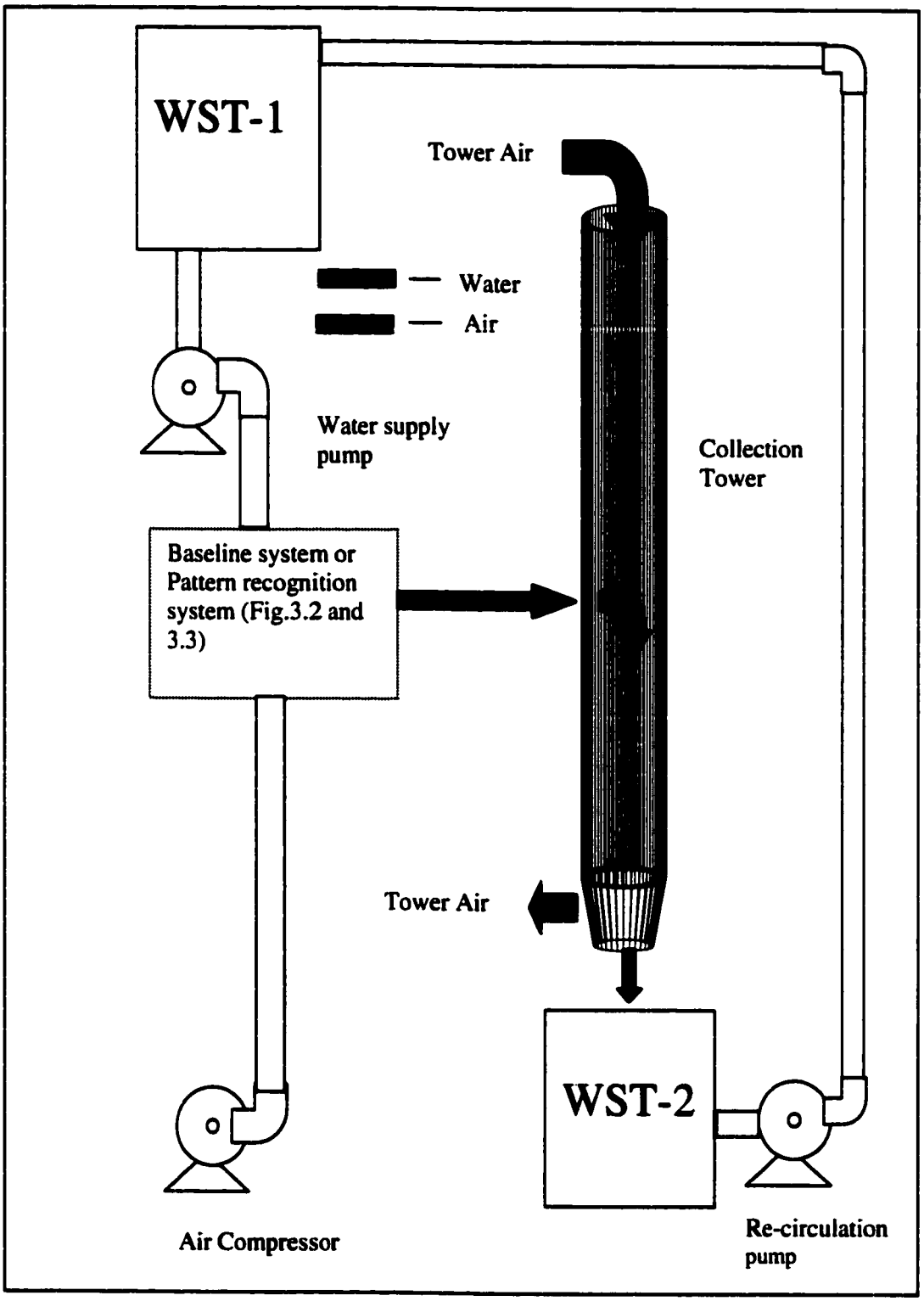

Figure 3.1: Schematic diagram for two-phase air/water flow system.

3.2 Baseline System for Single-Phase and Two-Phase Flows

The baseline system, shown in **Fig. 3.2**, provides a model arrangement for evaluating different pulsation patterns. Both, single and two-phase flow tests can be evaluated with this arrangement. The system is designed to operate with low liquid and air flow rates. The design principle for the baseline system is based on generating a regulated pulsation in water flow that can be tracked by a signal processing method and compared to the pulsation in an air-water mixture flow. Regular pulses of water flow are introduced into the system through a rotating ball valve coupled to a gear-reduced DC motor. This motorized valve provides a regular pulsation in flow at 222 pulses per minute (3.67 Hz.). The dynamic pressure transducer, used in the experimental work, is located 78 cm away from the mixing point of the two-phases. A manual needle valve, installed at the exit of the pipe, serves as a restriction device to control the pressure in the system.

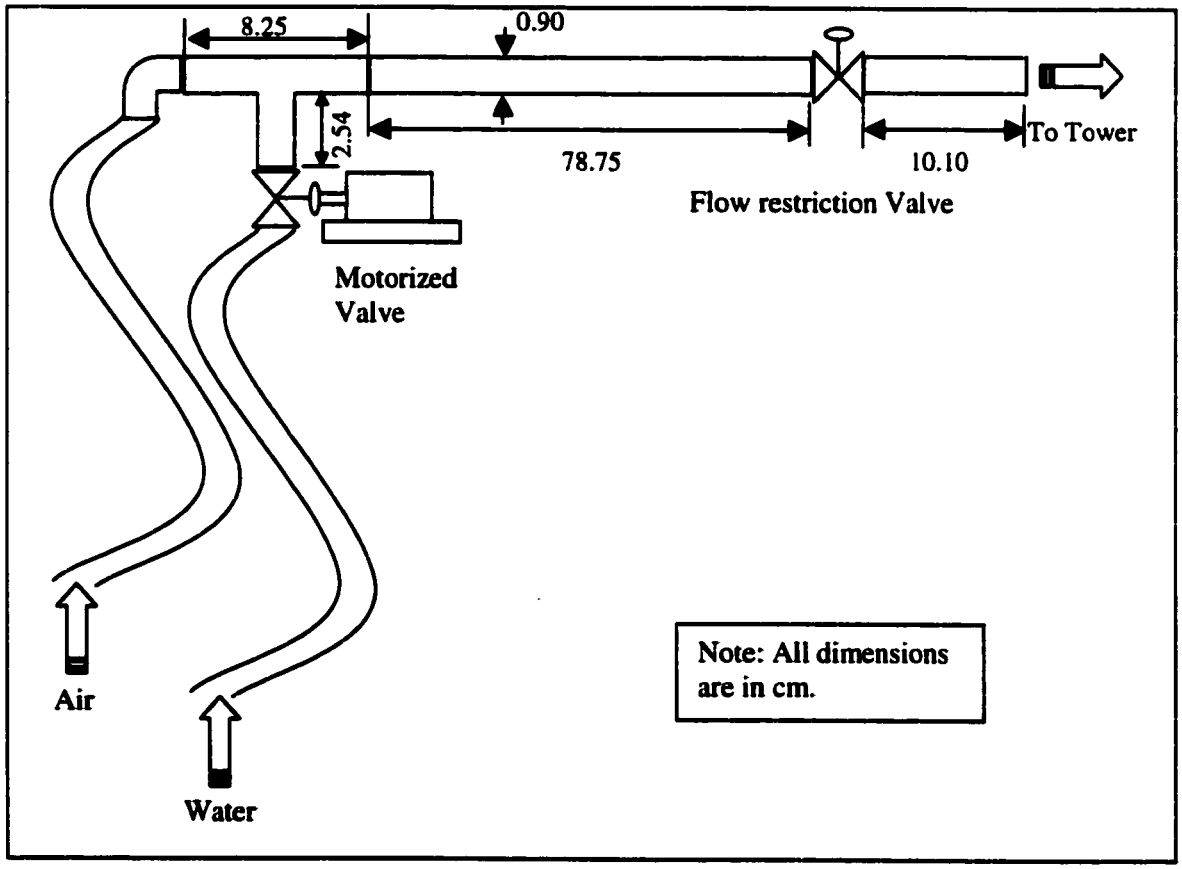

Figure 3.2: Baseline system for two-phase flow characterization.

3.3 Two-Phase Pattern Recognition System

Experiments conducted for characterizing different flow patterns are carried out on the two-phase flow pattern recognition system. **Figure.3.3** shows the schematic diagram of the flow system constructed. The two-phase flow apparatus consists of a Plexiglas® test section (2.43 cm. diameter and 345.2 cm. long) for observing the flow pattern developed. The mixing apparatus (Kirpalani et al., 1998) comprising two-pipes at 45° reduces the hysterisis effect discussed in chapter two. Also, the mixing point is located far away from the Plexiglas® section. Water exiting from the system is directed towards the water collection tower and is controlled by a restriction valve at the exit.

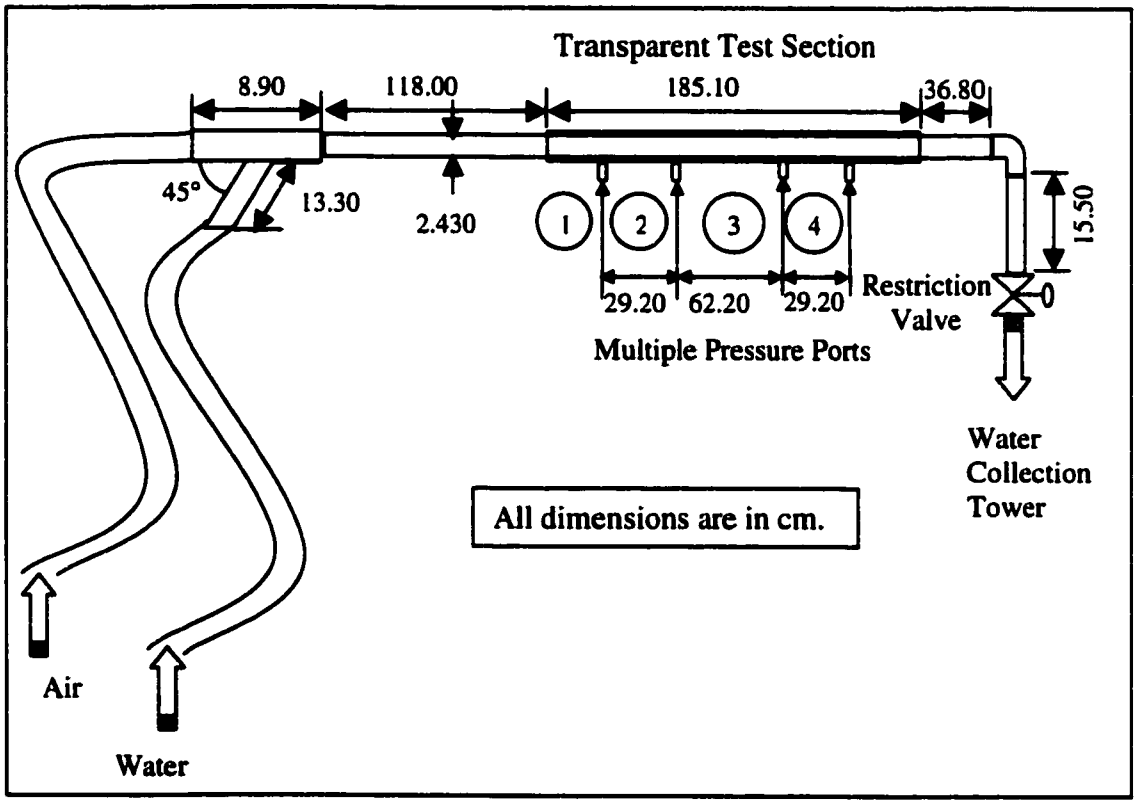

Figure 3.3: Two-phase flow system for characterization of flow patterns.

Multiple pressure ports on the Plexiglas® pipe, located as shown, were installed for recording pressure variations at the pipe walls. Position 2 was selected after preliminary experiments on the system.

The transparent tube allows photographs of the various flow structures in the pipe to be taken. For this research, only representative photographs of the flow structure for the annular, dispersed and slug flow are presented.

3.4 Process Diagnostic Sensors

The reasons for selection of pressure variation studies were described in chapter two. The specifications for the high-resolution dynamic pressure transducer chosen for this work are given below:

3.4.1 Pressure Transducer Specifications

The quartz pressure transducer (PCB Model No.: HS113A21) consists of a high resolution, acceleration compensated, quartz piezoelectric element coupled to a source follower type miniature electronic circuit. The transducer receives a constant excitation current of 4 mA. at 18-28 VDC from a transducer power supply (PCB Model No.: 482A10). This instrument is specially designed for applications involving shock tube and blast wave measurements, typical applications where transients in pressure occur. The selection of this unit was based on the large frequency range over which the transducer operates (up to 20 kHz.) and its special design. The output from the pressure transducer is bipolar in nature and ranges from -10V to +10 V. The transducer has a sensitivity to pressure change of 2.76 mV/kPa. (18.98 mV/psig) and has an operating range of 1378 kPa. (250 psig).

3.4.2 Extraneous Pressure Fluctuations

The pressure at any point in a two-phase flow system is caused either by the direct hydrodynamic nature of the two-phase flow itself, or by unwanted pressure pulsations from pumps, restrictions and intrusions to the flow or vibrations acting upon the flow loop from external sources (Samways et al., 1997). Unwanted pulsations such as pump vibrations and changes in geometry are reduced in the experimental arrangement used here by placing the Plexiglas ® test pipe on a different floor level. Also, flexible hosepipes eliminate any sharp changes in the direction of flow that could introduce a rotational component to the velocity along the axis of the flow.

3.5 Data Acquisition System Design

The pressure fluctuations for different operating conditions are collected with a data acquisition, control and processing system. The system flow chart, shown on **Figure. 3.4**, consists of a data acquisition and control board (National Instruments™ AT-MIO-16XE data acquisition and control card) and programs that were developed in LabVIEW®. This card is used for digitizing (12-bit) the dynamic pressure fluctuations in Volts. Hence the minimum analog signal detected from the transducer is +/- 5 mV. or 1.7926 kPa. (0.26 psig) while the signal frequency is below 10kHz. The signal-conditioned output from the pressure transducer amplifier is simultaneously observed with a 12-bit 100 MHz oscilloscope (Yokogawa). Counters from the card control a high-intensity light source for conducting flash photography to record the different flow patterns examined. The counters are optically isolated from the light source for this purpose.

LabVIEW® programs were developed in version 3.1 and upgraded to version 5.1 during this research. The data acquisition and control program flow charts are shown in **Figure 3.5.1 and 3.5.2**. The collected data is stored for further digital signal processing (DSP).

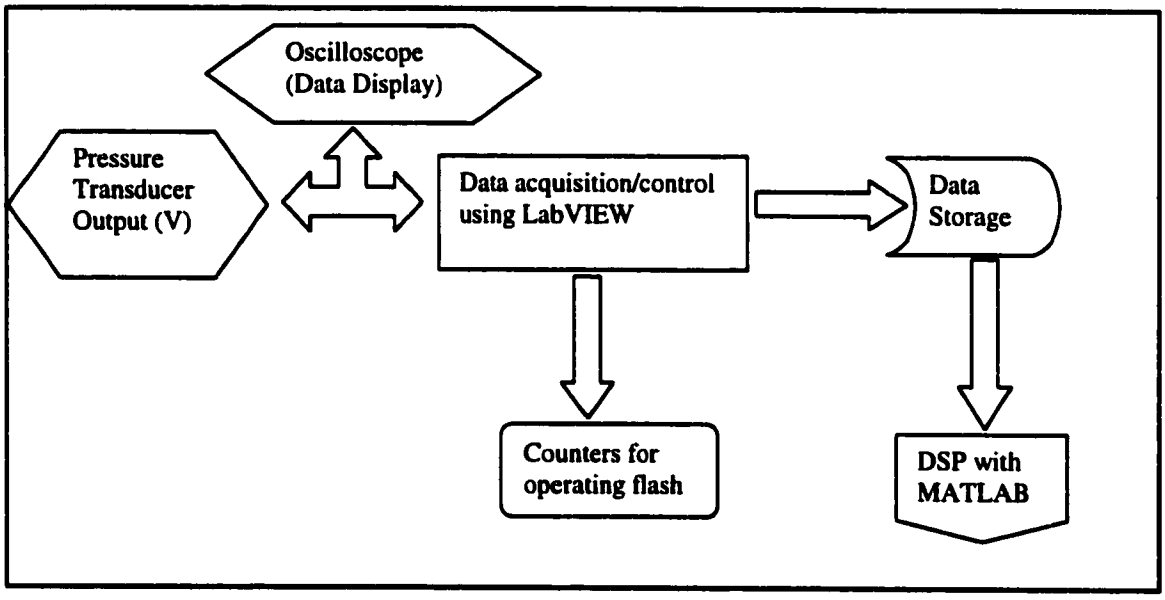

Figure 3.4: Program flowchart for data acquisition, control and processing system.

3.5.1 Data Collection

Data sampling rates of at least twice the highest frequency are required to satisfy Nyquist's sampling theory for signal analysis. The voltage output of the transducer was recorded at different sampling rates and analyzed to determine the peak frequencies. Initially, Fast Fourier Transform (FFT) analysis was implemented to investigate the occurrence of peak frequencies. After determining the maximum frequency of fluctuation to be less than 200 Hz., the sampling rate was set at 512 Hz., for all experimental conditions, to avoid any aliasing effects in data collection. Analog filters were also applied to confirm the maximum sampling rate for the data collection.

The pressure fluctuations for different flow conditions are conducted for a period of at least 60 seconds to examine multiple time segment analysis of the collected data.

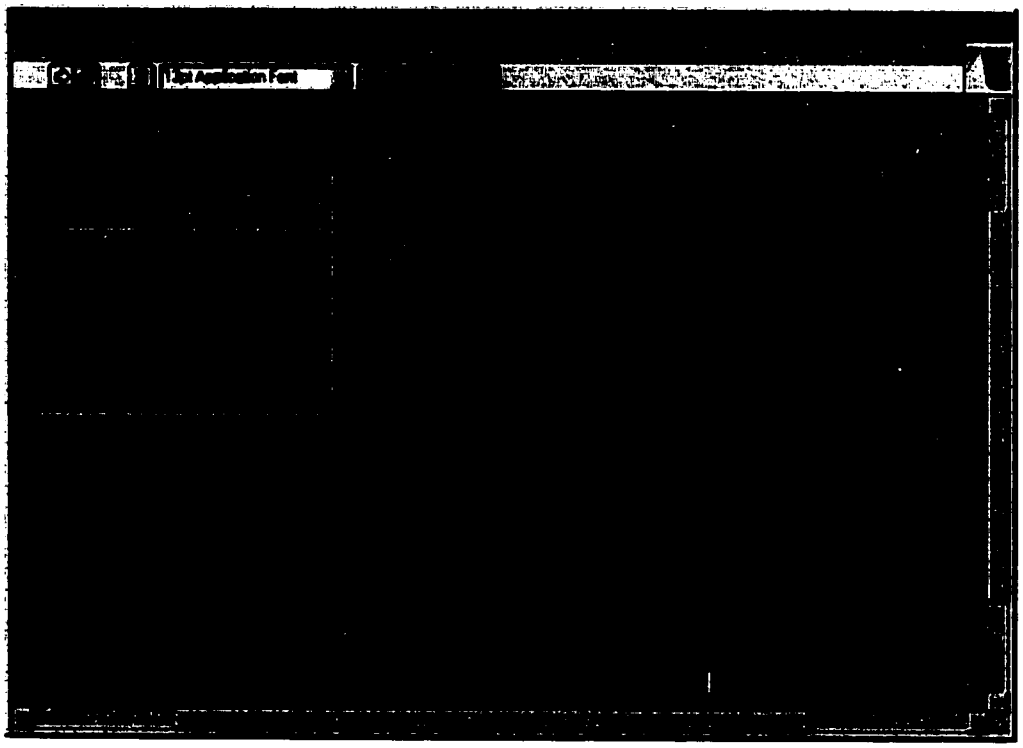

Figure 3.5.1: Main data acquisition front panel developed in LabVIEW ® software.

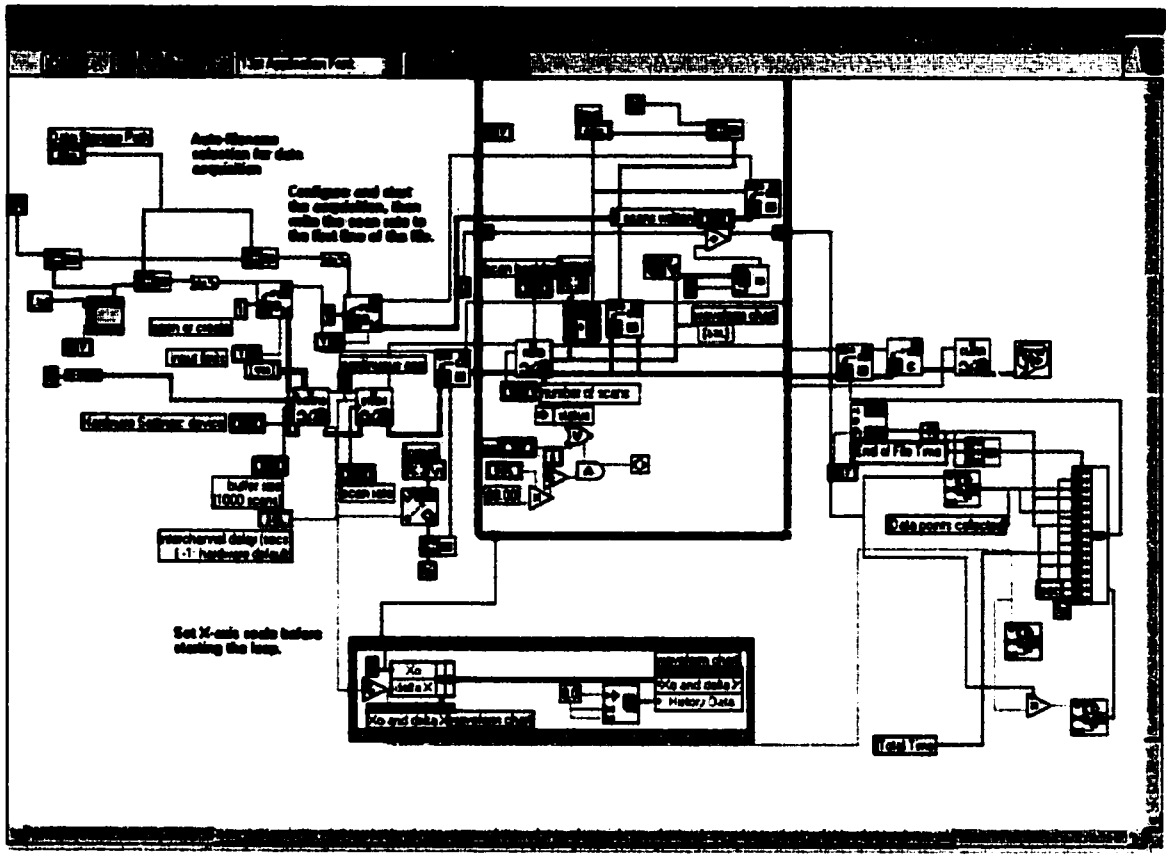

Figure 3.5.2: Main data acquisition block diagram (code) developed in LabVIEW ® software.

3.6 Experimental Methodology

3.6.1 Design of Experiments

A phased approach has been adopted for conducting experimental tests. Experiments are initially carried out on the baseline system and then transferred to the two-phase flow pattern recognition system. Experiments on the baseline system are used to test the data collection system and demonstrate the differences between single and two-phase systems.

The selection of experimental conditions for characterizing two-phase flows is described in chapter two. The experimental methodology is based on modeling experimental conditions using Baker's flow pattern map. Experiments are then conducted with the two-phase flow pattern recognition system. Two-phase flow tests conducted on the full-scale system cover both well-developed and transitional flow conditions.

3.6.1.1 Baseline Experiments

The experimental tests conducted on the baseline system are the principal means for verifying the data acquisition set-up. A single-phase pulsating flow experiment was carried out at a low water flow rate of 1627.20 m^3/s and the pressure fluctuations collected. The collected pressure variations were analyzed to detect the known pulsating pattern introduced in the system. In this manner, the data collection system is validated for conducting experimental tests.

While maintaining the water flow rate constant, an air flow rate of 3.36 m^3/s (STP) was introduced into the pulsating system. The complexity introduced into the pressure fluctuations was observed

These baseline experiments validated the pressure collection system and indicated clear differences in liquid and liquid-gas pulsation patterns.

3.6.1.2 Two-Phase Flow Pattern Recognition Experiments

Experimental conditions were selected to represent annular, dispersed and slug flow regimes by modeling on Baker's flow map. The experimental conditions selected are shown in **Table 3.1** and on **Figure 3.7**. These conditions are either well within the regime or near the transition zone. Air and water flow rates are varied to achieve the required conditions. Pressure fluctuations are collected for at least one minute for each experiment to allow multiple time segment analysis for each flow regime. Photographs representing annular, dispersed and slug flow patterns are shown on **Figure 3.8**.

Researchers (Dukler and Taitel, 1986) have concluded that pressure fluctuations in smooth slug flow conditions are fairly regular. Owing to experimental limitations, only one condition of slug flow that shows a fairly regular pattern was examined in this work.

The annular and dispersed flow regimes have been identified to exhibit a transient or irregular pressure fluctuation pattern. Therefore experiments have been concentrated on these regimes.

Flow Pattern	Operating Condition	Water Flow Rate (m^3/s)	Air Flow rate (m^3/s)	$L\lambda/\psi G$	cG/λ (kg/m^2-s)
Annular Flow	Conditon 1	7.69E-04	5.00E-03	128.18	9542.98
	Condition 2	1.89E-04	6.84E-03	23.04	13054.08
Dispersed Flow	Condition 1	1.06E-03	9.96E-02	8.87	189959.36
	Condition 2	2.21E-03	2.71E-02	67.79	51766.18
Slug Flow	Condition 1	1.89E-04	5.66E-04	278.42	1080.34

Table 3.1: Modeled experimental conditions from Baker's flow map.

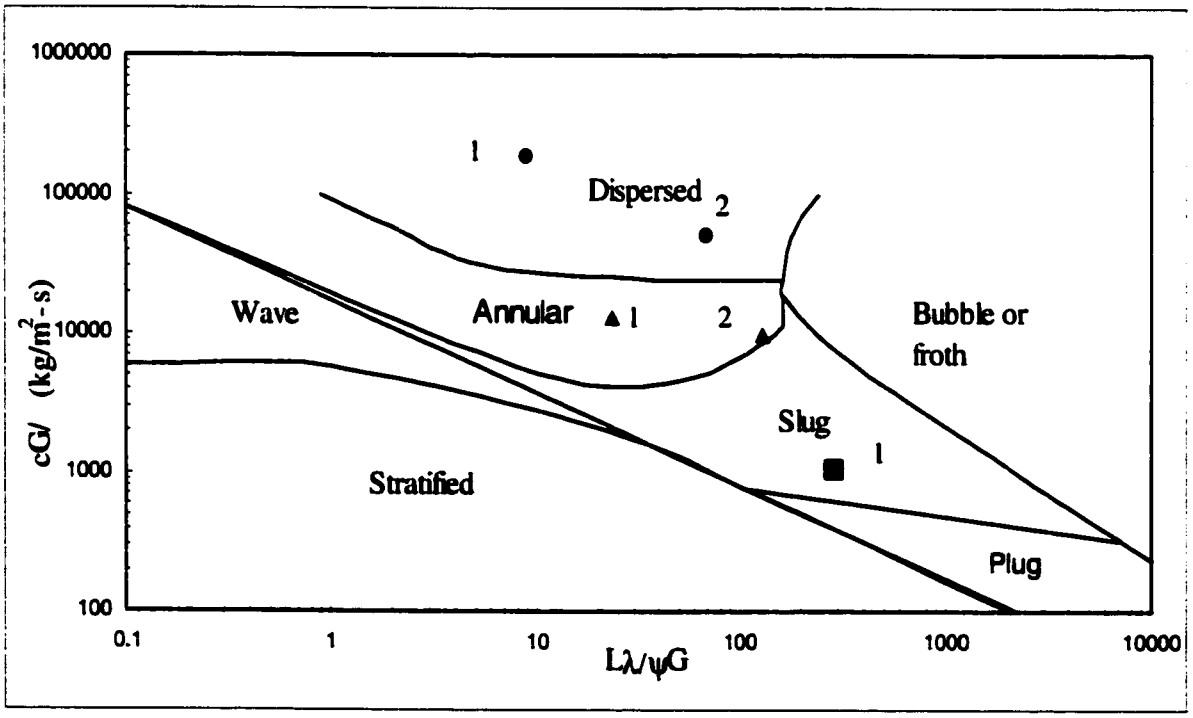

Figure 3.7: Operating conditions from Table 3.1 plotted on conventional two-phase flow map.

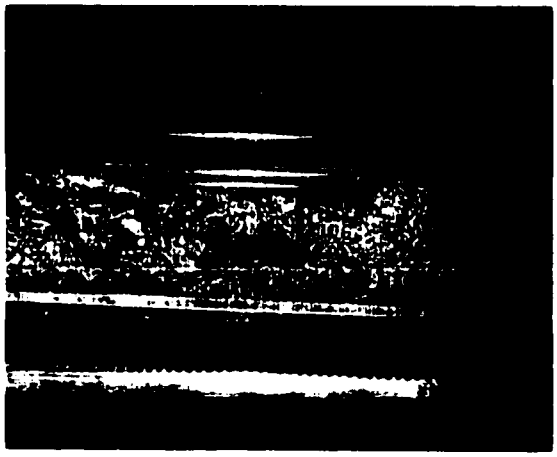

Figure 3.8.1: Picture of annular flow at operating condition 1.

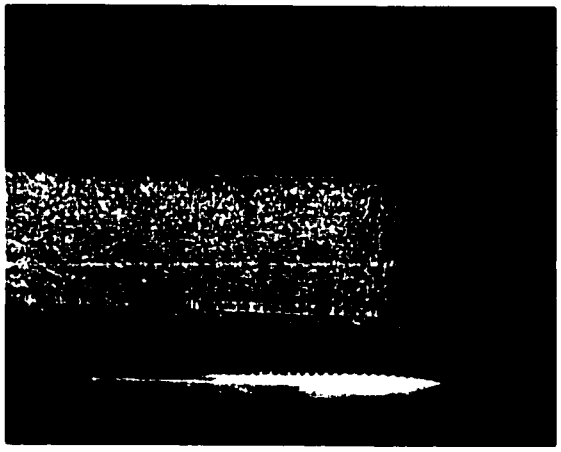

Figure 3.8.2: Picture of dispersed flow at operating condition 2.

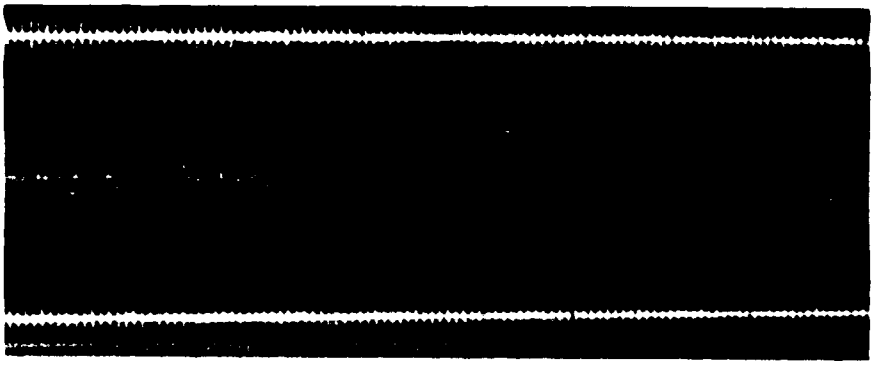

Figure 3.8.3: Picture of slug flow at operating condition 1.

Figure 3.8: Two phase flow regimes

3.7 Discussion

A systematic methodology for conducting experimental tests was developed and experiments conducted in the annular, dispersed and slug flow regimes on the two-phase pattern flow recognition system. The experimental collection of pressure fluctuations was validated and the collection of pressure fluctuations on the baseline system has differentiated single and two-phase flow systems. The pressure fluctuation data collected can be subjected to new signal analysis approaches for characterization work. Flash

photography was not conducted for all experimental conditions and only representative photographs for the different flow patterns examined in this research are shown on **Figures 3.8.1-3.8.3**.

Chapter Four

Signal Processing Methods for Flow Pattern Characterization

Chapter two summarizes the two-phase flow characterization work reported by other workers. Data from different sensor types, is typically handled by conventional signal analysis methods. However, recent developments have prompted the use of new approaches for flow pattern recognition. Novel signal processing methods for characterizing two-phase flows are described in this chapter. Example analyses, illustrating the use of these methods, are demonstrated on model data. The fixed pulsation pressure data collected from the baseline system, described in chapter three, is also analyzed using these new methods to carry out initial benchmarking and provide a basis for two-phase flow study.

4.1 Conventional Signal Processing Methods

In the past, flow patterns have been defined for fully developed two-phase flows using conventional analysis methods. These methods are based on observing the time, amplitude and positional variation of voids in the system. Conventional methods for characterizing two-phase flow patterns from fluctuating data are summarized as follows:

1) Govier and Aziz (1972) examined changes in the time averaged pressure gradient obtained at different flow rates of gas and liquid media.
2) Hubbard and Dukler (1966) suggested using Power Spectral analysis of wall-pressure fluctuations to determine flow patterns.
3) Tutu (1982) applied Probability Density Functions (PDF) to time-varying pressure drops across a section of two-phase flow in a pipe to analyze different flow patterns.

However, all of these approaches performed poorly in the prediction of flow patterns in the transition zone or near the regime boundaries where a large spectrum of

frequencies were present in time-varying data. Typically, prediction of flow pattern transitions has therefore been limited to modeling or visual observation through a transparent section in the pipe (DeGance and Atherton, 1970). Researchers (DeGance and Atherton, 1970; Barnea, 1980a, 1982, Barnea et al., 1989; Wambsganss et al, 1994; Cai et al, 1996) also predicted that two-phase flow is inherently unsteady or transient near the transition boundaries. In this work, advanced methods have been proposed for analyzing both fully developed and transitional flow patterns. Special emphasis is placed on analyzing the transient, or time varying aspect, of the pressure fluctuations. These methods are an enhancement to conventional techniques, such as spectral analysis, used for flow pattern recognition.

4.2 Signal Processing Approaches

Transform methods are useful in signal detection because a mathematical basis function will concentrate the signal onto relatively few of the basis elements (Graps, 1995). In this respect, the use of Fast Fourier Transforms (FFT) is an established signal processing method to determine the frequency content of a signal. The Fourier transform decomposes a waveform into sinusoids of different frequency and identifies or distinguishes the different frequency sinusoids and their respective amplitudes.

As discussed in chapter two, other two-phase flow researchers (Hubbard and Dukler, 1966.) have applied Power Spectral Density (PSD) analysis for characterizing flow patterns. Spectral analysis of time-varying signals can identify steady state or uni-variate conditions (Carter, 1993). However, during transient two-phase flow, often found near the transitional region, multi-variate signals are found to exist (Dukler and Taitel, 1986; Barnea, 1989; Maciejewski, 1996). The time of occurrence of these variations cannot be estimated as spectral analysis measures only the frequency of the signals. Consequently, this approach does not provide any information regarding the regularity of the signals.

4.3 Novel Methods for Signal Analysis

Preliminary attempts were made to characterize the unsteady behavior of two-phase flow by considering Short Time Fourier Transforms (STFT). In this method, the

signal is divided into segments small enough so that these portions of the total signal can be assumed to be steady, or stationary, in nature. A brief description of the STFT approach is presented below:

A window function 'w' (rectangular, gaussian etc.) is selected with a width equal to the segment of the signal where it is regular. This selected window function is first located at time t=0. If 'T' represents the width of the window, the window function will overlap with the first T/2 seconds. The window function and the signal are multiplied so that only the first T/2 seconds of the signal are selected and analyzed. If this portion of the signal is regular, the resultant will be a true frequency representation of the first T/2 seconds of the signal. Repeated translations, or shifting of the window, to other locations within the signal, results in a time-frequency representation of the signal. Because the transform is a function of both time and frequency, it can be plotted as a two-dimensional map. Initial analysis of pressure fluctuations was performed by generating time-frequency plots using STFT.

Unfortunately, time-frequency plots generated by this method suffer from a resolution problem. STFT does not provide information regarding the time intervals in which certain frequency bands exist. As the selected window is of a finite length, the frequency resolution is limited by the size of the window. If an infinite length (size of the window) is selected, the time resolution is completely lost. This analytical drawback can be briefly summarized as:

1) Small window size results in low resolution in the frequency domain.
2) Large window size results in low resolution in the time domain.

Graps (1995) confirmed that STFT is an inaccurate and inefficient method of time–frequency localization, as it imposes a scale or 'response interval (period T)' into the analysis. For analyses where a predetermined scaling may not be appropriate because of a wide range of dominant frequencies, a method of time–frequency localization that is scale independent must be employed.

4.4 Multi-Resolution Analysis

Time and frequency resolution problems are the result of a physical phenomenon (the Heisenberg uncertainty principle) and exist regardless of the transform used. However, it is possible to analyze signals by using an alternative approach called **multi-resolution analysis (MRA)**. MRA is designed to give good time resolution, but low resolution in frequency determination at high frequencies. Good frequency resolution at low frequencies is achieved at the cost of resolution in time (Kumar and Georgiou-Foufoula, 1994; Graps, 1995).

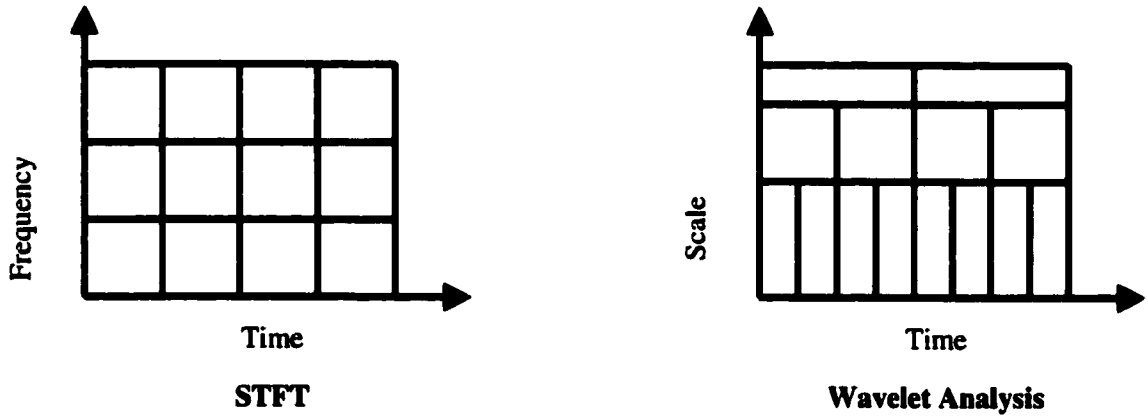

Figure 4.1: Comparison of Short Time Fourier Transform and Wavelet transform analysis.

4.4.1 Introduction to Wavelet Transforms

The wavelet transform is a tool that divides the data or functions into different frequency components and then analyzes each component with a resolution matched to its scale. A wavelet refers to a small wave, the reference to size (small) results from the condition that the window function or the analyzing wavelet is of finite length or is **compactly supported** (Kumar and Georgiou-Foufoula, 1994). The wave refers to the requirement that this function is oscillatory (Torrence and Compo, 1997).

Wavelets are functions that satisfy specific mathematical requirements in order to represent signals or other functions. Wavelet transforms adopt a wavelet prototype basis function, named the analyzing wavelet or the mother wavelet, for analyzing uni-variate and multi-variate signals. The term **mother** implies that the functions with different support lengths used in the transformation process are derived from one main function, or

the mother wavelet. In other words, the mother wavelet is a **prototype** for generating the other window functions.

The analysis in the time domain is performed with a contracted, high frequency version of the prototype wavelet while frequency analysis is performed with a dilated, low frequency version of the same wavelet. Because the original signal can be represented in terms of a wavelet expansion, using coefficients in a linear combination of wavelet functions, data operations can be performed by applying only the relevant wavelet coefficients.

4.4.2 Mathematical Definition of the Wavelet Transform

The wavelet transform is defined on the basis of a family of analyzing wavelets, $\psi_{a,b}(t)$, that are generated by varying the dilations or scales, a, and translations, b, from a mother wavelet, $\psi(t)$ (Kumar and Georgiou-Foufoula, 1994), as:

$$\psi_{a,b}(t) = \frac{1}{\sqrt{a}}\psi\left(\frac{t-b}{a}\right) \tag{4.1}$$

Where $a > 0$, $-\infty < b < \infty$, and $\int_{-\infty}^{\infty}\psi(t)\,dt = 0$ (4.1.1)

and:

$\psi_{a,b}(t)$ = analyzing wavelet function.

a = wavelet scales

b = translations of the wavelet

$\psi(t)$ = mother wavelet function

The characteristic properties of all wavelet functions are:

1) Localization in space by having a sufficiently fast decay to ensure that the wavelet is not a sustaining wave.
2) Zero mean, giving the wavelet function a wiggle, or wave-like structure.

The wavelet transform of a time series X (t) is defined as:

$$\overline{X}(a,b) = \frac{1}{\sqrt{a}} \int_{-\infty}^{\infty} X(t)\, \psi^*\left(\frac{t-b}{a}\right) dt \qquad (4.2)$$

The asterisk superscript indicates the complex conjugate of the wavelet function. Hence, the wavelet transform takes a one-dimensional function of time and converts it into a two-dimensional function with variables for space or time and scale (or frequency).

In practical applications, wavelets can be conveniently discretized by setting $a=2^s$ and $b = \tau 2^s$ in octaves where s and t are integers (Chui, 1992). Then the wavelet transform for the time series X(t) becomes:

$$\overline{X}(s,\tau) = \frac{1}{\sqrt{2^s}} \int_{-\infty}^{\infty} X(t)\, \psi^*\left(\frac{t}{2^s} - \tau\right) dt \qquad (4.3)$$

The variables s and τ are integers that scale and dilate the mother function ψ (t) to generate wavelets, such as the Daubechies wavelet family (Daubechies, 1992). The scaling index, s, indicates the width of the wavelet and the local index, τ, gives its position in space.

In order to analyze data at different resolutions, the analyzing wavelets are used in a scaling equation whose coefficients are obtained from solutions of higher order polynomials. It is helpful to think of these coefficients as filters. The coefficients are placed in a transformation matrix (cascade algorithm) and applied to the collected data. The coefficients are ordered using two dominant patterns, one that works as a smoothing filter (wavelet coefficients) and the other that brings out the detail (scaling coefficient).

Both Fourier transforms and wavelet transforms can be interpreted as a rotation in function space transforming the input time domain to a different domain. In the case of the fast Fourier transform (FFT) analysis, the new domain, frequency, has basis functions, which are the familiar sine and cosine functions.

The parameter **scale** in the wavelet analysis is similar to the scale used in geographical maps. As in the case of maps, high scales correspond to a non-detailed global view (of the signal), while low scales correspond to a detailed view. Similarly, in terms of frequency, low frequencies (high scales) correspond to a global description of a

signal, usually spanning the entire signal, whereas high frequencies (low scales) correspond to detailed information on a hidden pattern in the signal, usually lasting for a relatively short time. The conventional approach in wavelet based signal processing is to refer to signal occurrence as consequency. However, in this research the signal occurrence is referred to as frequency.

4.5 Classification of Wavelets

4.5.1 Orthogonal and non-orthogonal wavelets

In orthogonal wavelet analysis, the number of convolutions at each scale is proportional to the width of the wavelet basis at that scale. This produces a wavelet spectrum that contains discrete "blocks" of wavelet power, useful for signal processing, in that it gives the most compact representation of the signal. Unfortunately, in time series analysis, an aperiodic shift in the time series produces a different wavelet spectrum. Conversely, a non-orthogonal analysis is highly redundant at large scales, where the wavelet spectrum at adjacent times is highly correlated. The non-orthogonal transform is useful for time series analysis where smooth, continuous variations in wavelet amplitude are expected.

4.5.2 Complex and real wavelets

A complex wavelet function will return information about both amplitude and phase and is better adapted for capturing oscillatory behavior. A real wavelet function returns only a single component and can be used to isolate peaks or discontinuities. For determining wavelet power spectra, the obvious choice is that of a complex wavelet. The Daubechies wavelet (D4) is a real pseudo-orthogonal wavelet while the Morlet wavelet is a complex non-orthogonal wavelet (Torrence and Compo, 1997).

4.5.3 Daubechies Wavelet Function

The wavelets proposed by Ingrid Daubechies (Daubechies, 1992) provide a compromise between smoothness and compact support. She determined the appropriate scaling coefficients by using the cascade algorithm. The Daubechies wavelet function (D4), for a time series t and scaling function ($\phi(t)$), can be derived from:

$$f(\phi(t)) = \frac{1+\sqrt{3}}{4}(\phi(2t)) + \frac{1-\sqrt{3}}{4}(\phi(2t-1)) + \frac{3+\sqrt{3}}{4}(\phi(2t-2)) + \frac{3-\sqrt{3}}{4}(\phi(2t-3)) \quad (4.4)$$

The wavelet function, D4, is graphically shown on **Figure. 4.2.**

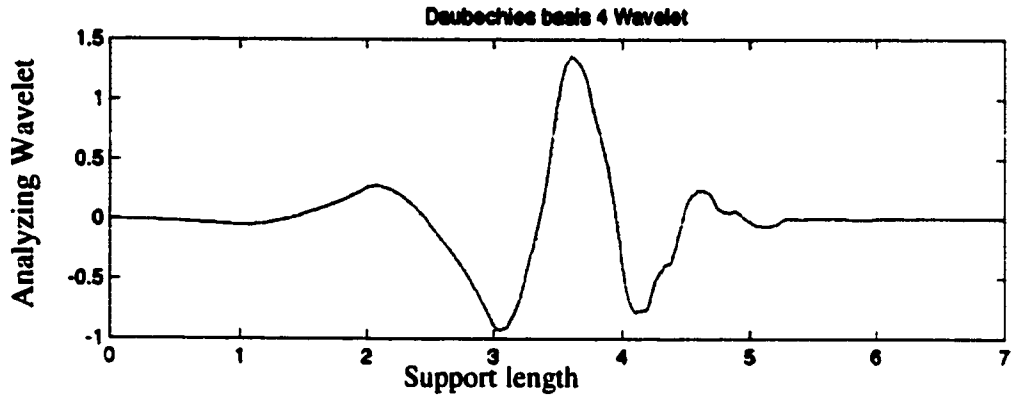

Figure 4.2: Daubechies (D4) wavelet (analyzing function) as a function of support length.

4.5.4 Morlet Wavelet

The Morlet wavelet consists of a plane wave modulated by a Gaussian. For a time series, x_n, with equal time spacing, dt, the Morlet wavelet function (ψ_0) that depends on a non-dimensional time parameter (η) is represented by the following equation:

$$\psi_0 = \pi^{-1/4} e^{i\omega_0 \eta} e^{-\eta^2/2} \quad (4.8)$$

where ω_0 is a non-dimensional frequency and i is a complex number.

Torrence and Compo (1997) concluded that $\omega_0 = 6$ satisfied the admissibility function. The Morlet wavelet function is shown graphically on **Figure 4.3.**

From the above discussion, it is observed that Daubechies (D4) wavelets are used for plotting time-scale plots (scalogram) to detecting discontinuities in signal fluctuations. Therefore, D4 wavelets are localized in time. For characterizing the pressure fluctuations the frequency of the fluctuations is also required. For this work, power spectral plots of pressure fluctuations are developed using Morlet ($\omega_0 = 6$) wavelets.

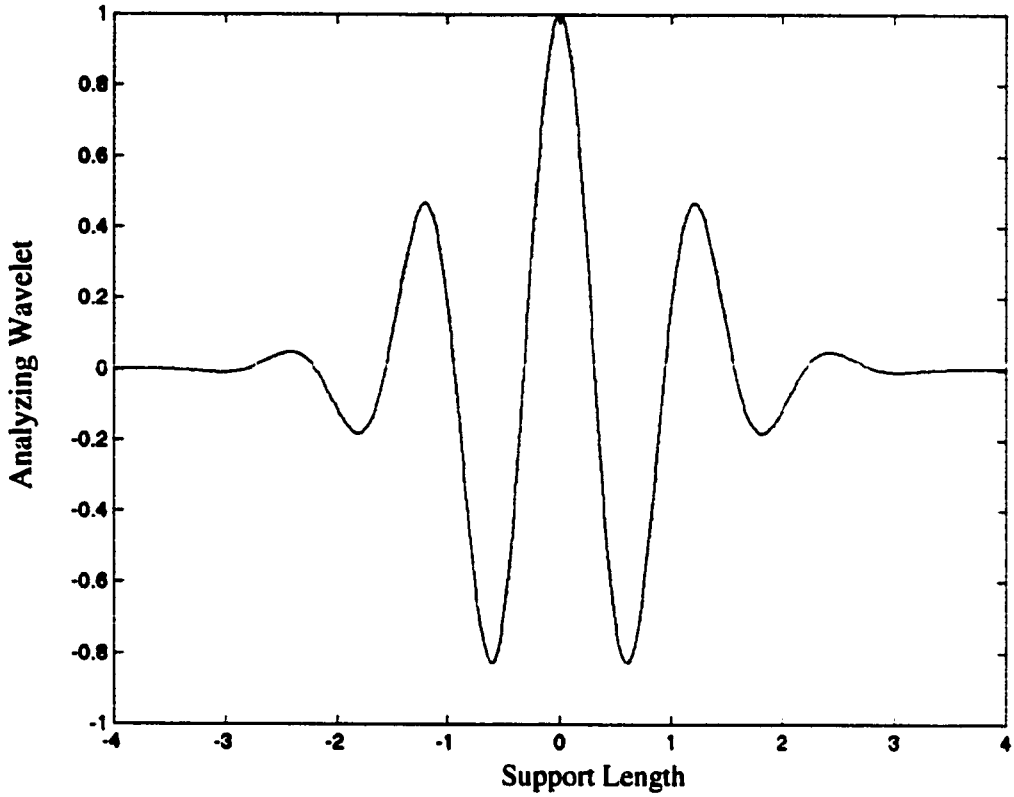

Figure 4.3: Morlet wavelet (analyzing function) as a function of support length.

4.6 Software Implementation

Software programs for analyzing both discontinuities and wavelet power spectra were developed using MATLAB. Fourier transform analysis was applied to collected pressure data to determine the frequency content of the signal.

1) The suggested analysis approach (Torrence and Compo, 1997) for characterizing fluctuating data is to normalize the data by standard deviation prior to wavelet transformation. Further analysis to determine the discontinuities in the signal is then carried out by analyzing the continuous wavelet transforms with D4 wavelets. Scalograms (or time-scale plots) are generated for the signal data. The wavelet toolbox supplied with MATLAB software is used for calculating the scalograms.

2) As reported in recent research (Lewalle, 1994, 1997, 1998; Torrence and Compo, 1997), wavelet spectra are developed to generate time-frequency plots and time-period plots using Morlet wavelets. The wavelet spectra give information on the relative power at a certain scale and a certain time.

3) Also, since Morlet is a complex wavelet, a phase or amplitude plot shows the

actual oscillation of the individual wavelets, rather than just their magnitude.
Using this approach, a comprehensive analysis of the signal is carried out simultaneously in the time and frequency domains.

A phased approach has been adopted to analyze signals by the proposed methods. Programmatically generated data are initially analyzed to evaluate the developed software. Experimental data from baseline experiments, discussed in chapter three, is then analyzed. Finally, these methods are applied to two-phase pattern recognition experiments.

4.6.1 Sample Analysis-Pure Sine Wave

The software developed for analyzing wavelets was first examined on sample data sets generated using MATLAB. Preliminary test results for a sine wave of 4 Hz. generated for 8 seconds and sampled at 32 Hz. are demonstrated with the procedure described above. The analyzed results are plotted stepwise on **Figures 4.4.1 to 4.4.6.**

1) A pure sine wave of 4 Hz., generated programmatically, is shown on **Figure 4.4.1.**
2) **Figure 4.4.2** shows the power spectrum computed by FFT analysis. A signal frequency of 4 Hz. is confirmed.
3) Wavelet spectra for the signal on time-period plots using Morlet wavelet (ω_0=6) are computed and plotted on **Figure 4.4.3.** The time-frequency wavelet spectrum, shown on **Figure 4.4.4,** demonstrates the differences between time and frequency domain analysis.
4) The wavelet phases are plotted on **Figure 4.4.5** to determine the actual oscillation of the individual wavelets.
5) To detect variations in the signal, the signal is analyzed using continuous wavelet transforms (Daubechies D4 wavelets). **Figure 4.4.6** shows the scalogram for the signal treated in this way.

Figures 4.4.1 to 4.4.6 clearly show that the wavelet analysis approach is capable of identifying the 4 Hz. signal and also traces its oscillations. In the event of a discontinuity, the oscillations of the waveform would change and the time at which a discontinuity occurs would be identified.

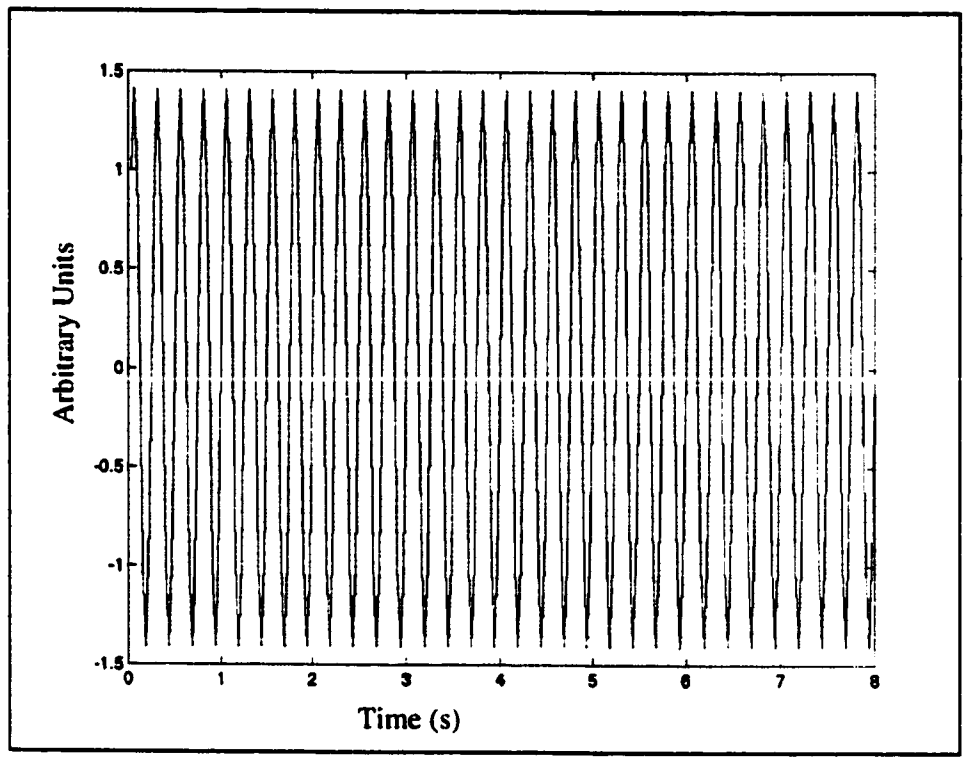

Figure 4.4.1: Programmatically generated sine wave of 4 Hz.

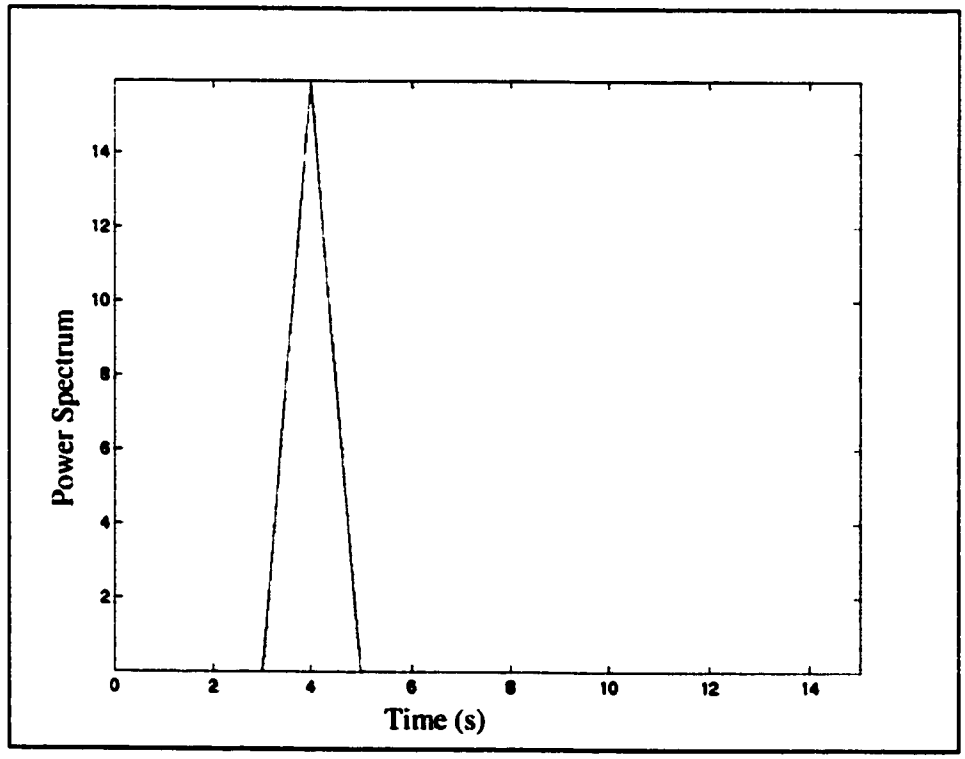

Figure 4.4.2: Spectral analysis (Fourier) for sine wave.

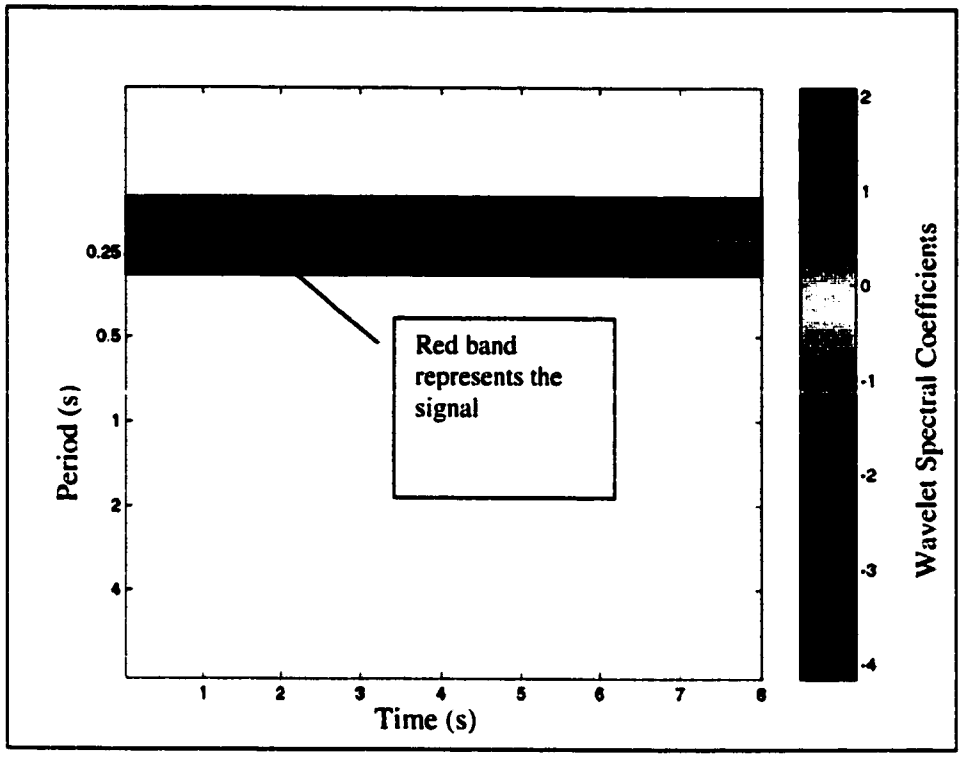

Figure 4.4.3: Morlet wavelet spectra on time-period axes for sine wave.

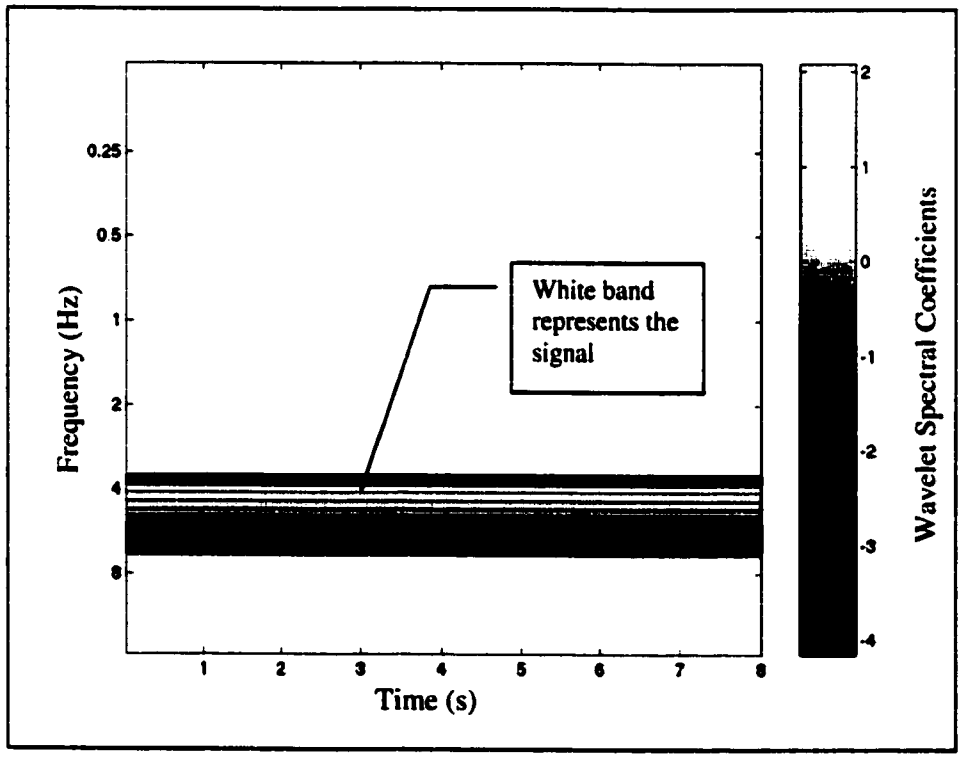

Figure 4.4.4: Morlet wavelet spectra on time-frequency axes for sine wave.

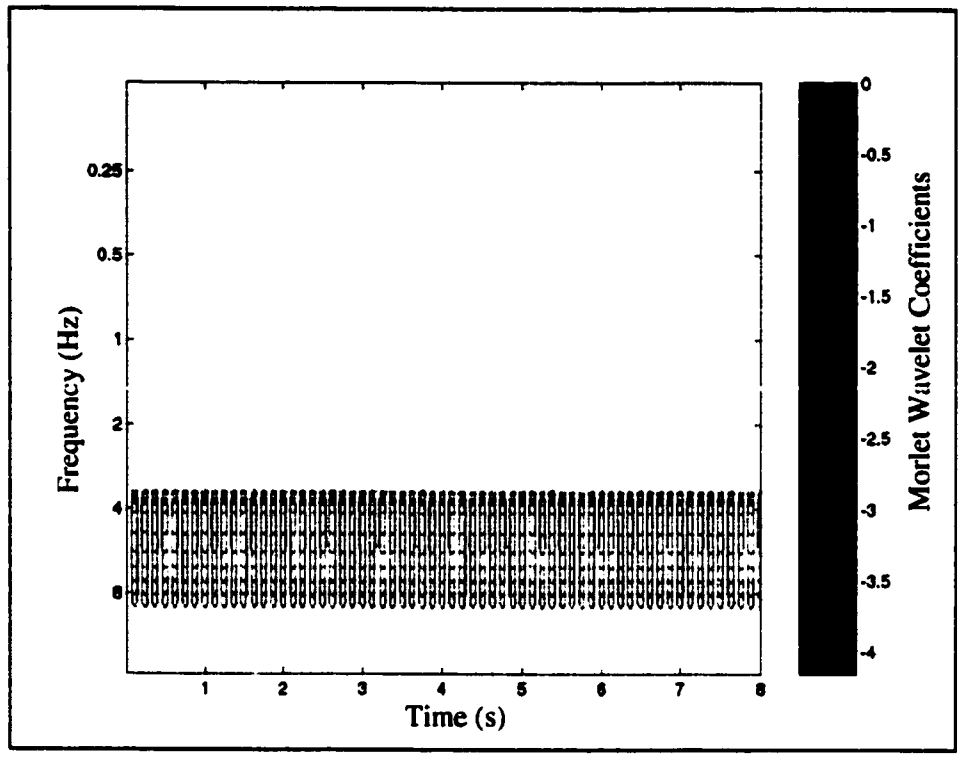

Figure 4.4.5: Wavelet phase plot on time-frequency axes for sine wave.

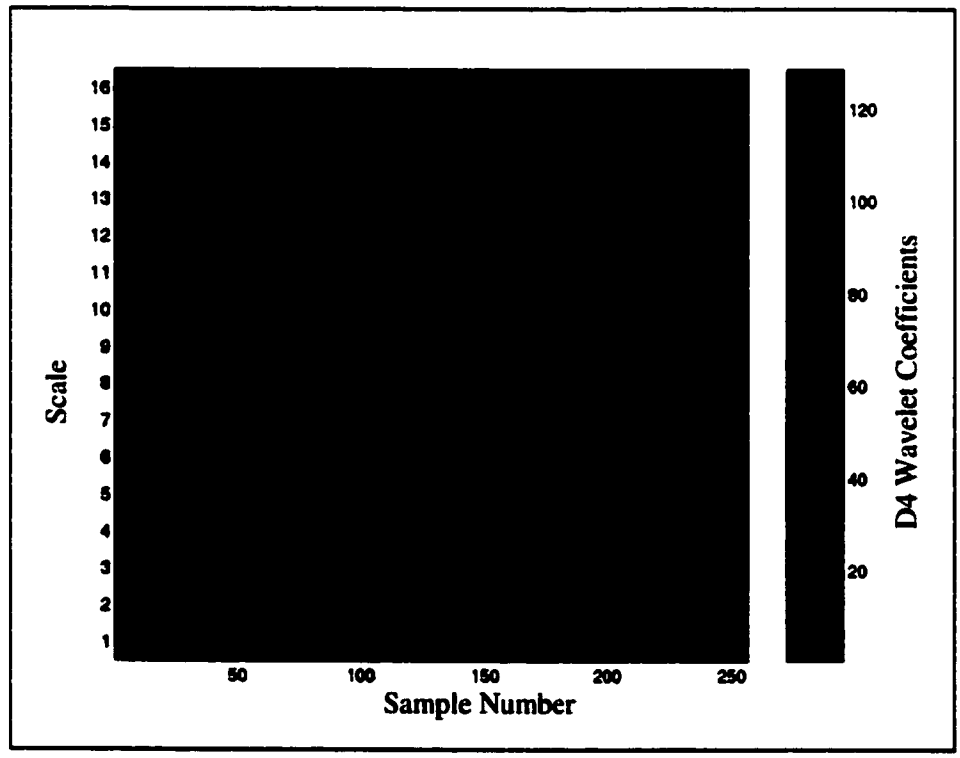

Figure 4.4.6: Continuous wavelet transform using D4 wavelets shows no discontinuities are present in the time domain.

4.6.2 Sample Analysis—Two-Frequency Data

A similar analysis was carried out on a two-frequency signal generated programmatically. The signal consists of two consecutive sine waves of 2 Hz. and 25 Hz. The objective of analyzing this signal is to confirm that the applied methods identify the location in the time domain at which the discontinuity occurs and simultaneously detects the two frequencies. The signal is sampled at 512 Hz. The results demonstrate the advantages of wavelets over Fourier transforms for analyzing non-stationary signals. The analysis procedure is followed stepwise and results are reported on **Figures 4.5.1 to 4.5.6**.

1) A pure sine wave of 2 Hz, followed by a sine wave of 25 Hz., generated programmatically, are shown on **Figure 4.5.1**.
2) **Figure 4.5.2** shows the power spectrum computed by FFT analysis confirming signal frequencies of 2 Hz. and 25 Hz. However, the location in the time domain when the change in frequency occurs cannot be predicted from the Fourier power spectrum.
3) Wavelet spectra for both time-period plots and time-frequency plots using Morlet wavelet (ω_0=6) are computed and plotted on **Figure 4.5.3 and 4.5.4**. These plots clearly represent the frequency band in which the two frequencies occur and simultaneously show the location in the time series where the change in frequency occurs.
4) The wavelet phases are plotted in **Figure 4.5.5** to determine the actual oscillation of the individual wavelets.
5) The discontinuity in the signal frequency is detected by similar analysis with continuous wavelet transforms (Daubechies D4 wavelets). **Figure 4.5.6** shows the signal scalogram obtained in the same way.

The change in frequency in the programmatically generated time series is analogous to a single discontinuity or a pulsation in a dynamic pressure signal. These tests on programmatically generated data show that the software developed identifies both frequency bands and time series variations.

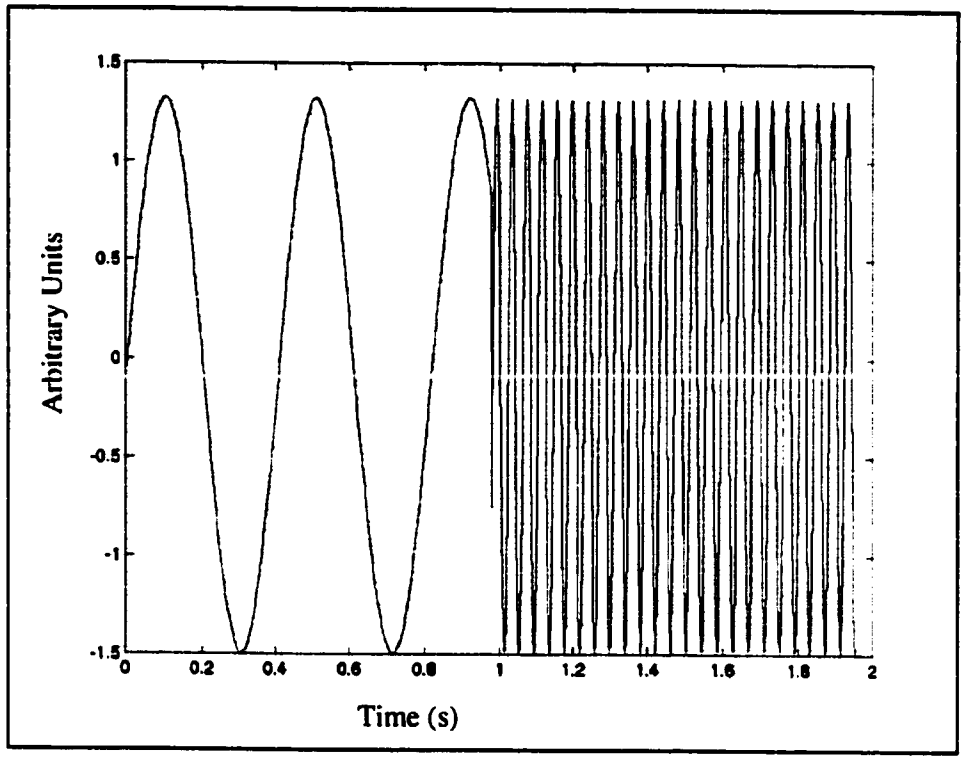

Figure 4.5.1: Programmatically generated two-frequency wave of 2 Hz. and 25 Hz.

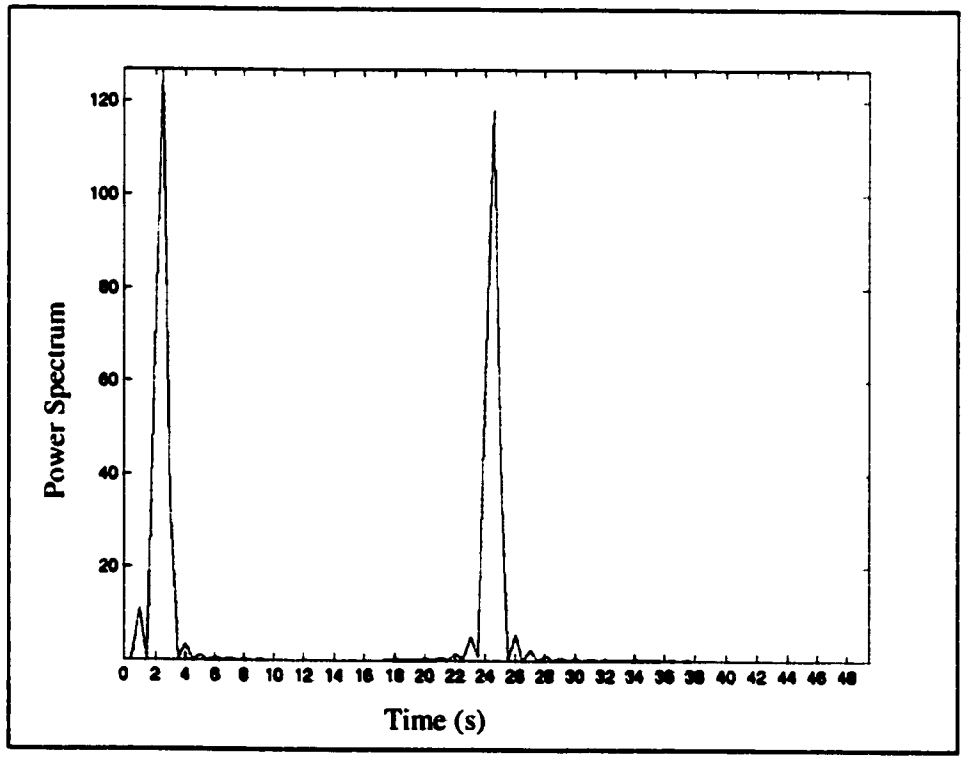

Figure 4.5.2: Spectral analysis (Fourier) for two-frequency wave.

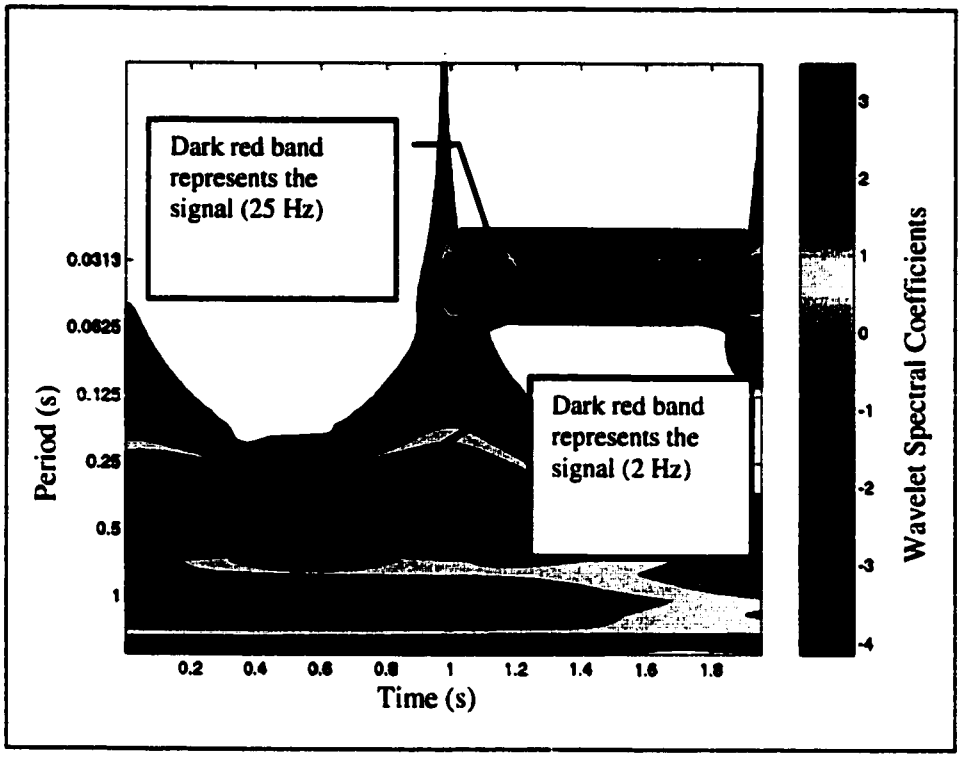

Figure 4.5.3: Morlet wavelet spectra on time-period axes for two-frequency wave.

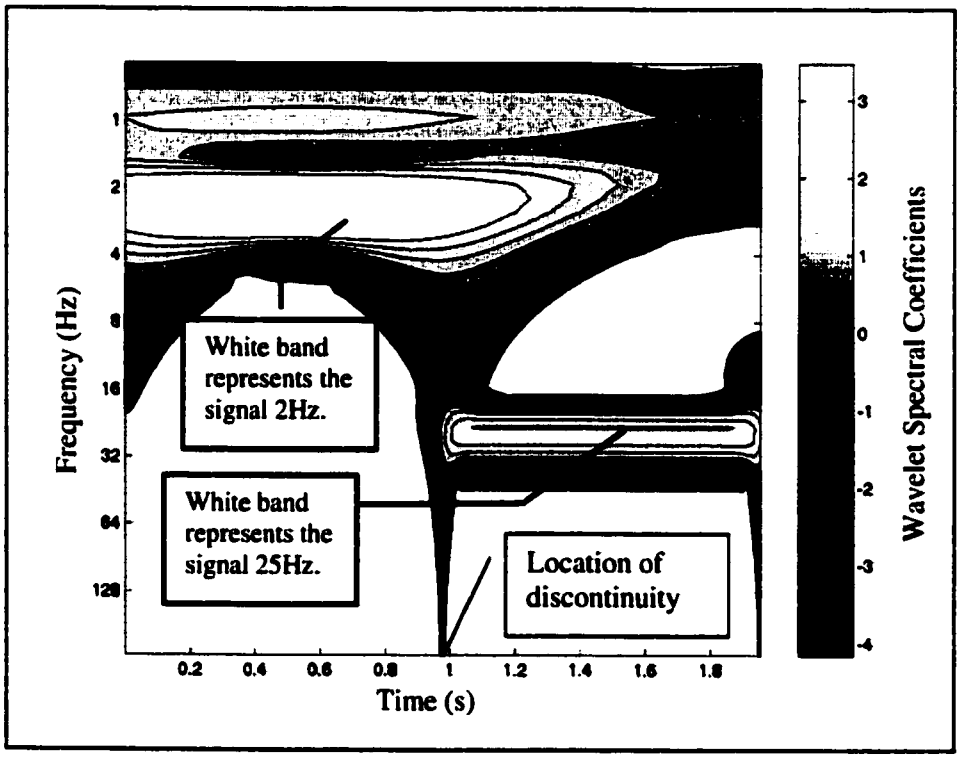

Figure 4.5.4: Morlet wavelet spectra on time-frequency axes for two-frequency wave.

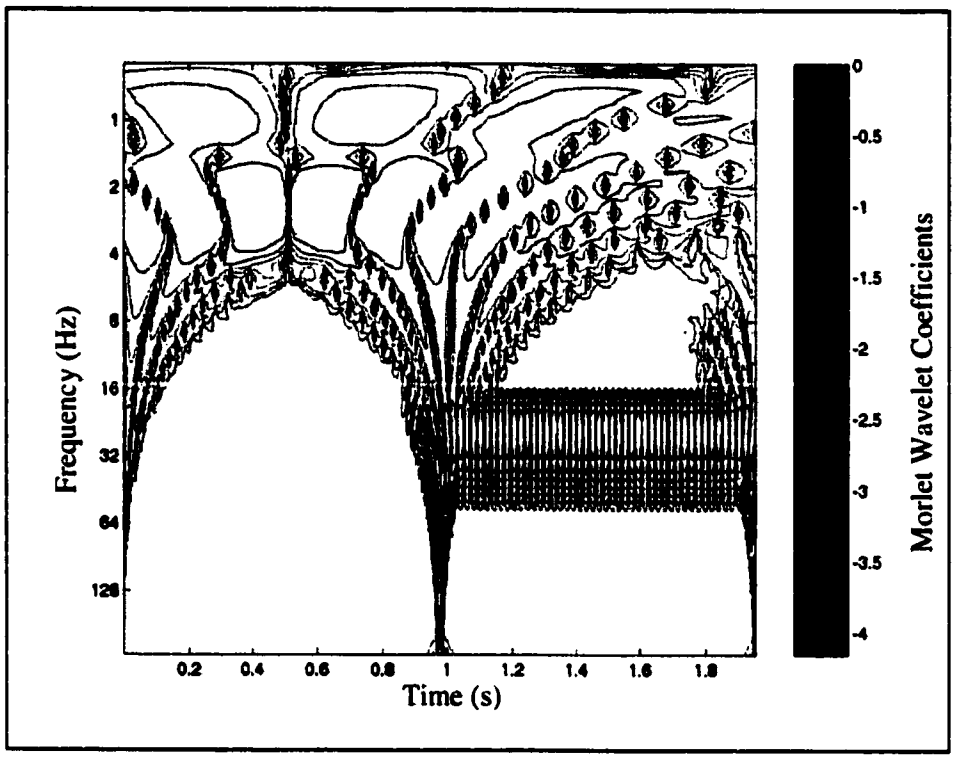

Figure 4.5.5: Wavelet coefficients on time-frequency plot.

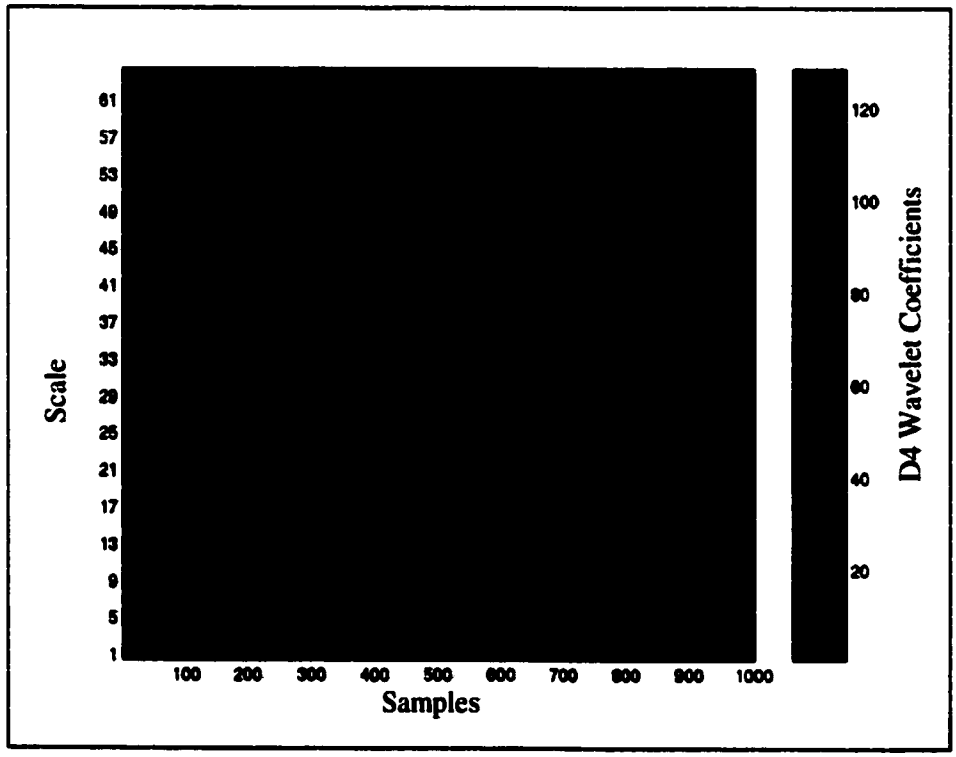

Figure 4.5.6: CWT using D4 wavelets to compare discontinuities with figure 4.5.5.

4.6.3 Baseline System

The model data confirm the applicability of the signal processing method to detect fluctuations. These methods are further applied to known pressure fluctuations from the baseline system. Single-phase water pulsations were analyzed initially because the frequency was known from the experimental set-up. A regular pulse of water flow (452.8 L/h) was fed to the system at 222 rpm (~ 3.67 Hz.). The fluctuating pressure data were collected and analyzed by applying the wavelet analysis approach. Analyzed results for the dynamic pressure signal are shown on **Figures 4.6.1 to 4.6.6**. The analysis clearly shows the liquid pulsation rate in the 2 to 4 Hz. band. The regularity of the pulses and the absence of extraneous signals is also observed in the pressure data.

Two-phase tests were also conducted on the baseline system with an airflow of 56 L/min. (at 25°C) and pulsing water flow of 7.55 L/min. The analysis of the collected dynamic pressure signals from the two-phase system shows characteristic differences between a single-phase and a two-phase system. The introduction of a second compressible phase causes visible complexities in the pressure data. The analysis for the two-phase experiments with the baseline system is shown on **Figures 4.7.1 to 4.7.6**. From the plots, it is observed that, multiple frequency bands are introduced owing to the introduction of air into the system.

The analysis on the baseline system can be summarized as an evaluation procedure for validating the data acquisition and control system. The system also shows that the introduction of air into the system causes complex pressure fluctuations.

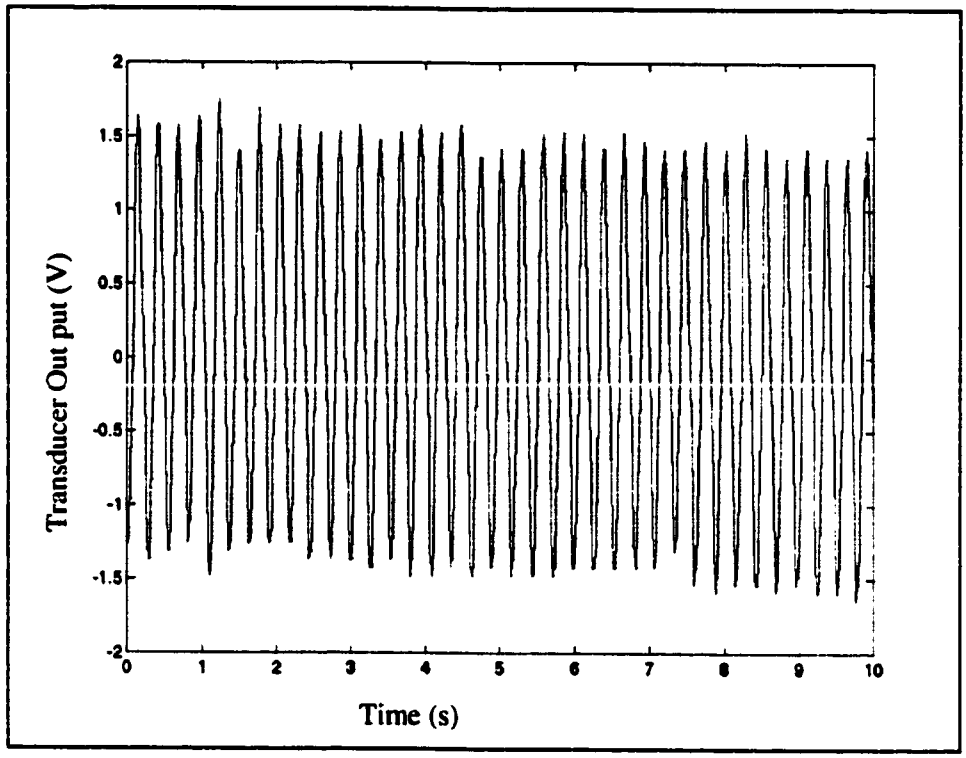

Figure 4.6.1: Single-phase (water) pressure variation in baseline system.

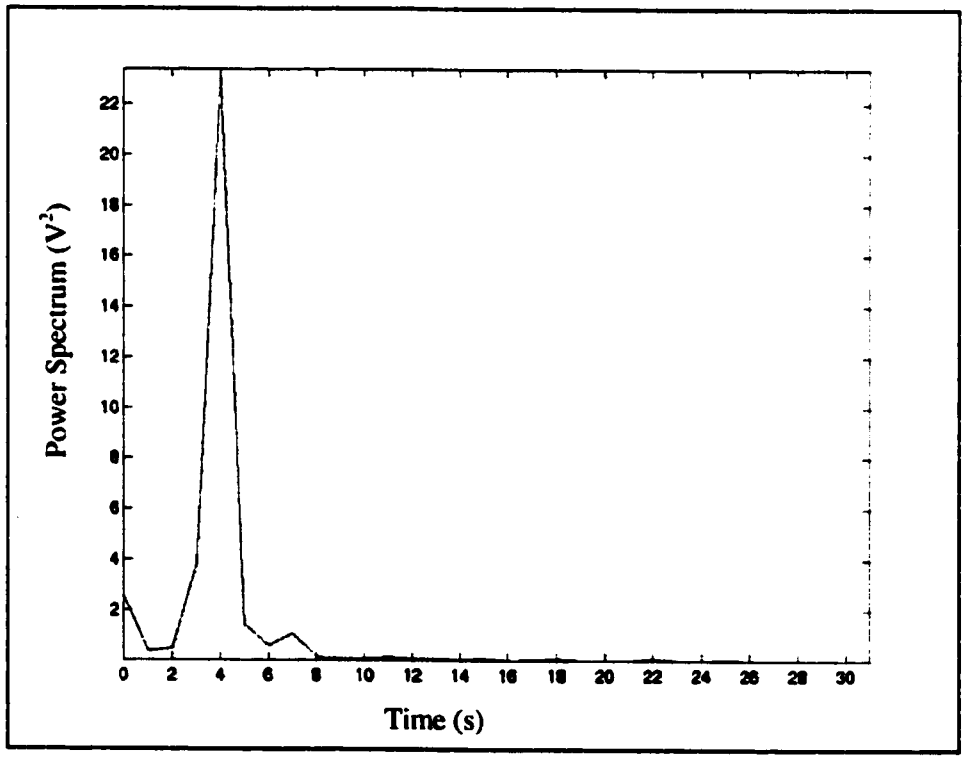

Figure 4.6.2: Spectral analysis (Fourier) for single-phase (water) pulsation induced in baseline system.

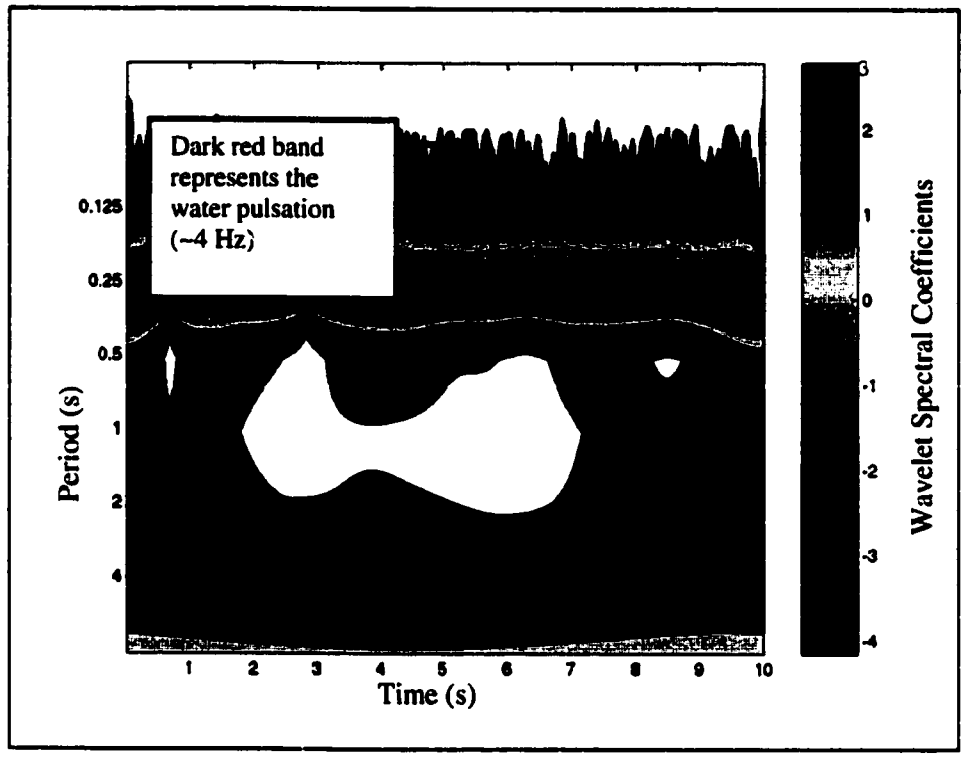

Figure 4.6.3: Morlet wavelet spectra on time-period axes for single-phase flow pulsation in baseline system.

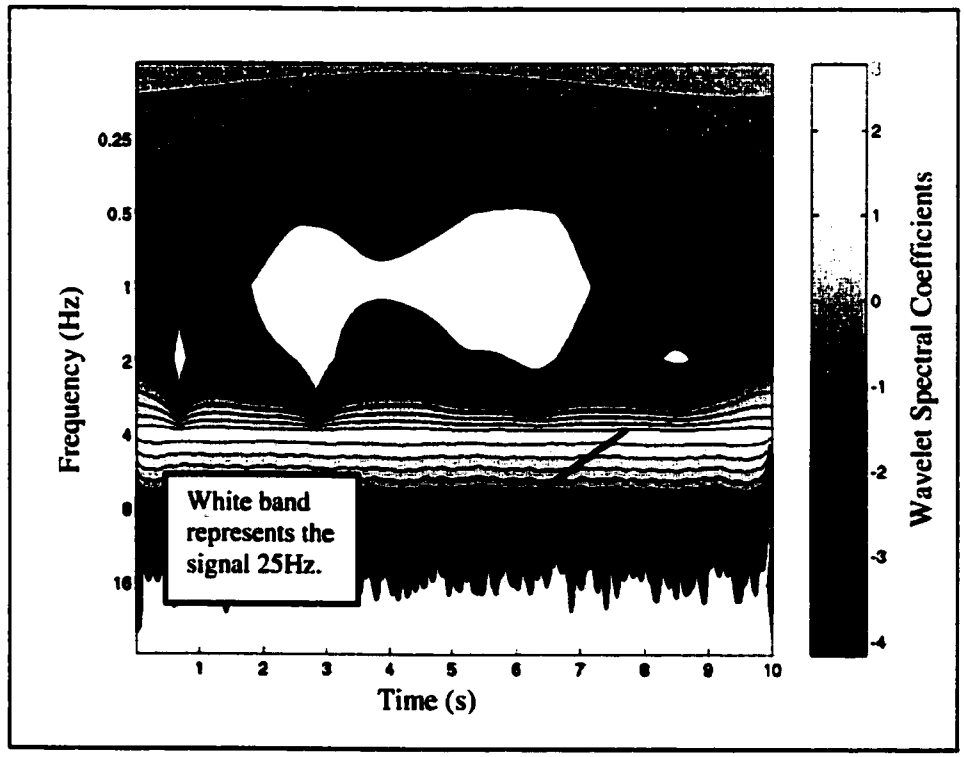

Figure 4.6.4: Morlet wavelet spectra on time-frequency axes for single-phase flow pulsation in baseline system.

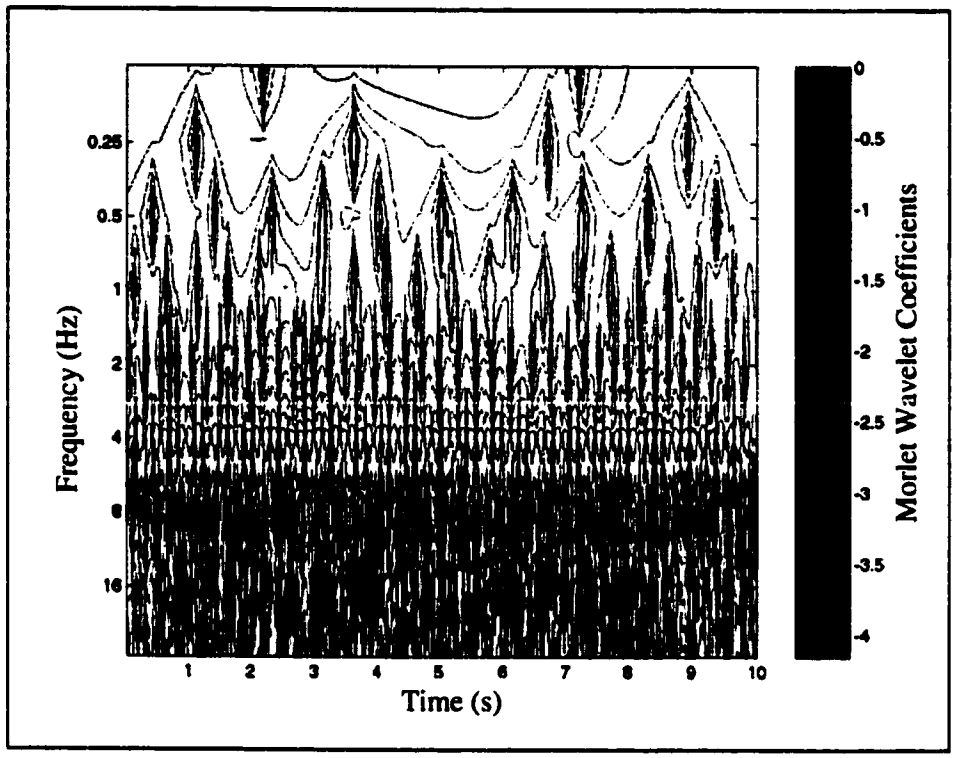

Figure 4.6.5: Wavelet phase plot on time-frequency axes for single-phase flow pulsation in baseline system.

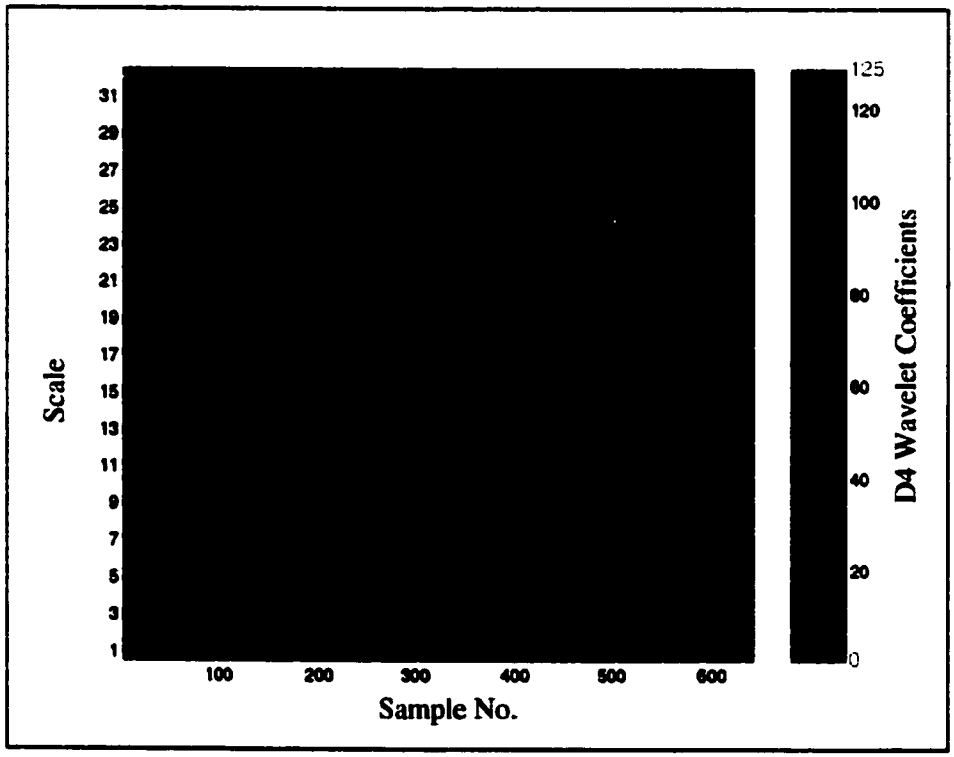

Figure 4.6.6: Continuous wavelet transform using D4 wavelets to detect variation for single-phase flow pulsation in baseline system.

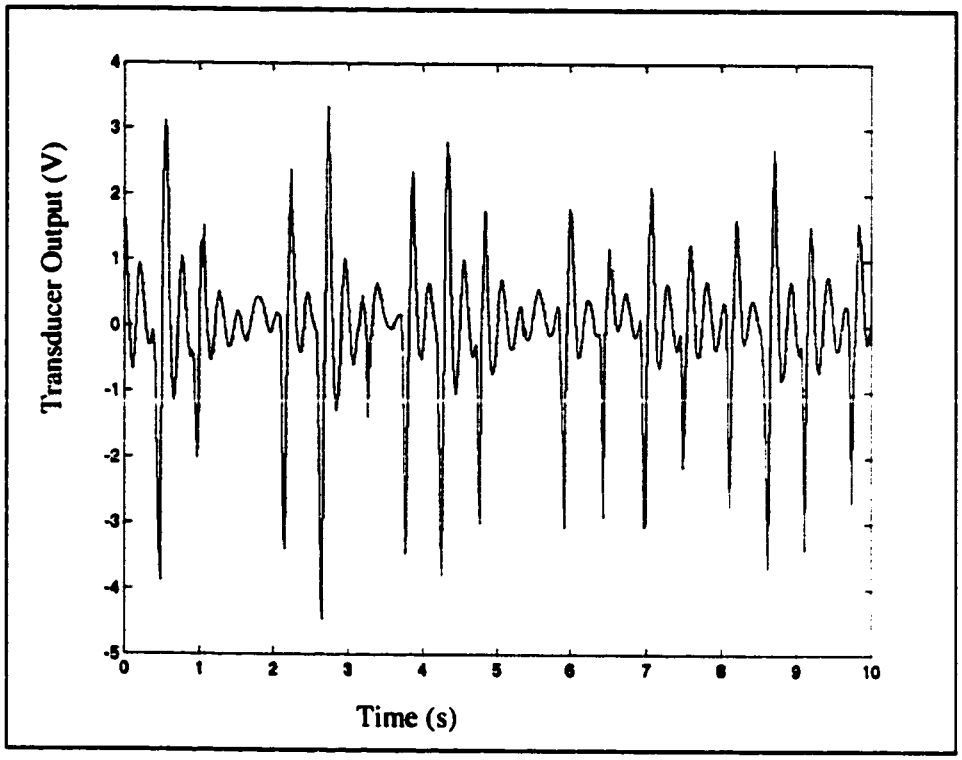

Figure 4.7.1: Air-water mixture pressure data for baseline system.

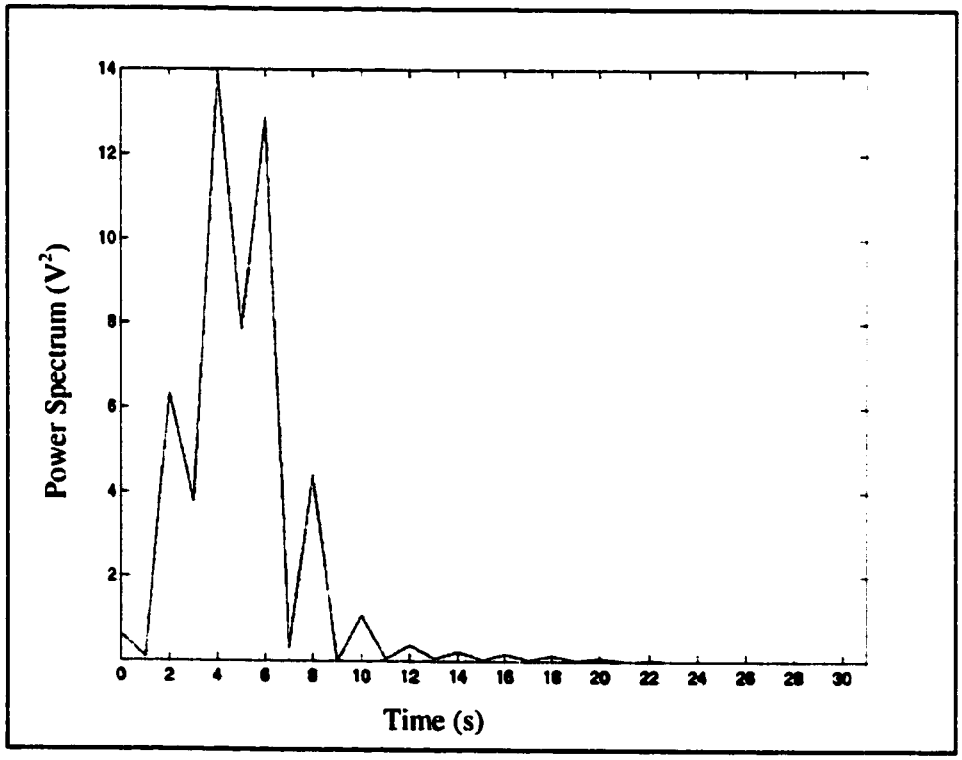

Figure 4.7.2: Spectral analysis (Fourier) for air-water pulsation induced in baseline system.

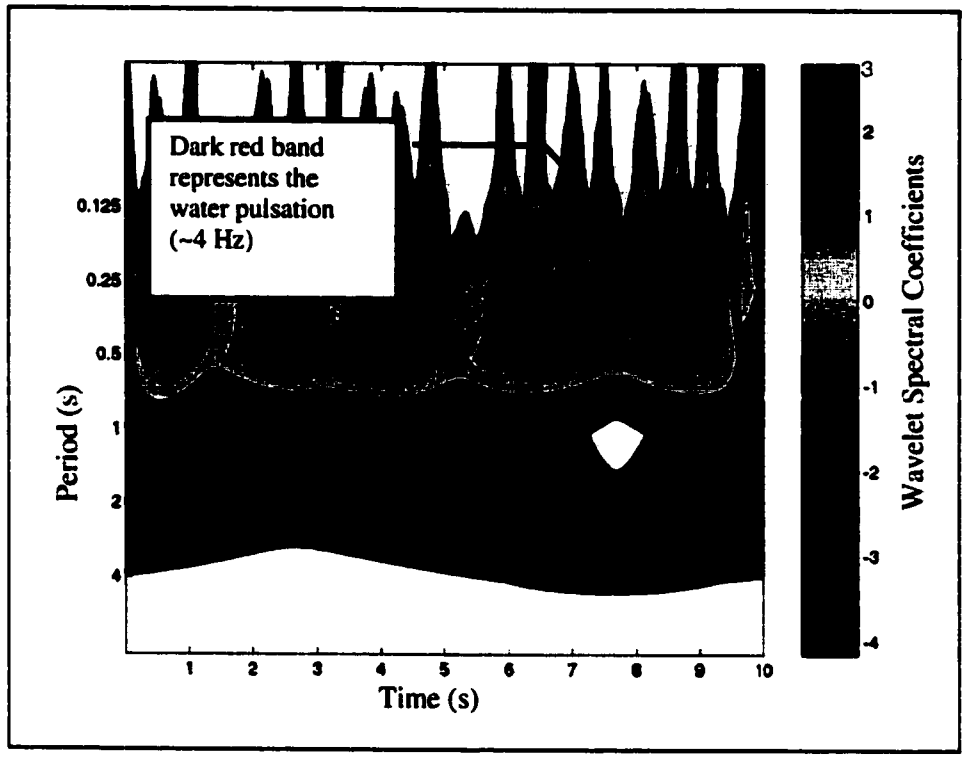

Figure 4.7.3: Wavelet spectra on time-period axes for air-water flow pulsation in baseline system.

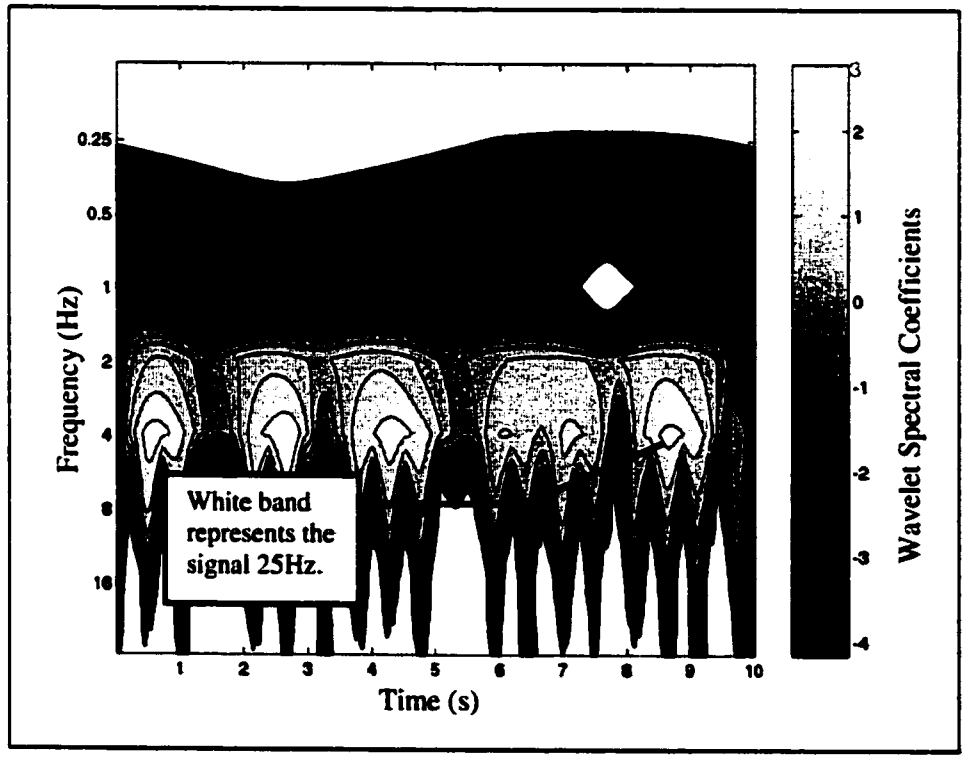

Figure 4.7.4: Wavelet spectra on time-frequency axes for air-water flow pulsation in baseline system.

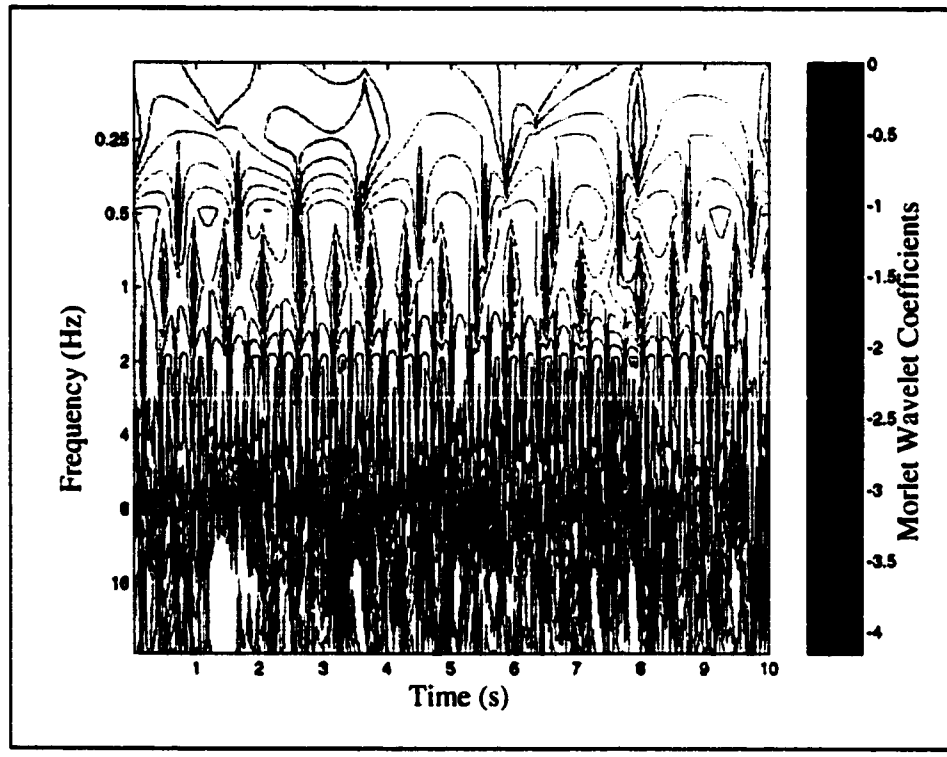

Figure 4.7.5: Wavelet phase plot on time-frequency axes for air-water flow pulsation in baseline system.

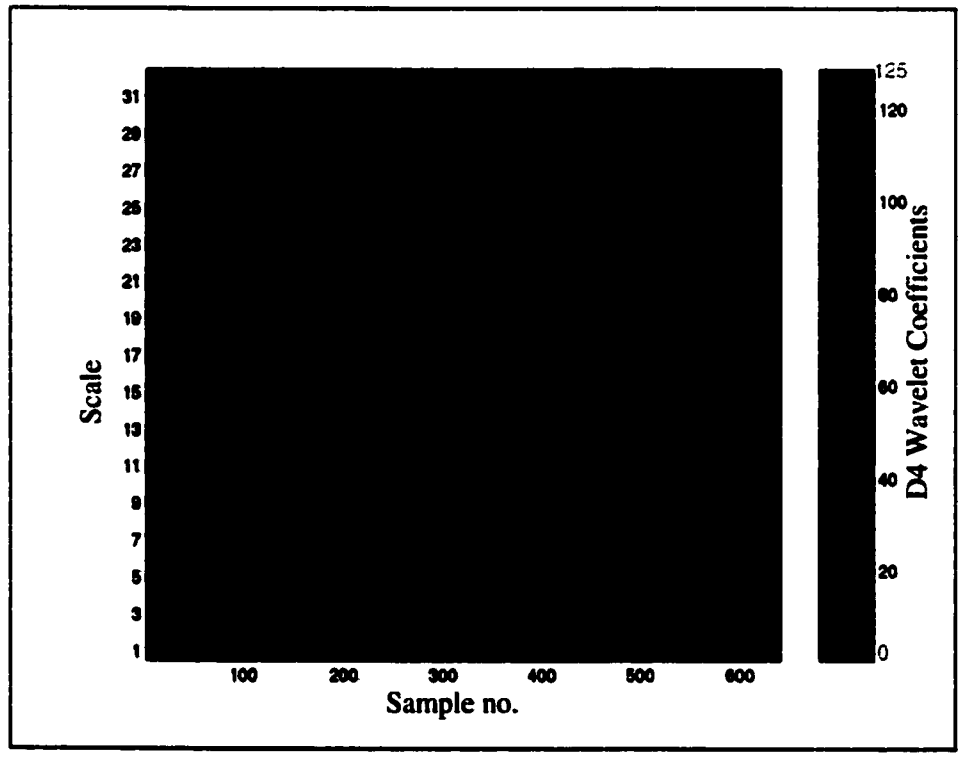

Figure 4.7.6: Continuous wavelet transform using D4 wavelets to detect variation for air-water flow pulsation in baseline system.

4.7 Discussion

The signal analysis for data generated both programmatically and with the baseline system provides a comprehensive means for analyzing steady (stationary) and transient (non-stationary) pressure or signal variations.

Analysis of baseline system experimental data leads to the following observations:

1) A single-phase pulsation pressure signal shows a regular or stationary signal.

2) The introduction of a compressible phase (air) creates irregularities or non-stationary signals in the pressure data. Hence, additional frequencies induced in the system need to be examined simultaneously. Distinct differences between single-phase and two-phase pulsation patterns are observed in the analyzed results. It should be observed that, besides detection of discontinuities, **Figure 4.7.6** could also be used for detection of similarities in the transient two-phase pressure pulsation.

Although, the Morlet wavelet function is more localized in the frequency domain, it is found to be fairly accurate in determining the location of pressure fluctuation peaks in the time domain. Further work in this research has been carried out using the Morlet wavelet basis function (Torrence and Compo, 1997) rather than the Daubechies wavelet code supplied with the MATLAB® Wavelet Toolbox.

Because, spectral intermittence can be studied by this novel approach to signal processing, the suggested methods are further applied for characterizing flow patterns.

Chapter Five

Results and Discussion

In this chapter, advanced wavelet spectral procedures are combined with the signal processing methods, described in chapter four, and applied to experimental data. The experimental data for flow pattern recognition, selected in chapter three compares distinctly visible flow patterns. These experimental conditions cover the three important flow regimes namely **annular, dispersed and slug regimes** that have been examined by most researchers in the field of flow pattern determination (Dukler and Taitel, 1986; Jones and Zuber, 1976).

Wavelet power contour plots and their spectral analysis results are shown for each experimental condition to demonstrate the applicability of the suggested methods. Applying wavelets to multiple consecutive intervals of pressure signal data circumvents limitations in developing contour-filled wavelet spectral energy maps.

The characteristics of two-phase flow patterns, discussed by various researchers in the past are compared with the current experimental results to interpret the spectral analysis plots.

5.1 Introduction to Wavelet Spectral Analysis

The recommendation of researchers in the field of wavelet analysis (Lewalle, 1994, 1998; Compo and Torrence, 1997) were considered for applying wavelet spectral analysis techniques to the wavelet spectral power/energy plots developed from the pressure data. Consequently, **Global Wavelet Spectrum and Scale-Averaged Wavelet Power** calculations were used in the current research for characterizing two-phase flow patterns.

5.1.1 Scale-Averaged Wavelet Power and Global Wavelet Spectrum

A global wavelet spectrum is the averaging in time of the spectral energy plot. If a vertical slice through a wavelet spectral plot can be considered to be a measure of the

local wavelet spectrum. Then the time-averaged wavelet spectrum over all the local wavelet spectra gives the **global wavelet spectrum:**

$$\overline{W}^2(s) = \frac{1}{N}\sum_{n=0}^{N-1}\left|W_n(s)\right|^2 \tag{5.1}$$

Where:

$\overline{W}^2(s)$ = Global wavelet spectrum coefficients,

N = Number of samples in time series,

$\left|W_n(s)\right|$ = Wavelet coefficients with respect to the number of samples N,

s = Number of scales.

The global wavelet spectrum is therefore analogous to the Fourier power spectrum because it averages the wavelet spectral plot in time and resembles a Fourier power spectrum. Several investigators (Lewalle, 1998, Graps, 1995) in this field are currently researching the analysis procedures for global or mean spectrum.

Similarly, to examine fluctuations in wavelet spectra over a range of scales or a frequency band, the **scale-averaged wavelet power** has been defined as the weighted sum of the wavelet power spectrum over the scales s_1 to s_2.

$$\overline{W}_n^2 = \frac{\delta_j \delta t}{C_\delta}\sum_{j=j_1}^{j_2}\frac{\left|W_n(s_j)\right|^2}{s_j} \tag{5.2}$$

Where:

$\overline{W}_n^2$ = Scale-averaged wavelet spectrum or power

$\left|W_n(s_j)\right|$ = Local scale-averaged wavelet spectral coefficients for scales s_j.

δ_j = Interval between the scales s_1 and s_2

δt = Time interval between samples.

C_δ = Empirically derived factor ($C_\delta = 0.776$ for Morlet's wavelet)

The scale-averaged wavelet power is therefore a time series of the average variance in a certain frequency band. Scale-averaged wavelet power shows the occurrence of fluctuations in power for a selected frequency band. The selection of the

frequency band is based on the global wavelet spectrum and a close examination of the contour-filled wavelet power plot.

5.2 Flow Pattern Recognition

Experimental data from the two-phase flow pattern recognition experiments is analyzed using this novel approach and relevant scale-averaged wavelet plots are developed for each condition.

5.3 Annular Flow Pattern Determination

Past research (Jones and Zuber, 1976) has confirmed that pressure fluctuations in the annular flow regimes are not definite in periodicity. This flow pattern requires a transient analysis approach for characterizing the two-phase flow pattern. Hence, the pressure fluctuations collected from experimental conditions in this flow pattern are useful for evaluation of the wavelet-based signal processing approach for two-phase flow characterization. Wavelet-based signal processing is applied to the pressure data for the **two conditions of annular flow** described in chapter three (refer to **Table 3.1**).

5.3.1 Exploratory Analysis for Annular Flow Pattern at Operating Condition 1

The measured pressure fluctuations for these flow conditions are shown on **Figure 5.1.1**. The corresponding contour-filled wavelet power plot, derived using Morlet's wavelet, is shown on **Figure 5.1.2**. Advanced spectral analysis is then applied to the wavelet energy/power plot. To examine the fluctuations in wavelet power, the global wavelet spectrum and the scale-averaged wavelet spectrum were calculated from the wavelet energy maps. The global wavelet spectrum was calculated by taking a vertical slice through the energy map and time averaging was carried out over the range of scales (< 512 Hz.). It provides the frequency band for calculating the scale-averaged wavelet power spectrum. From **Figure 5.1.2 and Figure 5.1.3 (a)**, it is clearly observed that the wavelet power is mostly in the frequency band of 1-16 Hz. **Figure 5.1.3 (b)** shows the scale-averaged wavelet power calculated over this frequency band. The global wavelet spectrum, an average of all the local wavelet spectra in time, is compared with the equivalent Fourier spectra in **Figure 5.1.4**. Both the wavelet spectra and Fourier power

spectra on this plot, show the pressure fluctuations possess a range of frequencies. This is in accord with Dukler's results for intermittent, including annular, flows that show sharp energy peaks at frequencies other than zero. To compare the modulations in pressure fluctuations for multiple 10-second time interval records of pressure data, consecutive data sets (3) are processed using this method and shown on **Figures 5.1.5 to 5.1.8**. The wavelet energy/spectral maps demonstrate the absence of periodicity in the signal as observed by Jones and Zuber (1976).

The wavelet power plots, shown on **Figures 5.1.2, 5.1.5, and 5.1.7** provide the spectral analysis for flow pattern recognition. Three consecutive pressure data sets have been analyzed to demonstrate the non-stationarity in the pressure fluctuations for this flow pattern. The spectral analysis of the wavelet power plots shows the transient nature of the pressure peaks. The different pressure data sets and corresponding plots for the Fourier and global or mean power spectrum are included in **Appendix C**.

Note: The units in the comparative spectral plots (**Figure: 5.1.4**) apply only to the Fourier spectra because wavelets are resizable functions that vary with frequency bands and do not represent absolute power.

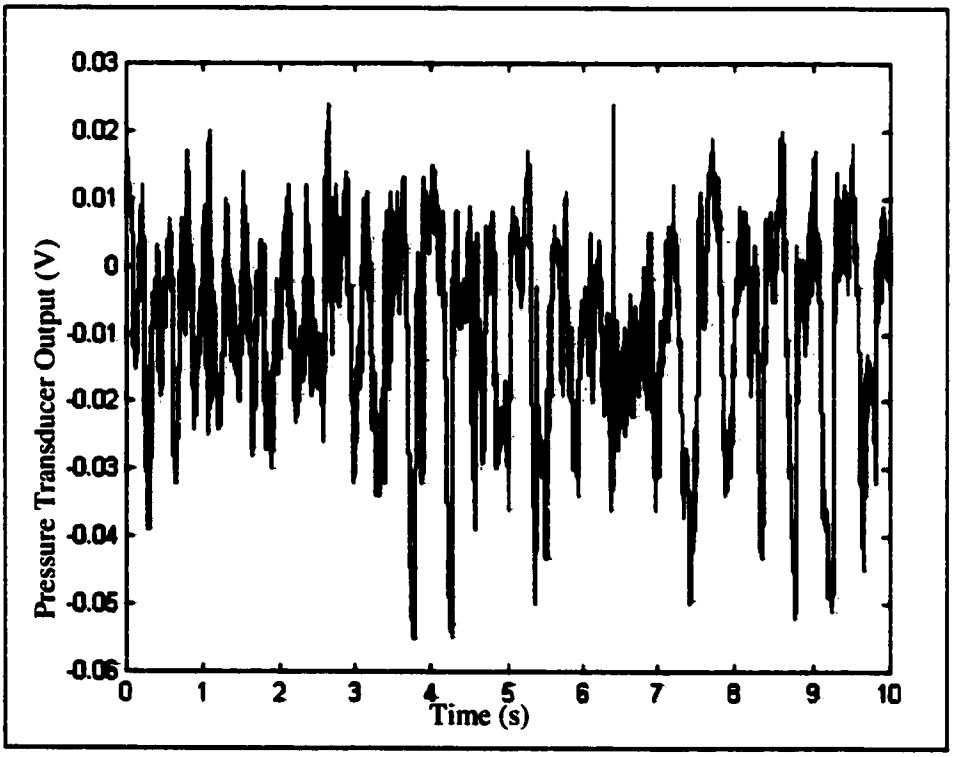

Figure 5.1.1: Pressure fluctuations in annular flow pattern at operating condition 1 for 0 ton 10 seconds.

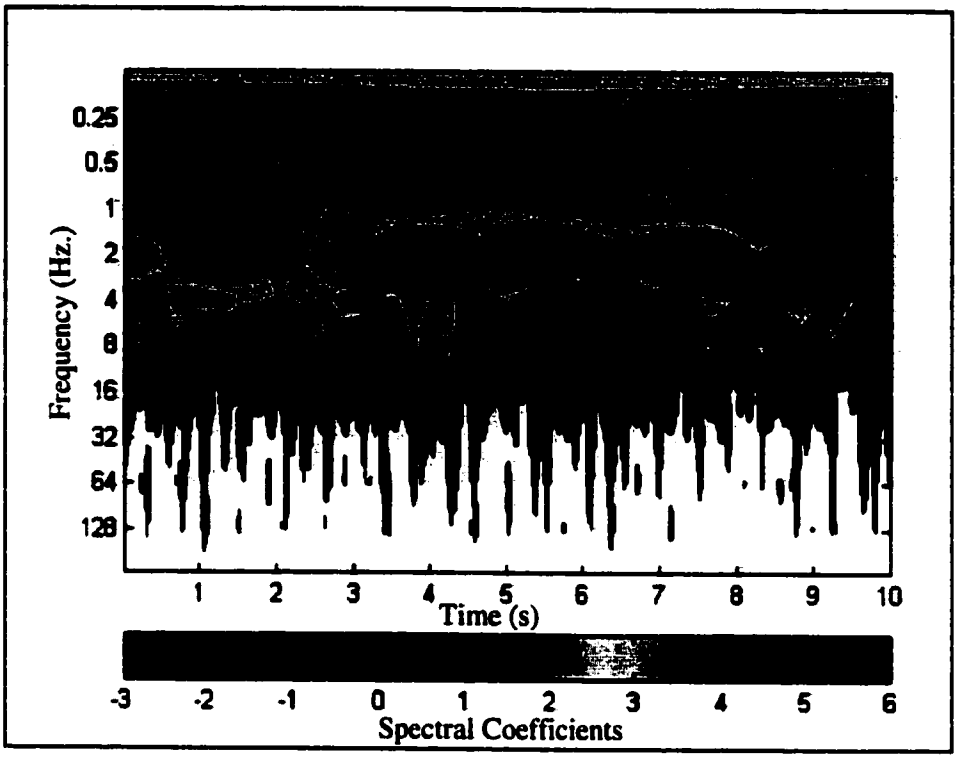

Figure 5.1.2: Morlet wavelet spectra on time-frequency axes at condition 1 from 0 to 10 seconds.

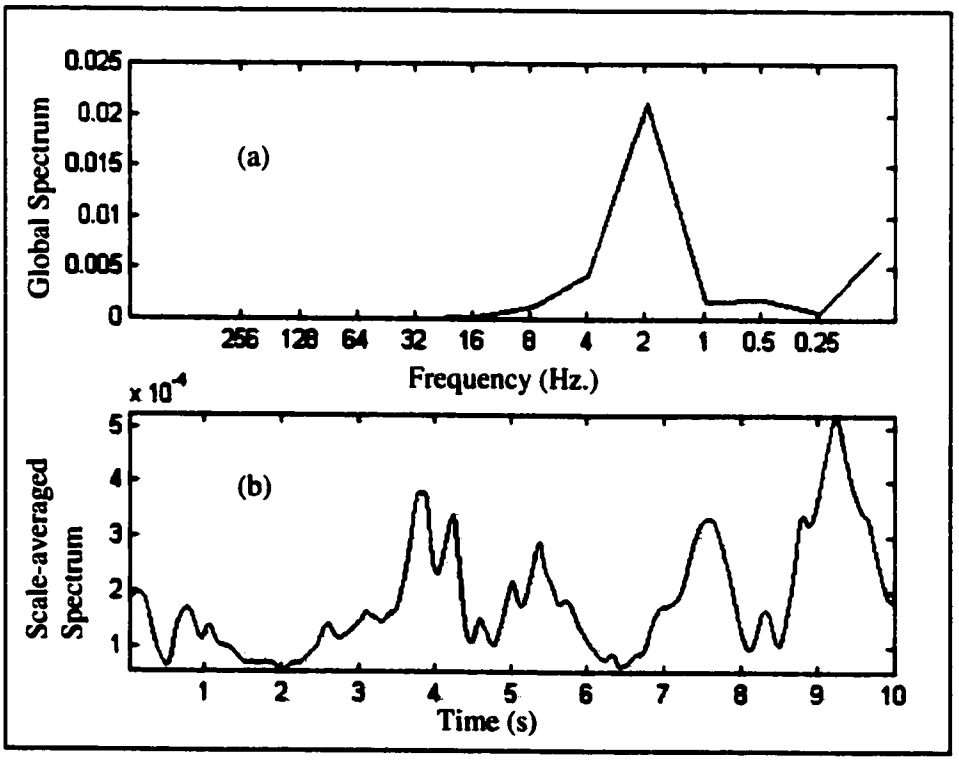

Figure 5.1.3: Morlet global spectra and scale-averaged wavelet spectra at condition 1 in the time interval from 0 to 10 seconds.

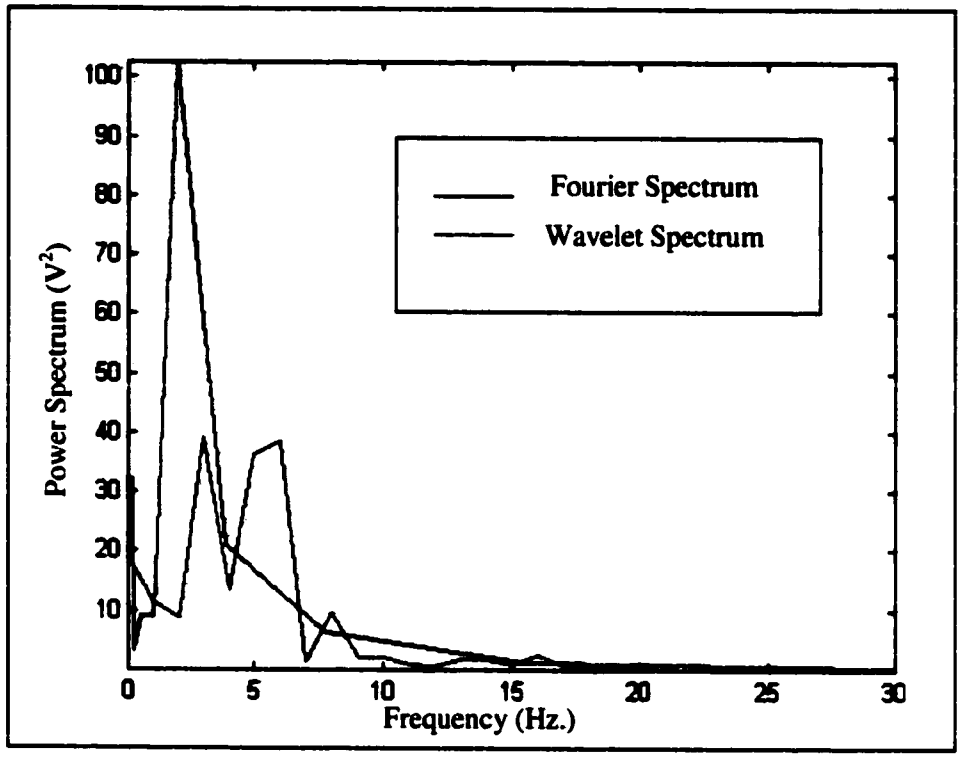

Figure 5.1.4: Comparison of wavelet spectra and power spectral analysis Fourier) for condition 1. The wavelet global spectrum is smoother due to averaging but peak location is within the frequency band.

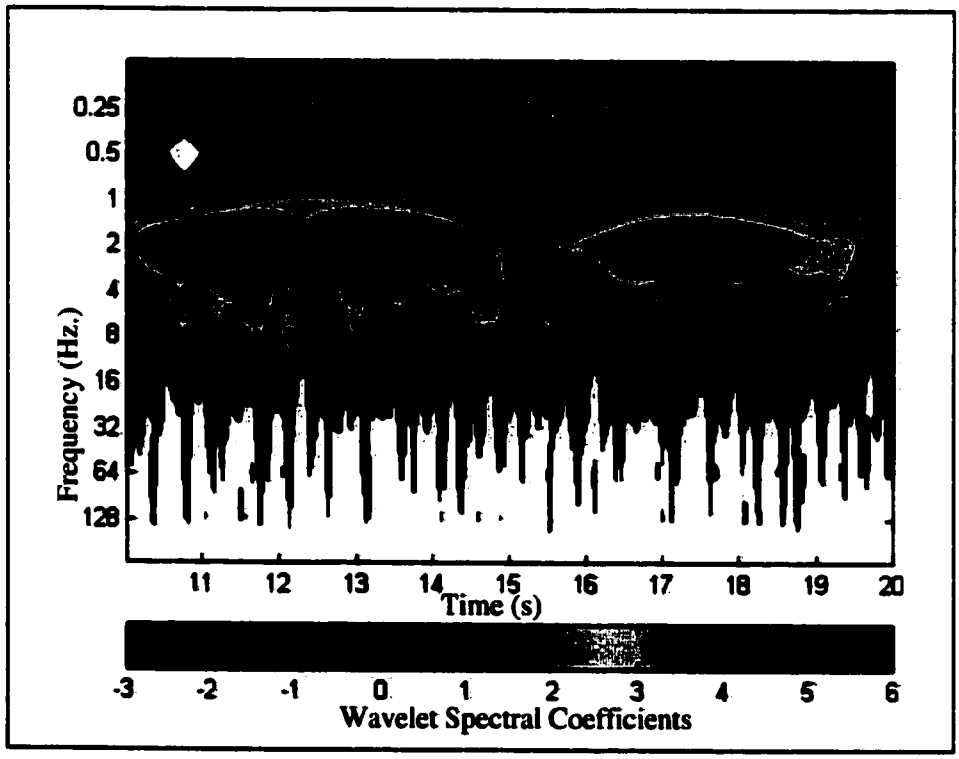

Figure 5.1.5: Wavelet spectra on time-frequency axes in time interval from 10 to 20 seconds at condition 1.

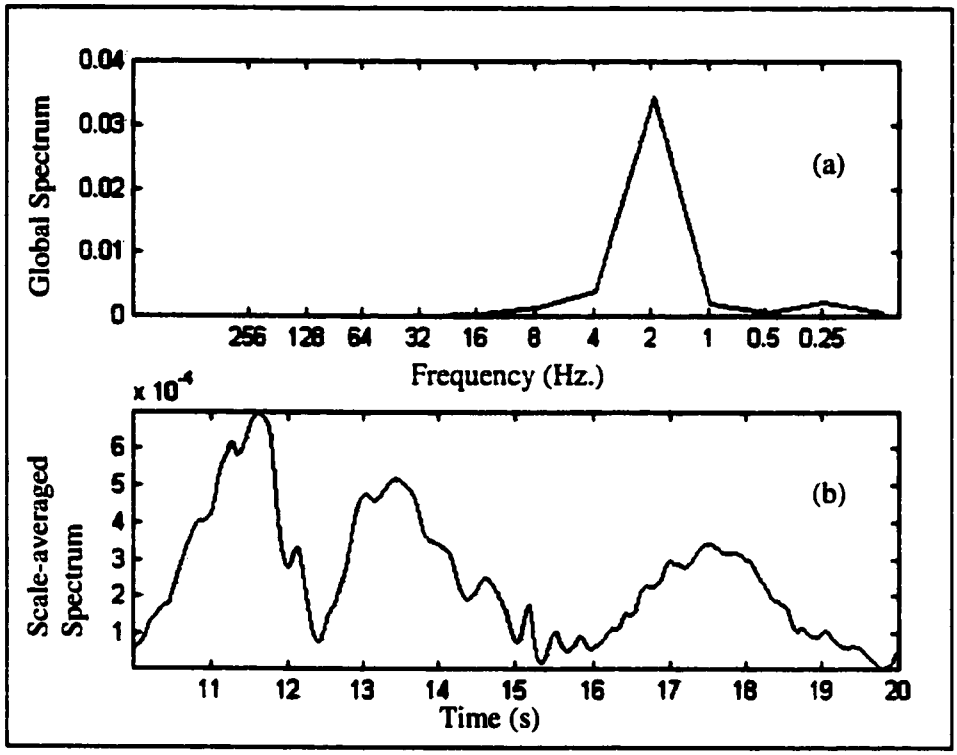

Figure 5.1.6: Global spectra and scale-averaged wavelet spectra for the time interval from 10 to 20 seconds.

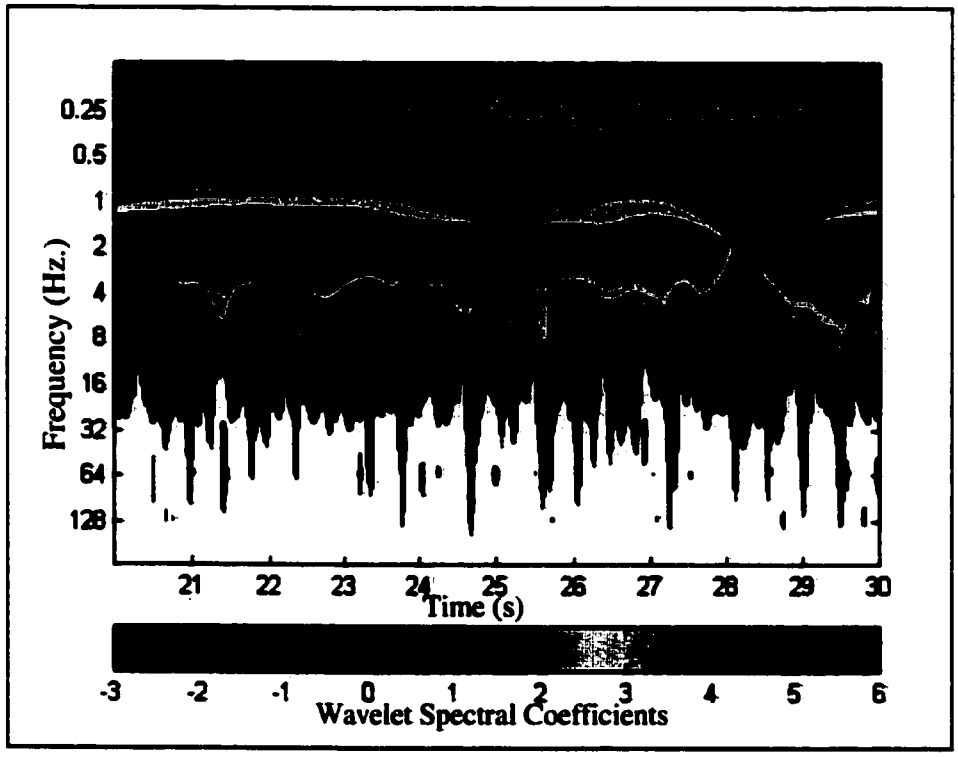

Figure 5.1.7: Morlet wavelet spectra on time-frequency axes for time interval from 20 to 30 seconds at operating condition 1.

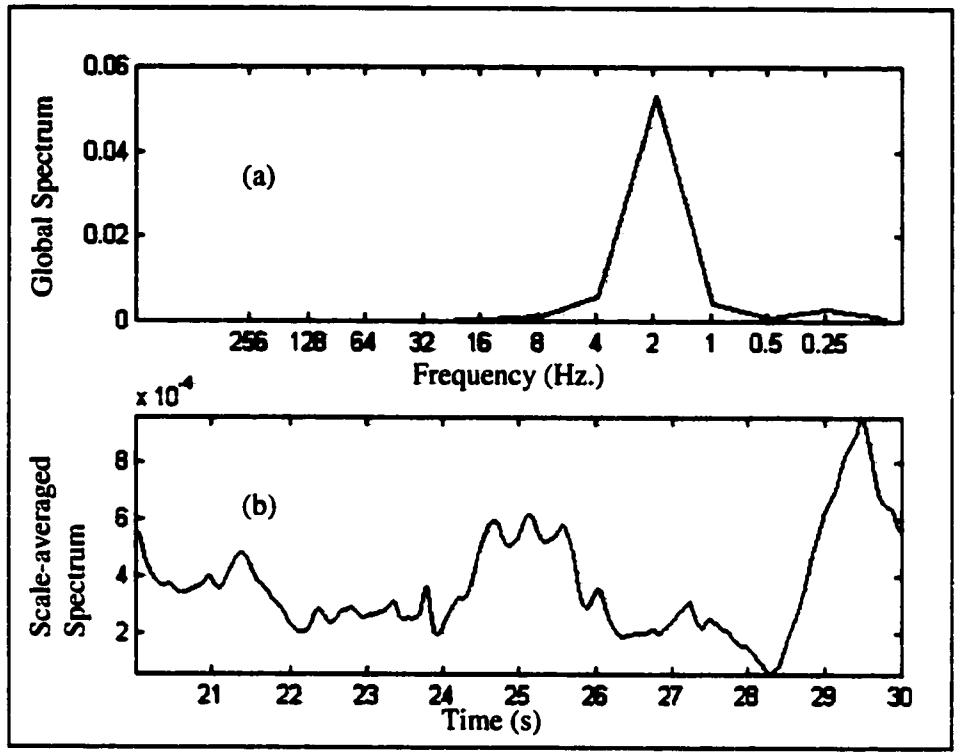

Figure 5.1.8: Global spectra and scale-averaged wavelet spectra in the time interval from 10 to 20 seconds.

5.3.2 Exploratory Analysis for Annular Flow Pattern at Operating Condition 2

Pressure fluctuations for a second operating condition in the annular flow region are also examined by wavelet analysis. Consecutive time intervals of data are plotted on wavelet power plots and their corresponding scale-averaged and global spectra are plotted in **Figures 5.2.1 to 5.2.6**. The contour-filled map shown on **Figures 5.2.1**, also shows wavelet power variations in the 0.5-1 Hz. frequency band. To account for the fluctuations in the lower band, the scale-averaged wavelet spectrum was calculated for the frequency band from 0.5 Hz. to 16 Hz. As in Condition 1, the analysis was carried out for multiple-time intervals of pressure data. The wavelet spectral plots, **Figures 5.2.2(b), 5.2.4(b) and 5.2.6(b)**, show the variations of the wavelet spectra in time by averaging over the relevant scales. From the analysis, it can be seen that the wavelet spectra are transient in nature and occur at irregular intervals of time. The different pressure data sets and the comparative plots for the Fourier and global or mean power spectrum are included in **Appendix C**.

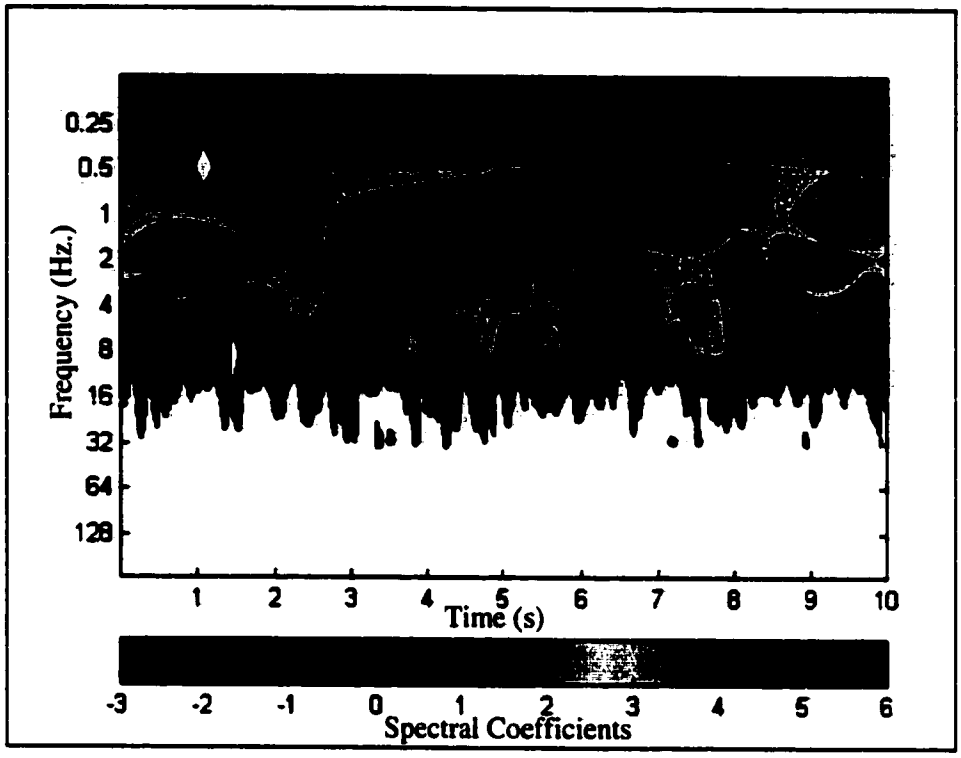

Figure 5.2.1: Morlet wavelet spectra on time-frequency axes for condition 2 for the time interval from 0 to 10 seconds.

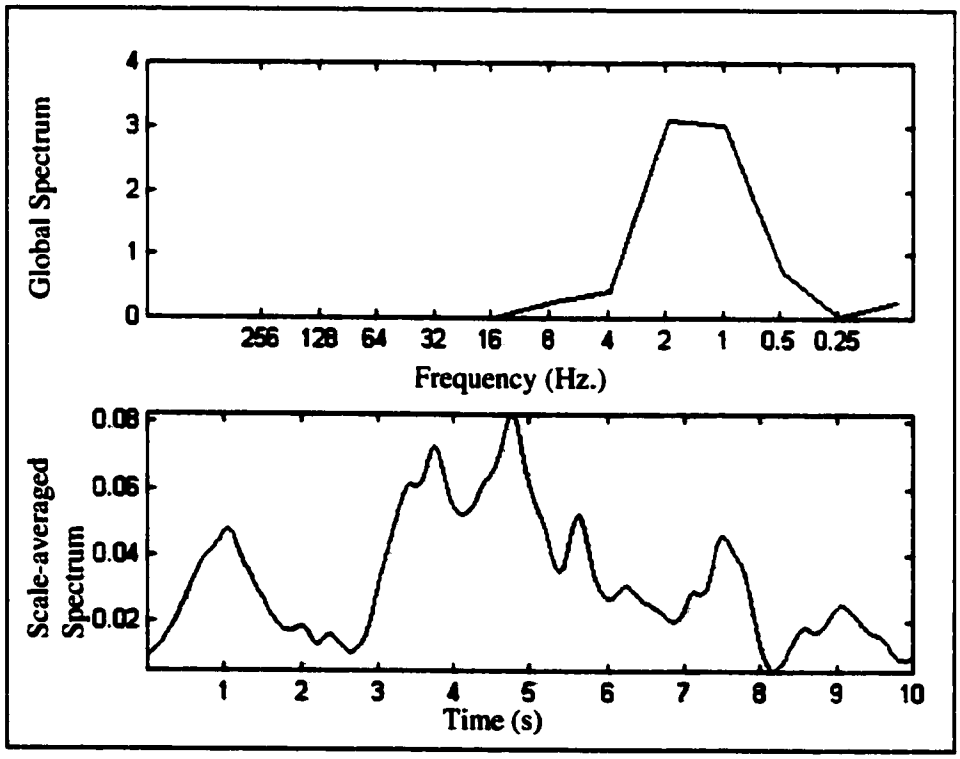

Figure 5.2.2: Global spectra and scale-averaged wavelet spectra for the time interval from 0 to 10 seconds.

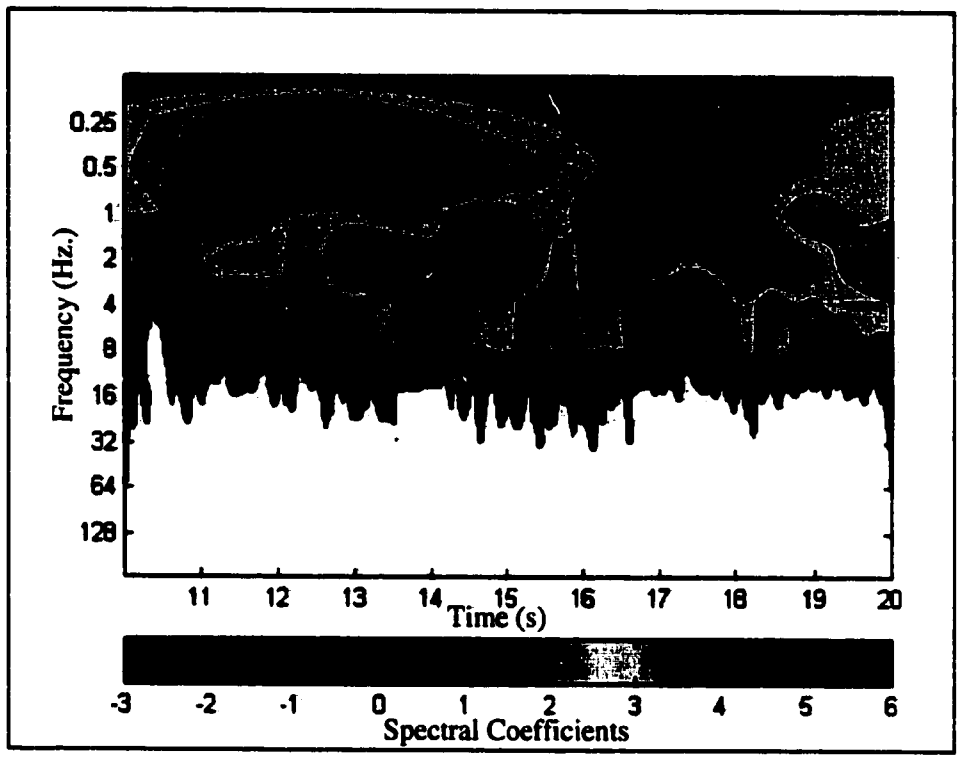

Figure 5.2.3: Morlet wavelet spectra on time-frequency axes for condition 2 in the time interval from 10 to 20 seconds.

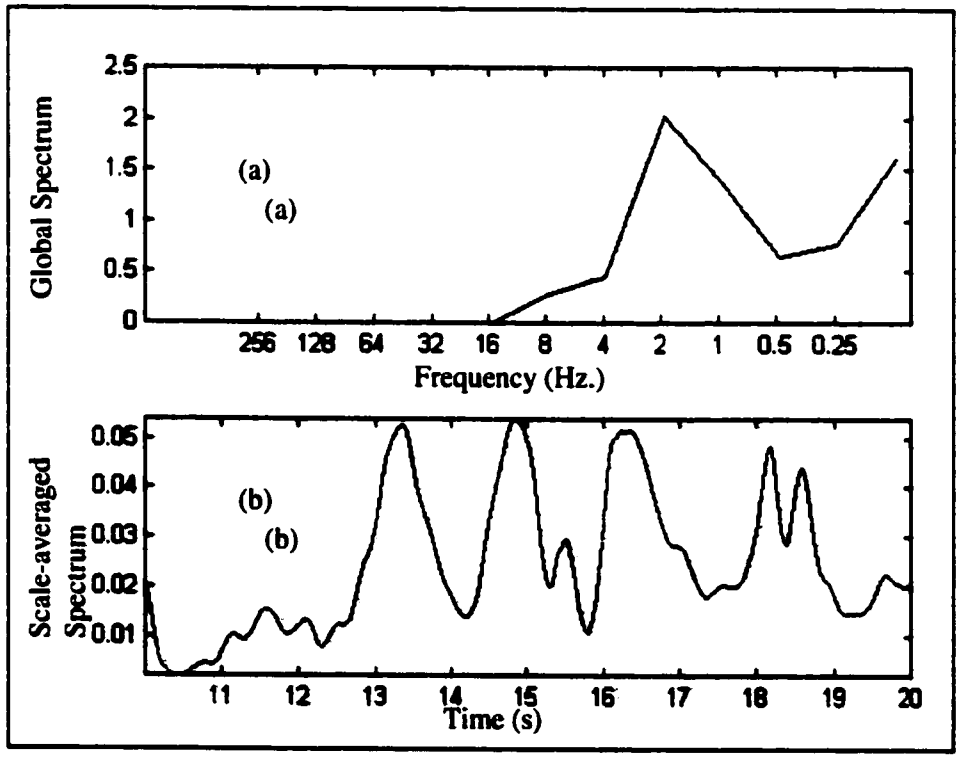

Figure 5.2.4: Global spectra and scale-averaged wavelet spectra in the time interval from 10 to 20 seconds.

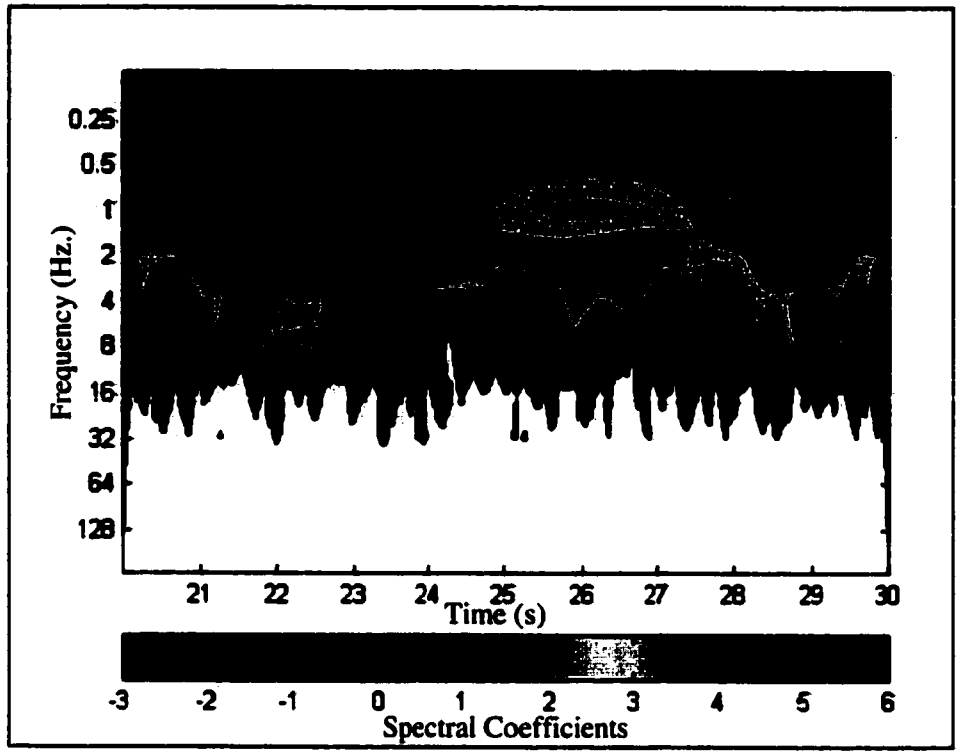

Figure 5.2.5: Morlet wavelet spectra on time-frequency axes at condition 2 in the time interval from 20 to 30 seconds.

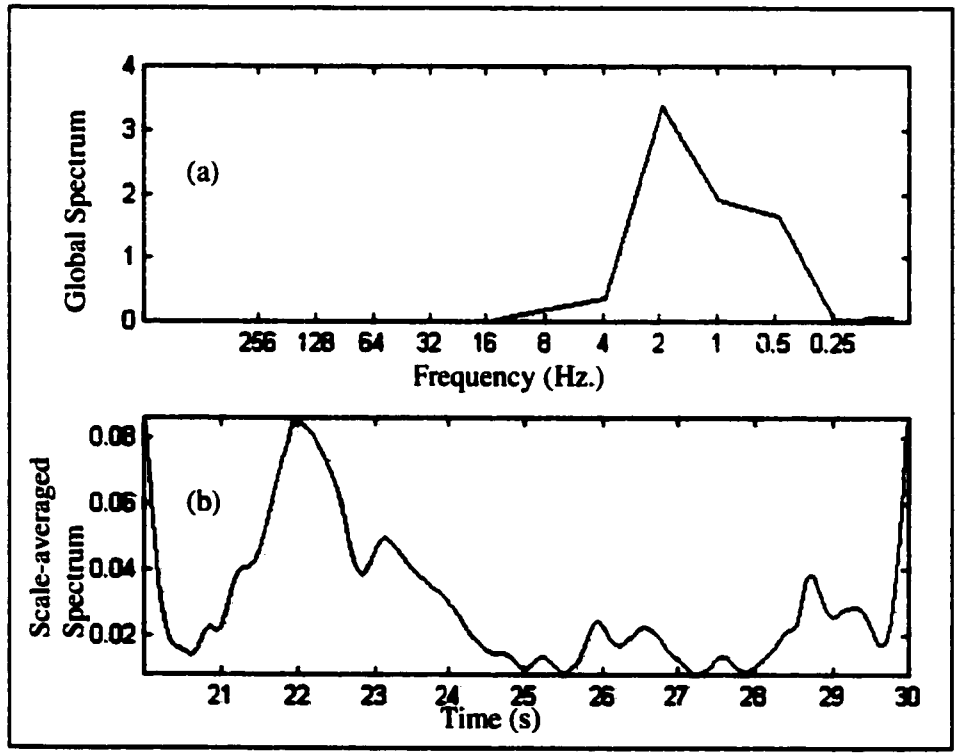

Figure 5.2.6: Global spectra and scale-averaged wavelet spectra for the wavelet energy map for the time interval from 20 to 30 seconds.

5.3.3 Interpretation of Graphical Results

From the wavelet energy or power plots and the spectral analysis plot, the following observations are made:

1) As predicted by other two-phase flow researchers (Dukler and Taitel, 1986), the peak frequency is observed to occur in a high band greater than near zero frequency.
2) The calculated scale-averaged wavelet plots show that intermittent spectra peaks are formed in annular flow patterns. This agrees with Jones and Zuber's (1976) description. The peaks are observed to be irregular in occurrence.
3) Multiple 10-second time intervals of recorded pressure fluctuations, for both conditions, have been examined for confirmation purposes. The spectral results derived for each pressure record show that the global wavelet spectra have similar characteristics. The formation of peaks is intermittent.

The contour plots representing the energy map show that the suggested signal processing methods are suitable for annular flow pattern determination.

5.4 Dispersed Flow Pattern Determination

Dispersed flow is the most widely examined condition observed in two-phase flow systems. Work by earlier researchers (Jones and Zuber, 1976), determined that void fluctuations in bubbly flow are completely random with no periodicity. Zuber also concluded that **dispersed flow patterns** appear to be relatively homogeneous over a significant length of time and analysis of recorded data sets should be quite similar. Dukler and Taitel (1986) determined that pressure variations in dispersed flows are uniformly spread over a large frequency band. Here, wavelet-based signal processing is applied to the pressure data for two conditions in the dispersed flow regime (refer to **Table 3.1**).

5.4.1 Exploratory Analysis for Dispersed Flow Pattern at Operating Condition 1

The pressure fluctuations for this flow condition are shown in **Figure 5.3.1** while the corresponding wavelet spectral map is shown in **Figure 5.3.2**. Multiple 10-second intervals of pressure fluctuation data were processed using the signal processing procedures described earlier for annular flow pattern determination. The energy/wavelet

spectral maps demonstrate the absence of periodicity in the signal previously observed by Jones and Zuber (1976). The wavelet power maps developed for subsequent 10-second intervals show a higher range of frequencies in this flow pattern. Also, the similarity in the wavelet power plots for the different pressure records (10 seconds each) prompts the use of further spectral analysis. The analysis procedure is similar to that conducted for annular flow pattern recognition.

The scale-averaged wavelet spectrum provides a measure of the intermittence in two-phase flows. Based on the global wavelet spectral plot shown in **Figure 5.3.3 (a)**, the frequency band for calculation of the scale-averaged wavelet power is determined to be about 1-64 Hz. for this condition. Similarly, scale-averaged wavelet power is calculated over a range of scales (frequency band of 1-64 Hz.) as shown in **Figure 5.3.3(b)**. A comparison of the Fourier power spectrum and the scale-averaged wavelet spectrum is shown in **Figure 5.3.4**. Also, similar contour-filled wavelet energy maps and their corresponding global and local wavelet spectra for consecutive 10-second time intervals of recorded pressure transducer data are shown in **Figures 5.3.5 to 5.3.8**. Raw pressure data and the comparative plots for the Fourier and global or mean power spectrum are included in **Appendix C**.

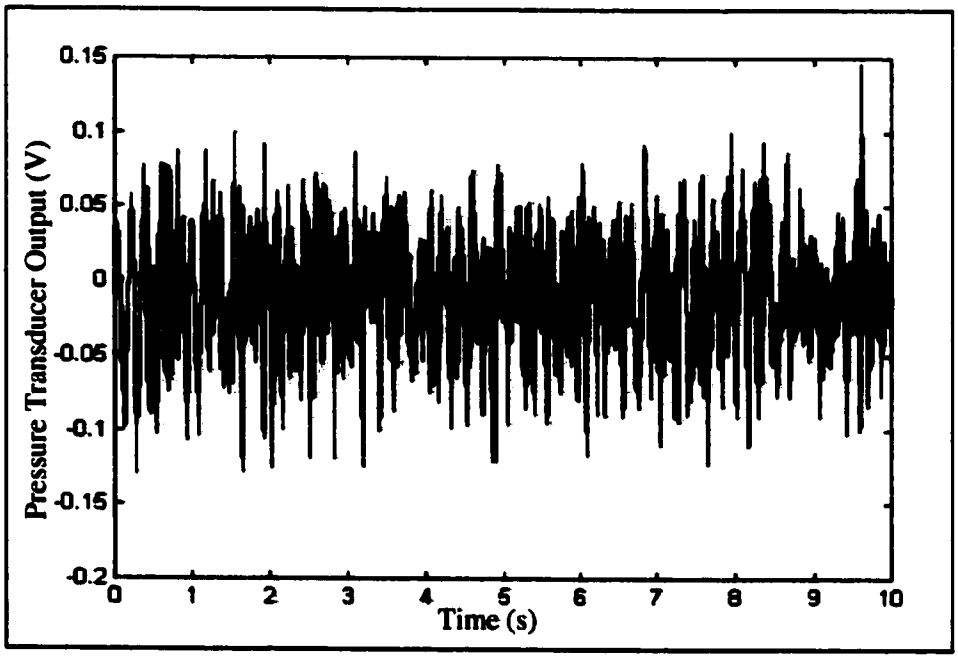

Figure 5.3.1: Pressure fluctuations in dispersed flow pattern at operating condition 1 for 0 to 10 seconds.

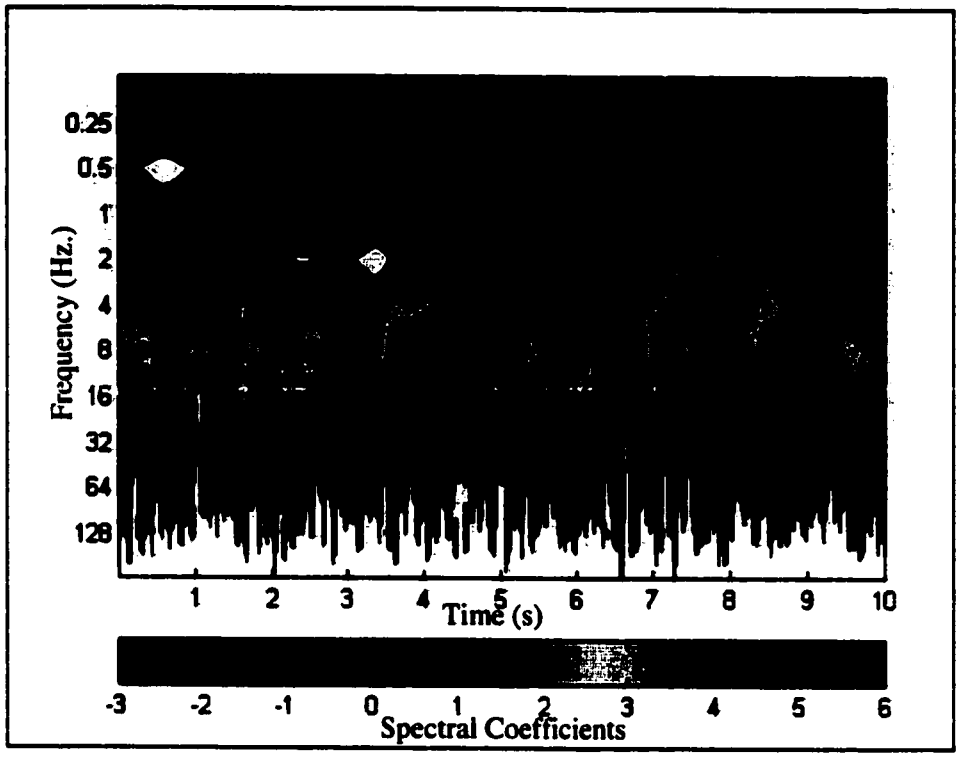

Figure 5.3.2: Morlet wavelet spectra on time-frequency axes at condition 1 from 0 to 10 seconds.

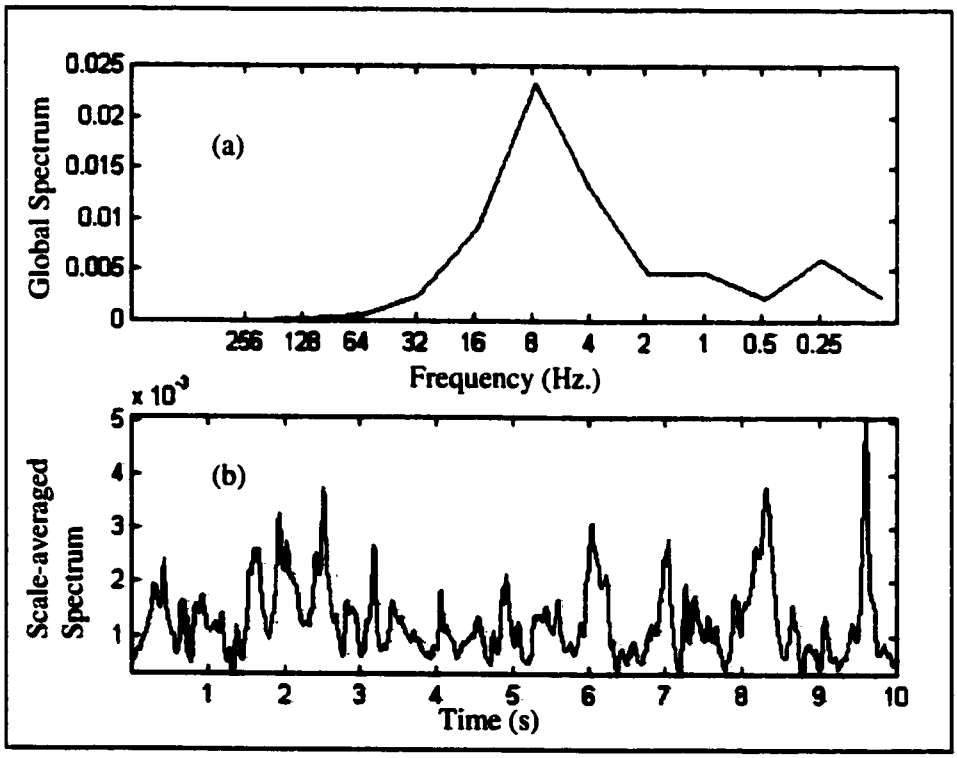

Figure 5.3.3: Global spectra and scale-averaged wavelet spectra at condition 1 for the time interval from 0 to 10 seconds.

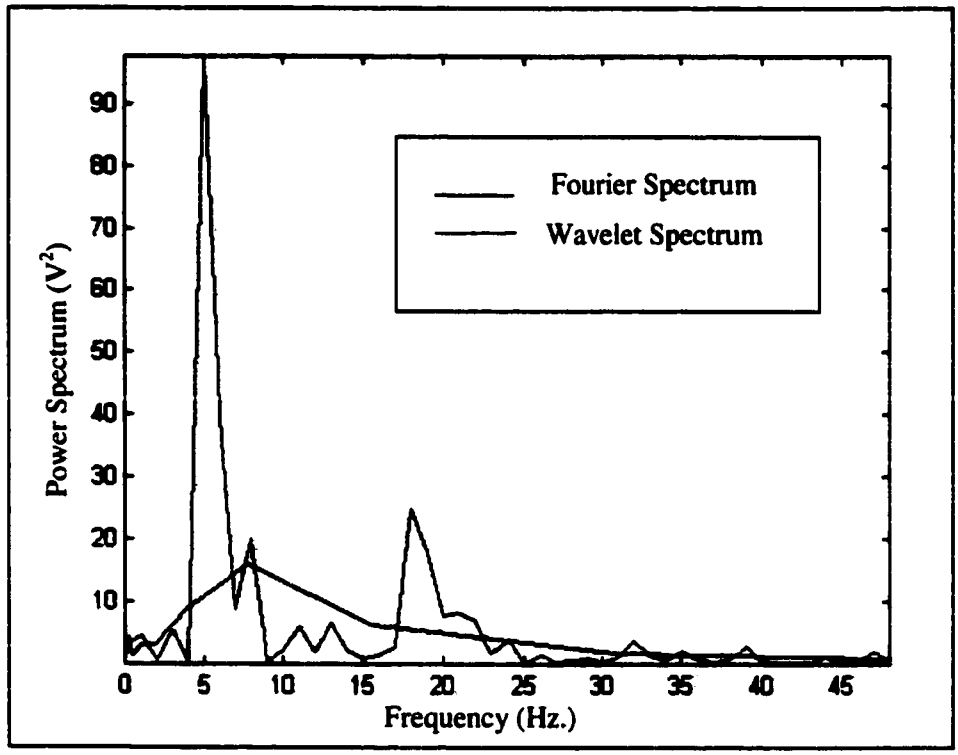

Figure 5.3.4: Comparison of wavelet spectra and power spectral analysis (Fourier) for condition 1. The wavelet global spectrum is smoother due to averaging but peak location is within the frequency band.

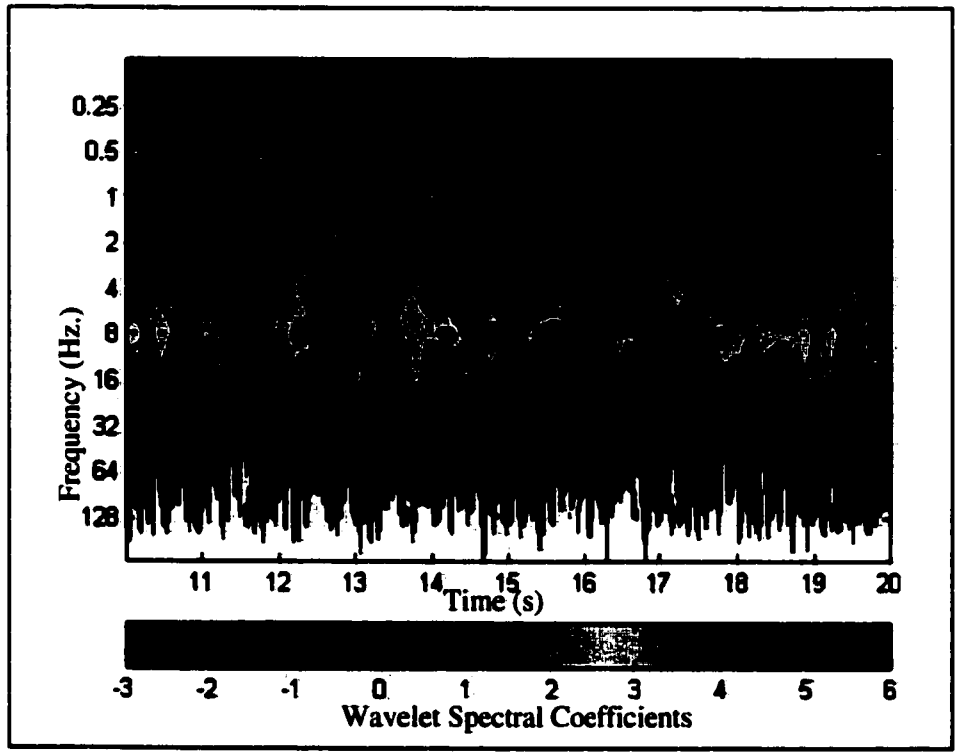

Figure 5.3.5: Wavelet spectra on time-frequency axes in time interval from 10 to 20 seconds at condition 1.

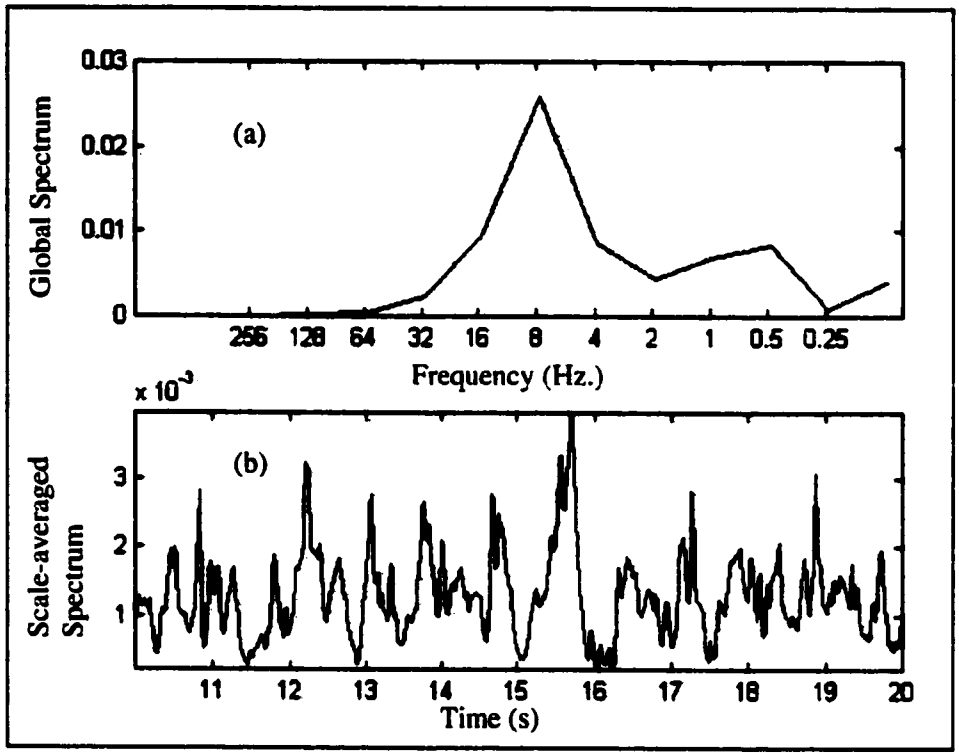

Figure 5.3.6: Global spectra and scale-averaged wavelet spectra for the wavelet energy map in the time interval of 10 to 20 seconds.

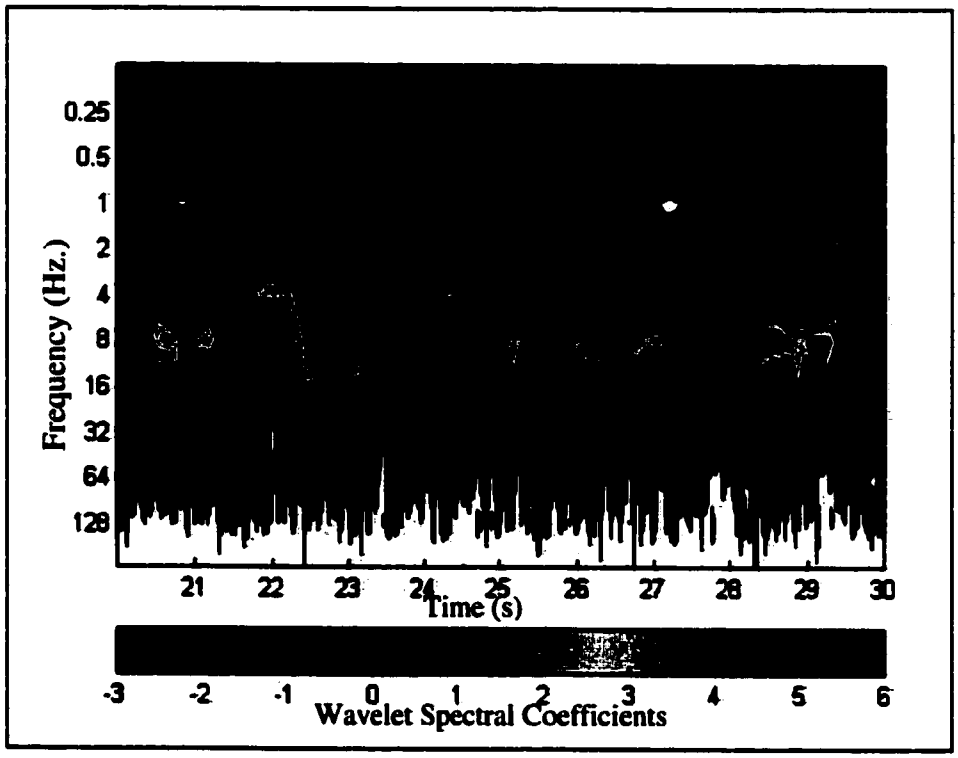

Figure 5.3.7: Morlet wavelet spectra on time-frequency axes in time interval 20 to 30 seconds at operating condition 1.

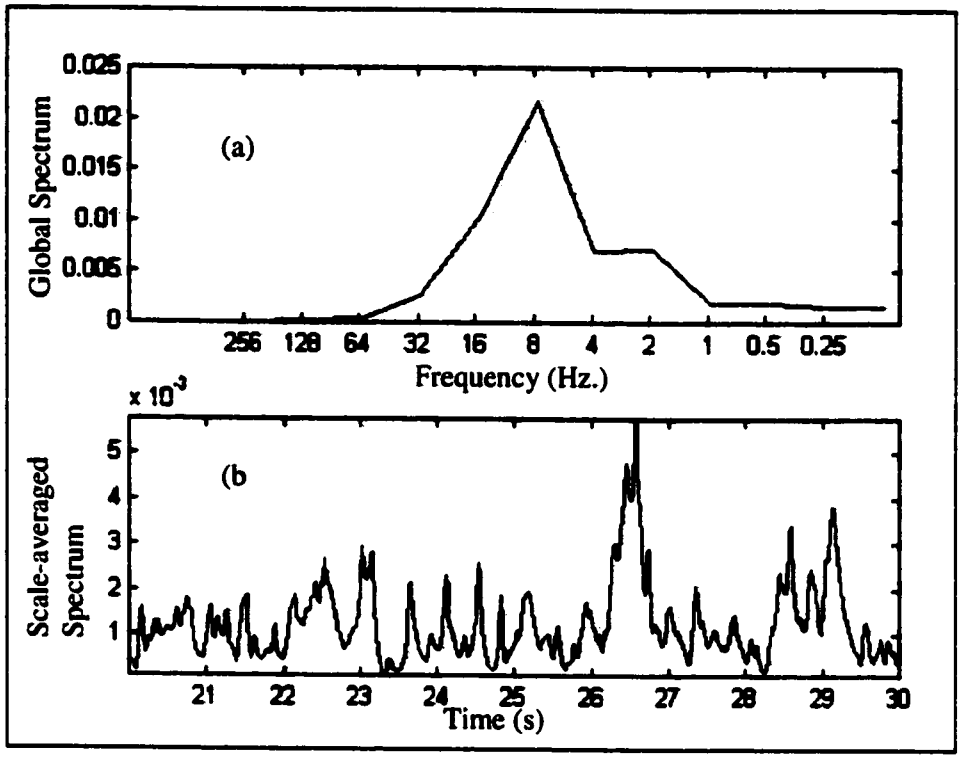

Figure 5.3.8: Global spectra and scale-averaged wavelet spectra in the time interval of 20 to 30 seconds.

5.4.2 Exploratory Analysis for Dispersed Flow Pattern at Operating Condition 2

Similarly, condition 2 is selected for further exploratory analysis in the **dispersed/bubble flow regime**. Again, the wavelet spectral plots for multiple 10-second time intervals of data sets show similar trends to those observed for condition 1, as demonstrated in the contour-filled wavelet energy maps. From the analysis, it can be seen that the wavelet spectra possess a much higher frequency and the pulsations occur much more rapidly than those observed in annular flow. The scale average wavelet power is therefore calculated for the frequency band of 1-64 Hz. Wavelet spectral maps and their corresponding scale-averaged and global spectra are plotted on **Figures 5.4.1 to 5.4.6.** From the analysis, fast transients in the scale-averaged wavelet power are observed. The different pressure data sets and the comparative plots for the Fourier and global or mean power spectrum are included in **Appendix C.**

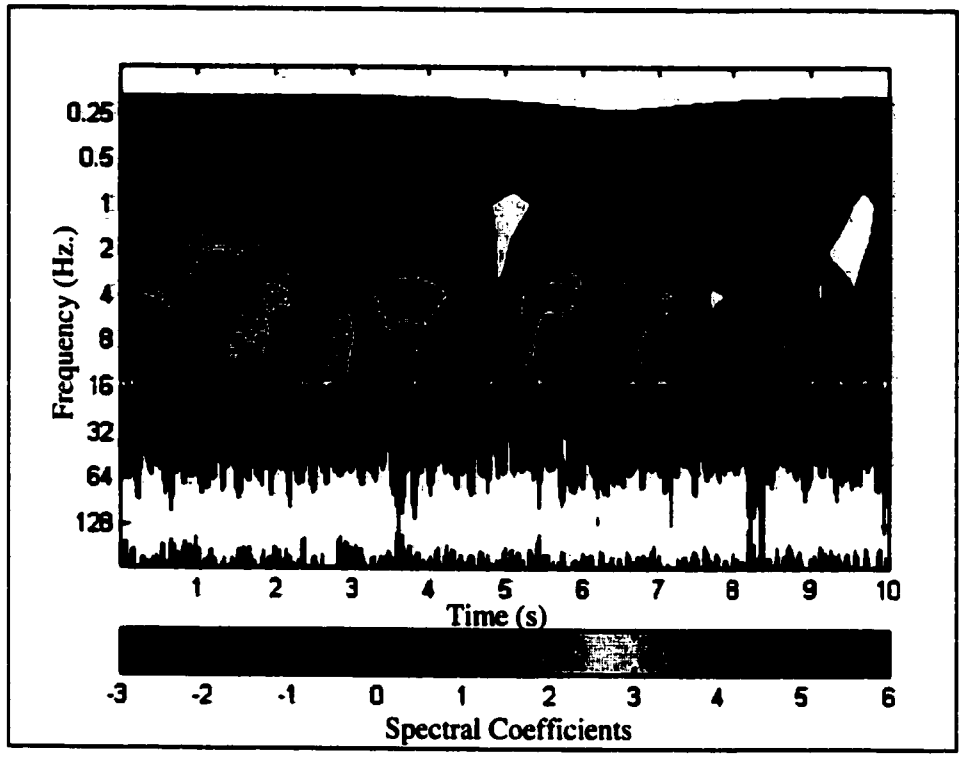

Figure 5.4.1: Morlet wavelet spectra on time-frequency axes for condition 2 (dispersed flow) in the time interval from 0 to 10 seconds.

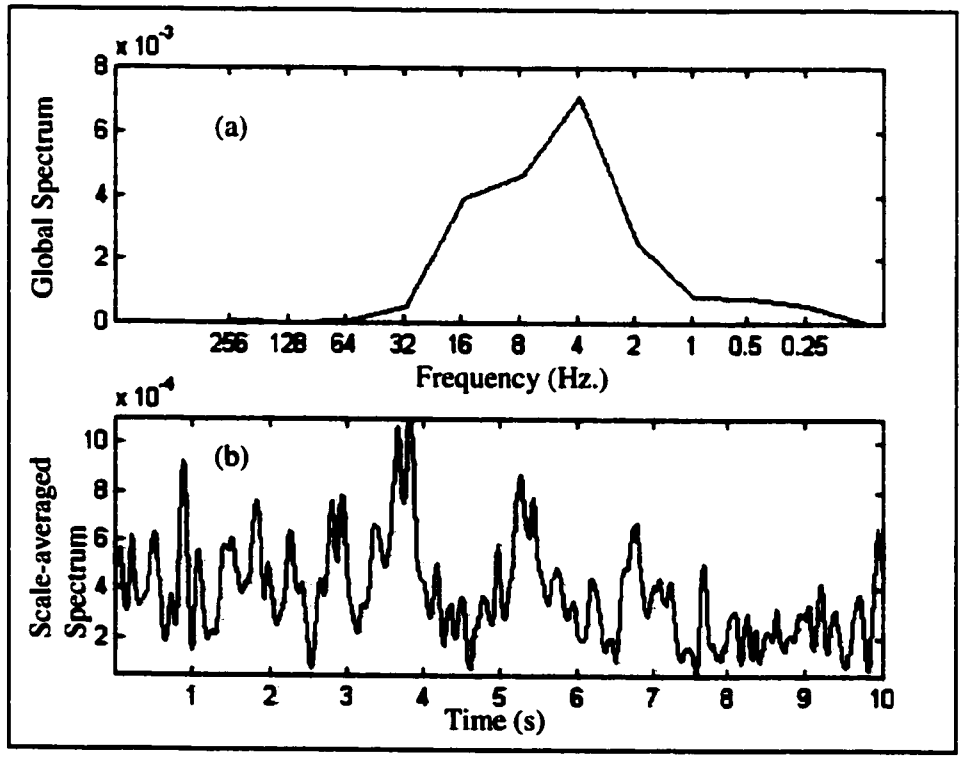

Figure 5.4.2: Global spectra and scale-averaged wavelet spectra in the for the time interval of 0 to 10 seconds.

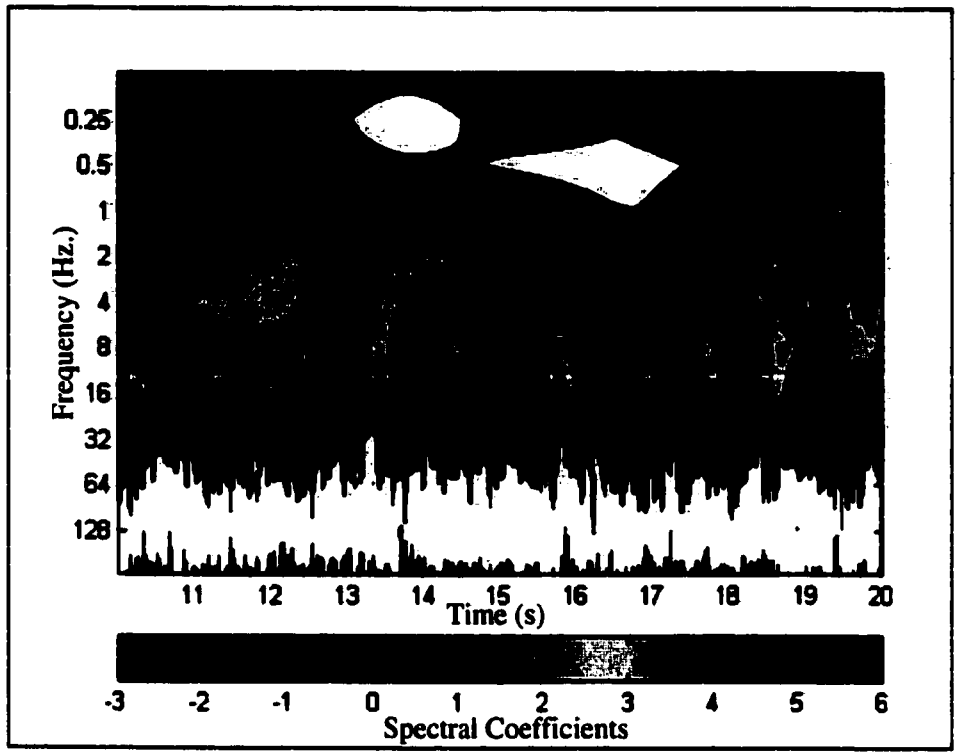

Figure 5.4.3: Morlet wavelet spectra on time-frequency axes in condition 2 (dispersed flow) for the time interval from 10 to 20 seconds.

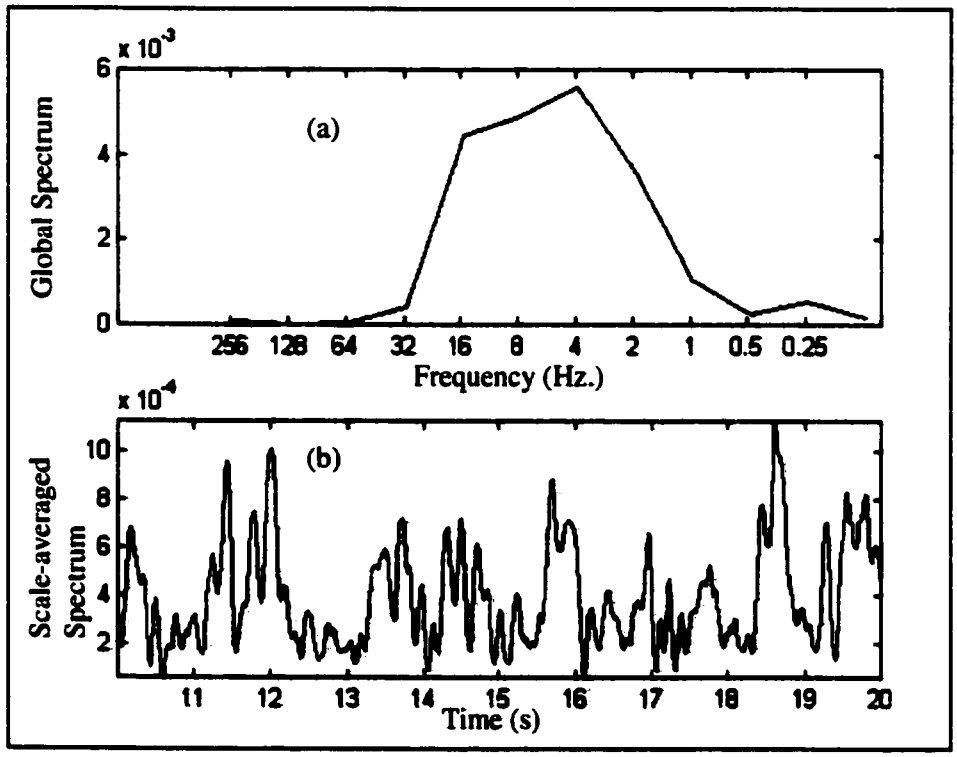

Figure 5.4.4: Global spectra and scale-averaged wavelet spectra in the wavelet energy map time interval from 10 to 20 seconds.

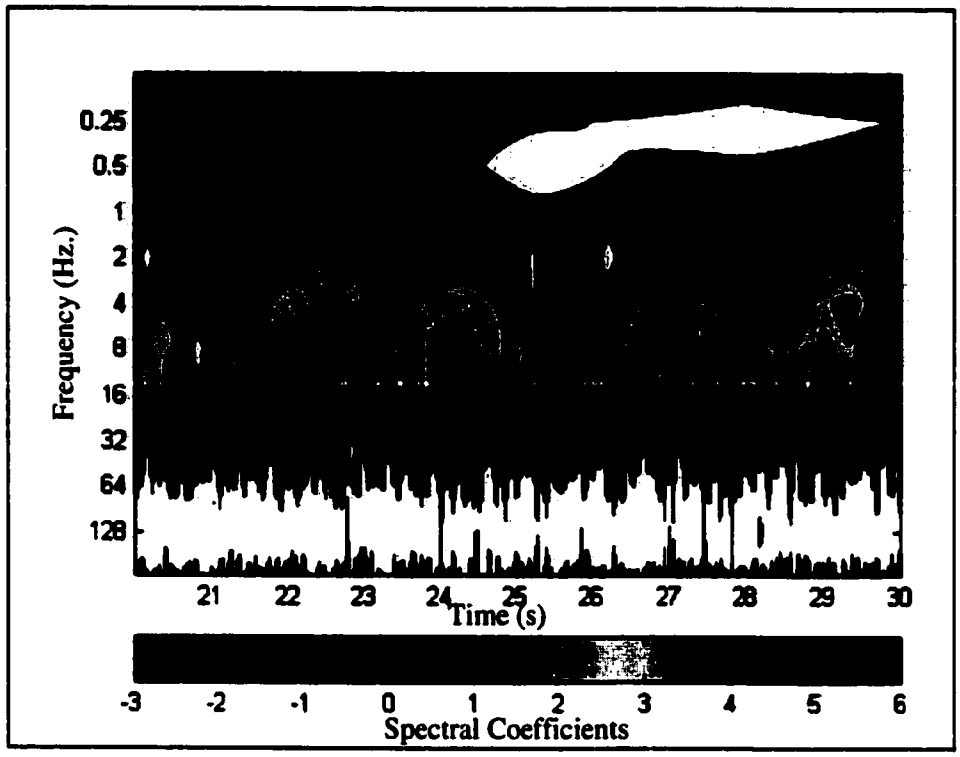

Figure 5.4.5: Morlet wavelet spectra on time-frequency axes at condition 2 (dispersed) in the time interval from 20 to 30 seconds.

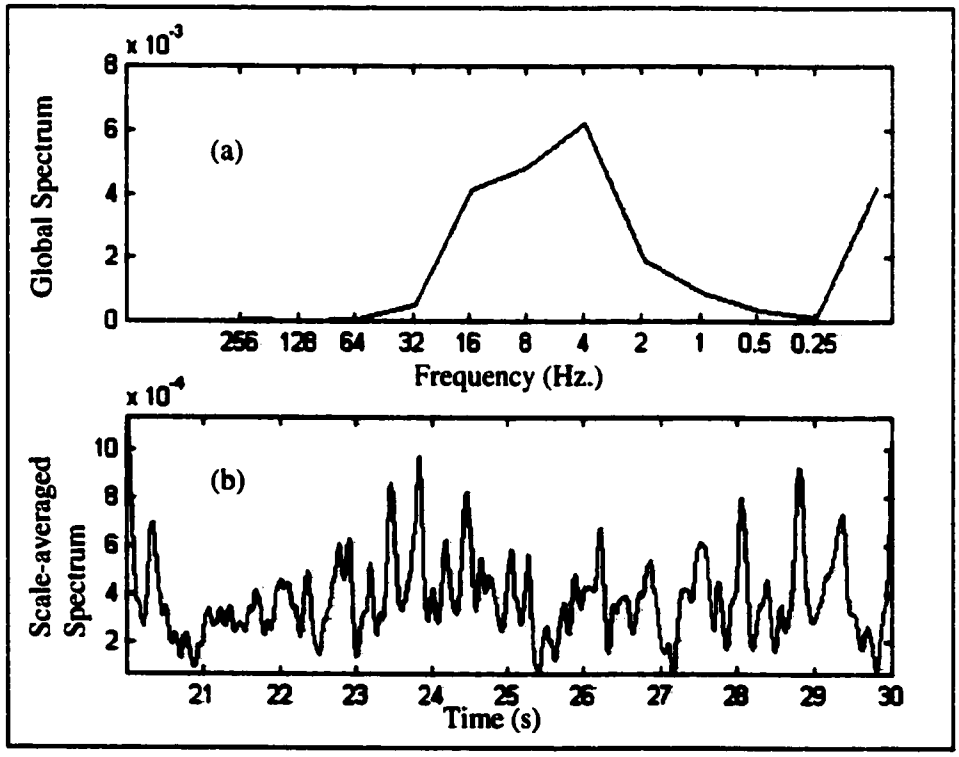

Figure 5.4.6: Global spectra and scale-averaged wavelet spectra in the time interval from 20 to 30 seconds.

5.4.3 Interpretation of Graphical Results

The wavelet power plots and advanced spectral analysis plots allow the following observations to be made:

1) The global wavelet spectrum for each condition shows that the fluctuations occupy a higher frequency band than observed in annular flow. Similar results are seen with Fourier power spectra but the intermittence is observed only with the scale-averaged wavelet plot.
2) The scale-averaged wavelet plot generated for this flow pattern shows that intermittent pressure peaks occur much more rapidly than in the case of annular flow. The two-phase mix is quite homogeneous in nature for dispersed flows. Some researchers (Jones and Zuber (1976)) have attributed this characteristic to the intense mixing between the two-phases.
3) Consecutive time records of pressure data show similar results for the two conditions examined.

Thus, for the dispersed flow pattern, the scale-averaged wavelet power plot filters the required band of frequency and characterizes the system on the basis of intermittence.

5.5 Slug Flow Pattern Determination

As described in chapter two, the historical method for flow pattern determination is based on a combination of spectral and statistical analysis. Jones and Zuber (1976) proposed that slug-like flow is a localized condition with the appearance of two separate yet statistically significant maxima in the probability density function of the void fluctuations. Also, Dukler and Taitel (1986) suggested that separated flows consisted of spectra with distributions centered about zero frequency and with amplitude decaying rapidly with increasing frequencies.

Only one operating condition was examined for slug flow (refer to **Table 3.1**) by the wavelet-based signal processing method.

5.5.1 Exploratory Analysis for Slug Flow Pattern at Operating Condition 1

The pressure fluctuations for the given operating condition are shown on **Figure 5.5.1**. The corresponding wavelet power plot is shown on **Figure 5.5.2**. The energy/wavelet spectral map conforms with Dukler's results for separated flow pattern recognition because the peak frequency is near zero with a rapid decay in amplitude with increase in frequency. Further the wavelet power plot shows that wavelet peaks occur less rapidly compared to the other regimes.

Spectral analysis of the wavelet power/energy plot is shown on **Figure 5.5.3**. The global wavelet spectral plot, shown on **Figure 5.5.3(a)**, indicates that the frequency band for the peak frequency is between 0.25 Hz. and 4Hz. The scale-averaged wavelet power plot is then calculated over this frequency band. It shows that the fluctuations occur less frequently in this flow pattern and are fairly regular in their occurrence. Consecutive data sets have been analyzed to confirm the regularity of peak occurrence. The wavelet spectral energy plots and the corresponding scale-averaged and global spectrum plots are shown on **Figures 5.5.5 to 5.5.8**.

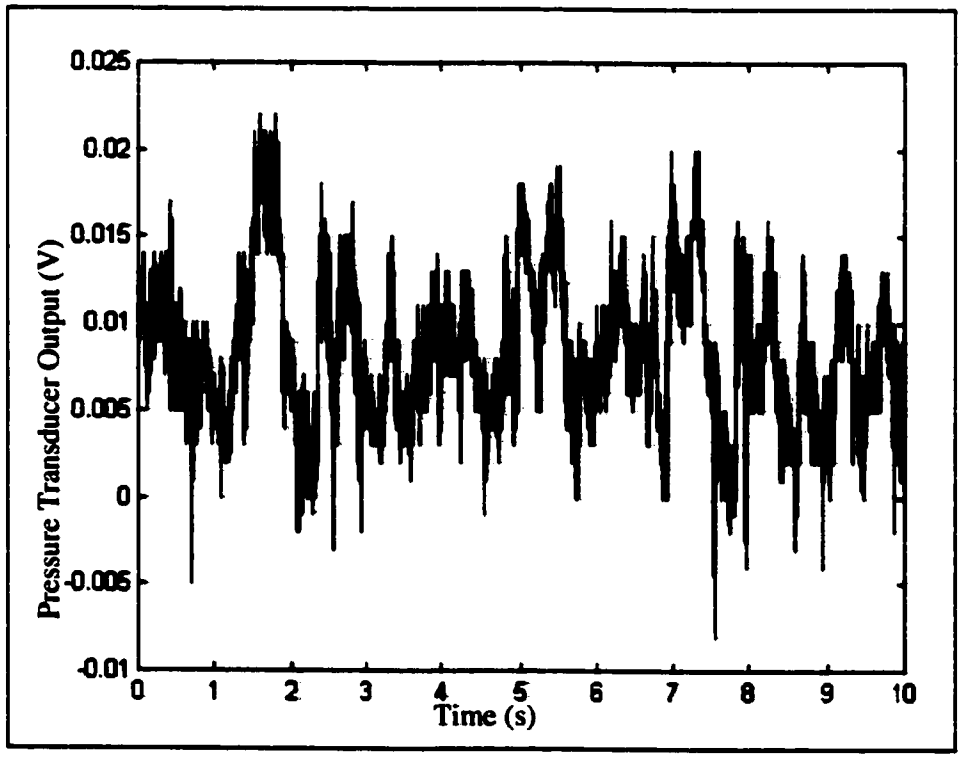

Figure 5.5.1: Pressure fluctuations in annular flow pattern at operating condition 1 (slug flow) for 0 ton 10 seconds.

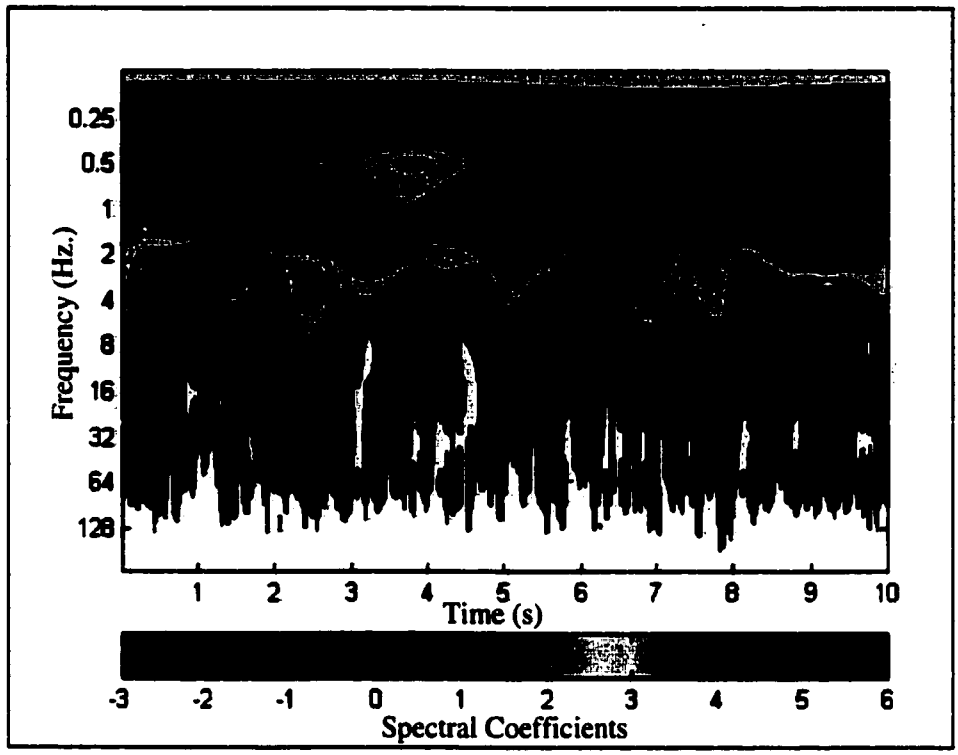

Figure 5.5.2: Morlet wavelet spectra on time-frequency axes at condition 1 (slug flow) from 0 to 10 seconds.

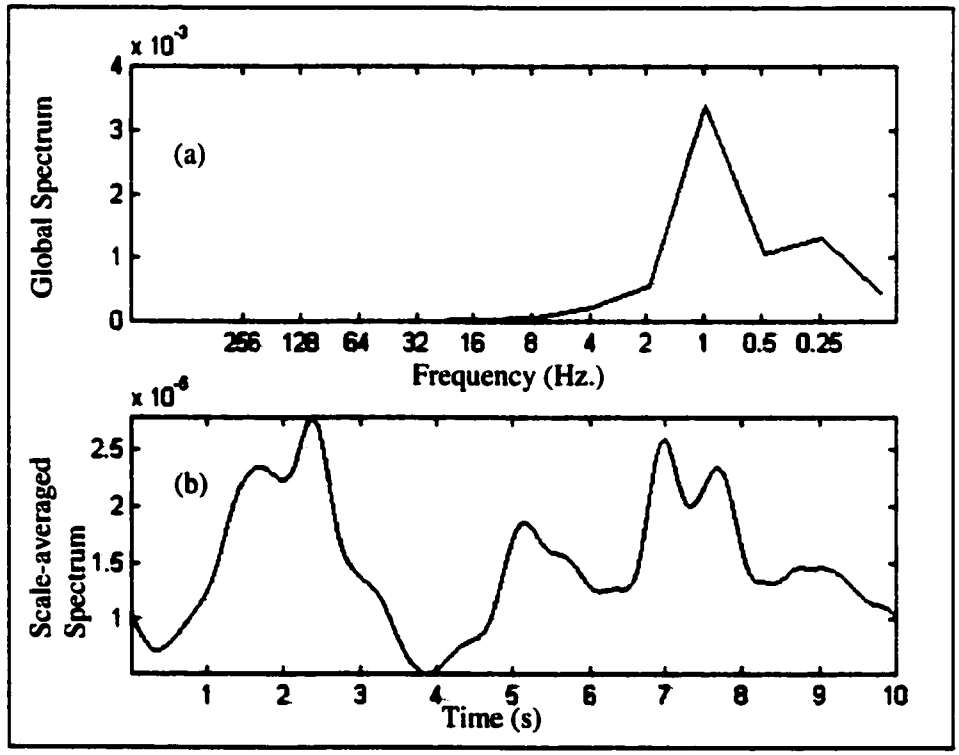

Figure 5.5.3: Global spectra and scale-averaged wavelet spectra at condition 1 (slug flow) for the time interval from 0 to 10 seconds.

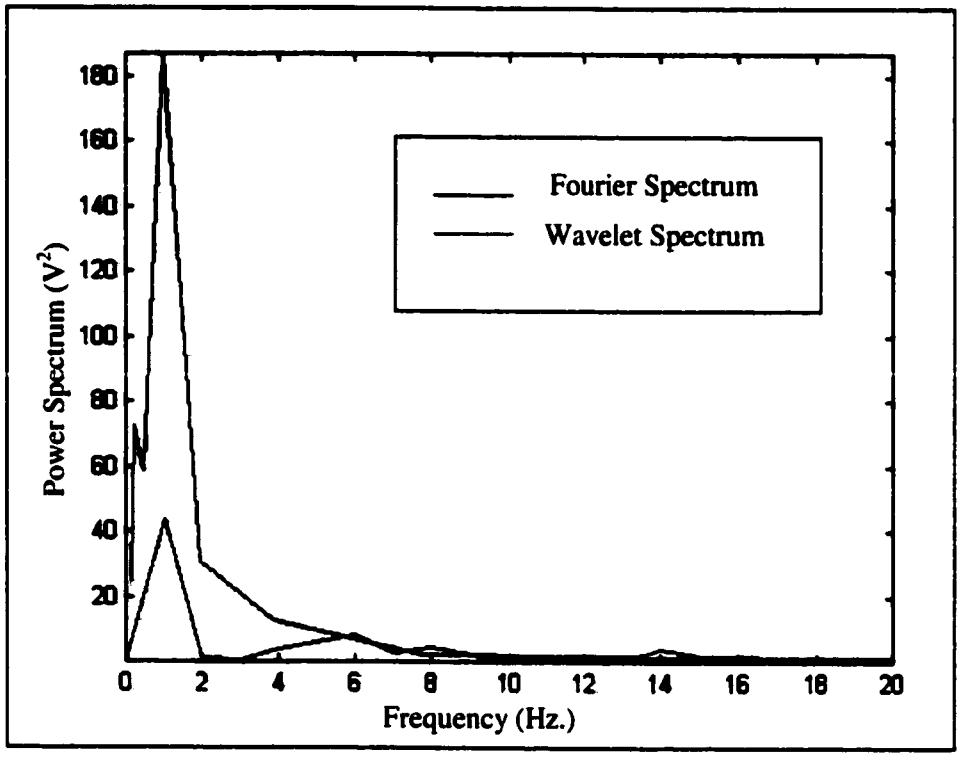

Figure 5.5.4: Comparison of wavelet spectra and power spectral analysis (Fourier) for condition 1 (slug flow). The wavelet global spectrum is smoother due to averaging but peak location is within the frequency band.

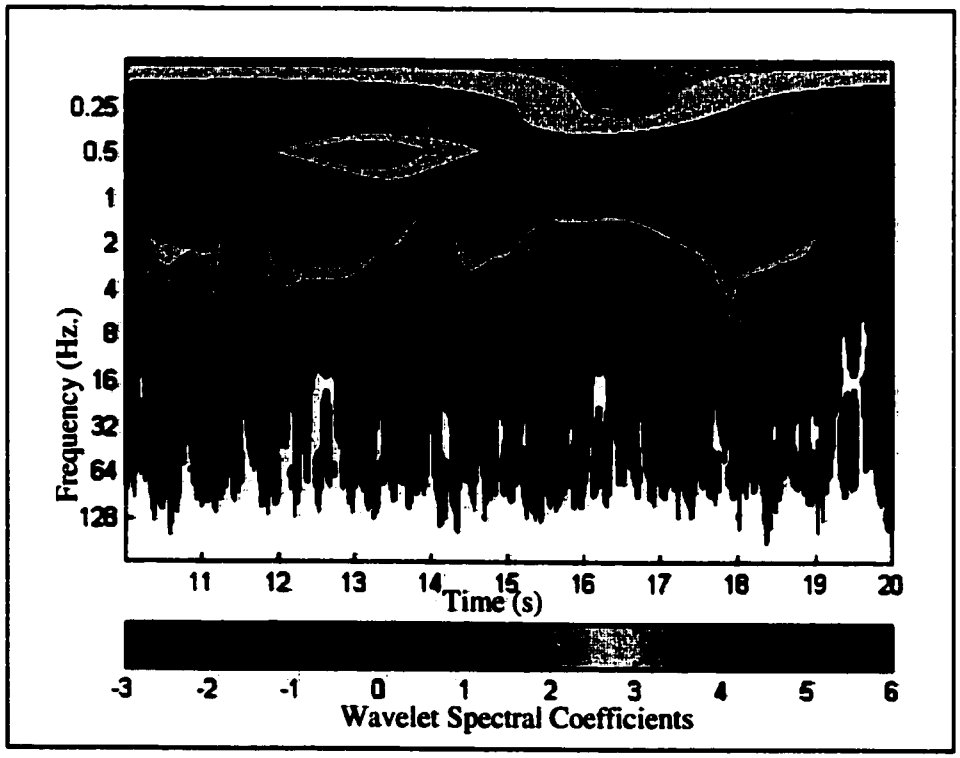

Figure 5.5.5: Morlet wavelet spectra on time-frequency axes in the time interval from 10 to 20 seconds at condition 1 (slug flow).

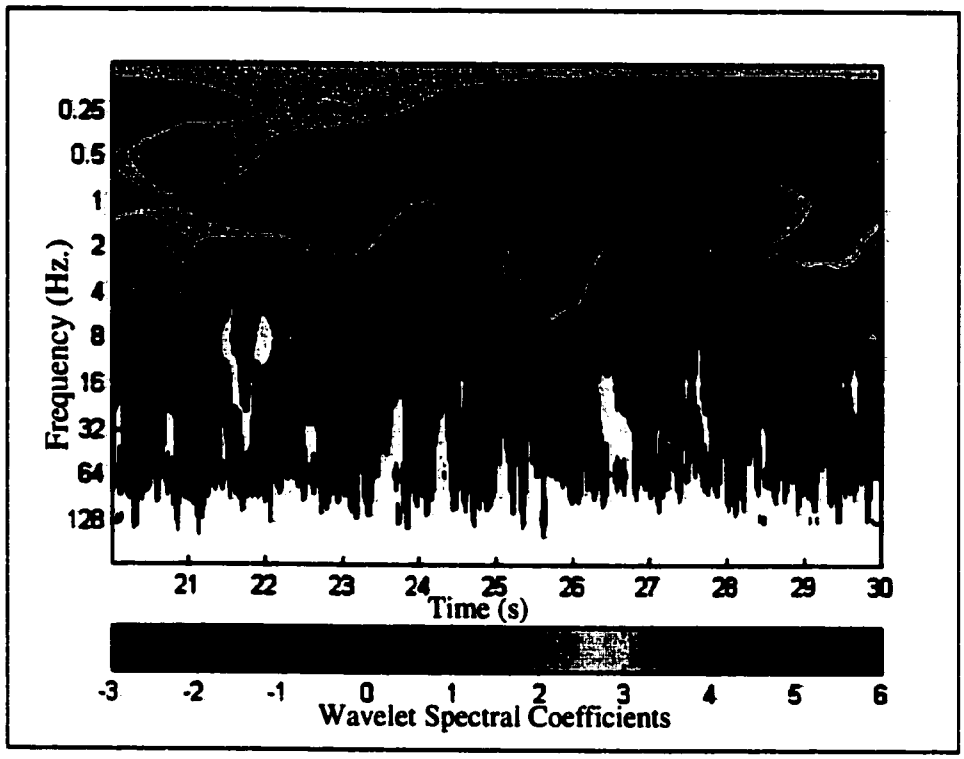

Figure 5.5.6: Morlet wavelet spectra on time-frequency axes in time interval from 20 to 30 seconds at operating condition 1 (slug flow).

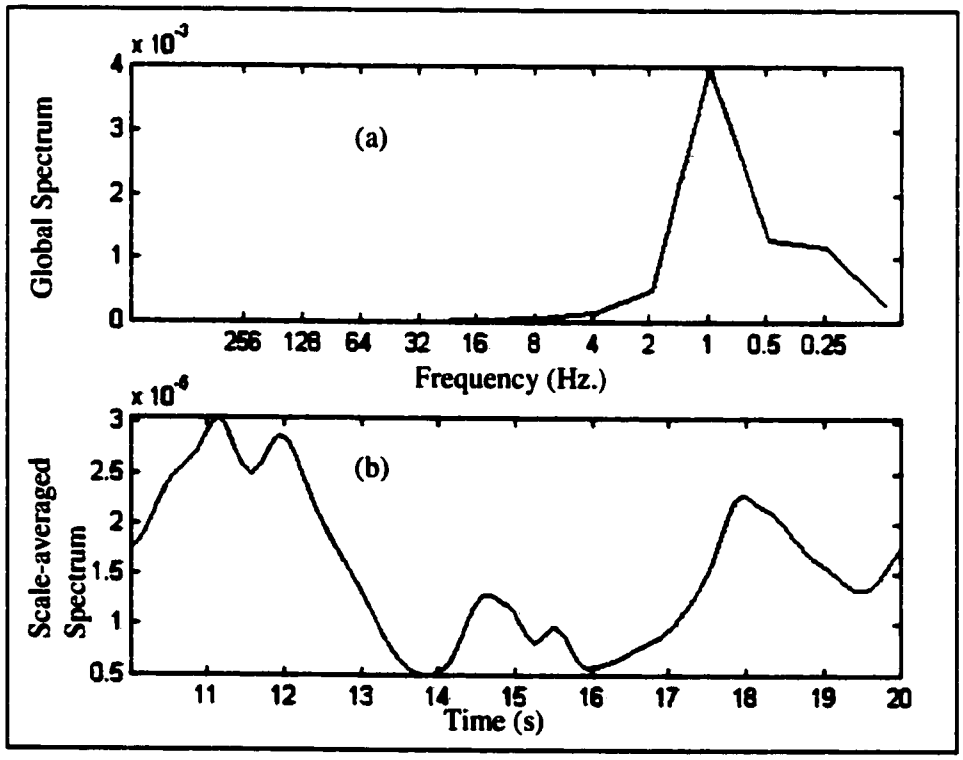

Figure 5.5.7: Global spectra and scale-averaged wavelet spectra in the time interval from 10 to 20 seconds.

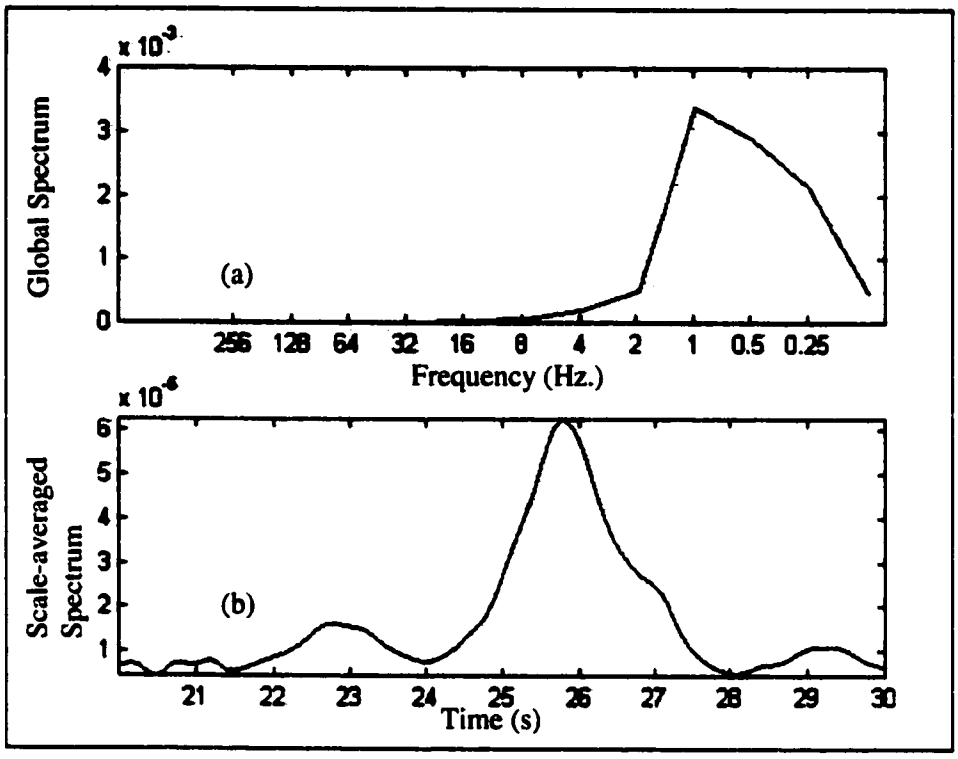

Figure 5.5.8: Global spectra and scale-averaged wavelet spectra in the time interval of 20 to 30 seconds.

5.5.2 Interpretation of Graphical Results

The wavelet power plots and advanced spectral analysis demonstrate the following:

1) For both conditions, the global wavelet spectrum exhibits a much lower frequency band for this flow pattern. Near-zero frequencies are observed in the spectral analysis plots. Similar results are seen with Fourier power spectra.
2) The scale-averaged wavelet plots generated for this flow pattern show that fluctuations seldom occur in this flow regime. Smooth variations in the selected frequency band are observed for this flow pattern.
3) Consecutive time records of pressure data show similar results.

Longer time records (>10 sec.) need to be processed to observe this flow pattern clearly. Pulsations in this smooth slug-like flow pattern are anticipated to be regular in nature (Jones and Zuber, 1976). Therefore limited work with wavelets has been carried out for this regime. Unsteady slug flow could not be generated due to experimental limitations.

5.6 Quantifying Intermittency

The annular and dispersed flow regimes show transient characteristics as observed in the scale-averaged wavelet spectral plots. The intermittent formation of the scale-averaged wavelet peaks is also observed to be typical for a given flow pattern. Intermittency has many manifestations depending upon the physical context (Hagelberg and Gamage, 1994). An intermittency index has been developed to characterize flow patterns quantitatively. Preliminary attempts to characterize the intemittency, based on calculating kurtosis values or other statistics as recommended by other workers (Torrence and Compo, 1997; Lewalle, 1998), were not successful because that approach was dependent on different bands of frequency occurring in the signal. The intermittency index used here is defined as the fraction of the record time occupied by a scale-averaged spectral peak. A peak is defined as 80% of the maximum scale averaged wavelet power.

$$intermittency = \frac{time\ for\ scale-averaged\ power\ peak}{sampling\ time} \tag{5.3}$$

This index represents the amount of time peaks are in existence. In the case of dispersed flow, it is observed that the peaks occur rapidly leading to low intermittence, while in annular flow the peaks occur less frequently but last for a fairly long period of time. Experimental results for unsteady slug flow were not available owing to experimental difficulties. Therefore slug flow is not included in the intermittency index.

The intermittency index is calculated for the conditions in the annular and dispersed flow regimes. The indices are reported in **Table 5.1**

Flow Pattern	Operating Condition	Analysis time intervals		
		0-10 sec	10-20 sec	20-30 sec
Annular Flow	Condition 1	0.0348	0.0672	0.0441
	Condition 2	0.092	0.1297	0.0793
Dispersed Flow	Condition 1	0.0035	0.0119	0.007
	Condition 2	0.0215	0.0264	0.0123

Table 5.1: Intermittency index values for annular and dispersed flow regimes.

5.7 Discussion

Conventional flow pattern maps, such as Baker's flow pattern map, are system-specific e.g., for an air-water mixture in a pipe with similar dimensions. Therefore, the maps cannot be extended to other two-phase flow systems Also, transition regions show unsteady behavior. Two-phase flow systems operating in these regimes are difficult to identify with flow maps.

Based on the findings of this research, a novel method using wavelet-based signal processing has been recommended for characterizing flow patterns by analyzing pressure fluctuations from two-phase flow systems. A phased approach was adopted for examining the suggested method. Initial development was carried out on programmatically generated model data. The developed methods were evaluated on a baseline system where a known pulsation rate was induced into a liquid flow. The baseline system was also used to examine the differences between single-phase and two-phase pulsation patterns. Using the results of the baseline system, further spectral analysis methods were designed for characterizing flow patterns.

Using this approach, distinct differences in the scale-averaged wavelet plots are observed for different regimes. Frequency bands, where peak fluctuations are localized, are determined from the wavelet variance. Intermittent pulsations are characterized with an intermittency index. Differences in the index values for the two annular and dispersed flow conditions are sufficient to allow discrimination between the flow patterns. Transition regions between flow patterns also show different index values. The results from **Table 5.1** confirm the low intermittence in dispersed flow compared to the annular flow regime. The intermittency index has not been designed to include regular flow pattern conditions such as smooth slug flow. Such flow patterns are recognized by frequency values that are nearly zero. Additional parameters such as a ratio of the scale-averaged wavelet peaks are recommended to be incorporated into the index in future work.

5.8 Experimental Difficulties

The experiments conducted for these tests require large quantities of air and water at high pressure. A thick-walled Plexiglas tube was fabricated so that the flow in the pipe

could be visualized and recorded. This restricted the maximum pressure attainable. For practical purposes, the pressure transducer probe must be located far from the fluid mixing point. This required nearly 2 m. of additional piping.

All the regimes could not be examined because of experimental limitations. Experiments for unsteady slug flow could not be conducted owing to practical difficulties in obtaining the fluid flows required for these conditions.

Considerable time was spent on determining the highest sampling rate that was required for collection of pressure fluctuation data. Development, evaluation and optimization of the wavelet techniques was a fairly long process. The experiments conducted for the thesis, are limited to the three most important regimes because experimental equipment installation and operation is time-consuming. Additional experiments are required to develop the intermittency index further.

5.9 Software Processing Limitations

The introduction of wavelets for processing of transient signals from process systems is a recent introduction in the field of chemical engineering. The development of the digital signal processing system for pressure collection and analysis involved an extended learning curve in the newly emerging field of wavelets. Previously, developed wavelet code available with the Wavelet Toolbox in MATLAB® does not cover complex wavelets used in time-frequency or time-period analysis. Further, the concepts of spectral analysis for wavelets are still under development.

The processing software developed has been limited to a minimum frequency band of 0.125 Hz to 0.25 Hz. for a data-sampling rate of 512 Hz. This is a limitation as a large amount of redundant information is associated with analysis at lower frequency bands.

Chapter Six

Conclusions and Recommendations

Conventional methods for characterization of two-phase flows are limited in application. These methods are not suited for evaluating the transient nature of some two-phase flow patterns. The study of pressure fluctuations, for characterizing two-phase flow patterns, has been ongoing for a long time. Recent developments in wavelets have been used in this research to characterize two-phase flows. Novel applications in wavelets such as scale-averaged spectrum generation and associated intermittency measures like intermittency index estimation, have been introduced through this thesis.

As stated earlier, the primary objectives of this work can be summarized as follows:

1) To gain a better understanding of conventional two-phase flow pattern detection methods,

2) To study recent developments in signal processing for transient signal characterization,

3) To design and implement a novel transient signal processing method to collected sensor data for characterizing different two-phase flow patterns.

6.1 Conclusions

The following conclusions may be drawn from this work:

1) A two-phase flow dynamic pressure collection and processing system has been designed and is fully operational for examining different two-phase flow patterns.

2) A baseline system has been developed for conducting single and two-phase flow tests. A comparison of single-phase to two-phase flow has been shown to demonstrate the complexity introduced by the addition of a compressible phase (air) into the system.

3) Owing to experimental limitations, in pump and compressor capacities and piping materials, such as Plexiglas® for the visual test section etc., three important flow patterns; annular, dispersed and slug flow have been investigated in this research.

4) Two-phase flow experiments have been carefully selected to accommodate operating conditions well within the boundaries of a flow regime as well as near the transition zone of the pattern for annular and dispersed flows.

5) Pressure data sampling rates were optimized to 512 Hz. This sampling rate is selected by conducting FFT analysis and applying on-line filters to the signal.

6) A novel approach to signal processing involving wavelet analysis of pressure fluctuation for two-phase flow studies has been introduced. The wavelet power has been computed as a function of sampling time and pulsation frequency. Further spectral analysis with the global wavelet spectrum has evaluated the resultant contour-filled wavelet power plot. Based on the global wavelet spectrum, the intermittency in wavelet power has been demonstrated in the scale-averaged wavelet spectral plots. Finally, an intermittency index has been introduced for quantifying the transient nature of the flow.

7) The intermittency index is significantly higher for annular flow as compared to dispersed flow pattern and allows the two regimes to be identified unequivocally.

6.2 Recommendations for Future Work

The following suggestions are provided for future work in this area of research.

1) Additional validation of the two-phase flow pattern determination technique should be carried out using the novel signal-processing method described in this work. For this, a number of different flow conditions can be calculated from Baker's flow pattern chart and experimentally evaluated using the two-phase flow system.

2) To quantify the flow pattern from the scale-averaged wavelet plot, refinements to the intermittency index have been proposed. In this respect, the association of statistical parameters to the scale-averaged wavelet plots may be considered.

3) Different mixing arrangements are known to have a significant effect on the flow pattern generated. Future tests should include different mixers to determine their effect.

4) Although the signal processing methods developed have been designed for two-phase flow systems, they may very well be used to examine other transient process signals from turbulent, mixing and fluidization processes that are commonly found in the chemical industry.

References

1) Al-Sheikh, J. N, Saunders, D. E. and Brodkey, R. S., "Prediction of Flow Patterns in Horizontal Two-Phase Pipe Flow", Can J. Chem. Eng. **48**, 21–29, (1970).

2) Baker, O., "Simultaneous Flow of Oil And Gas", Oil Gas J. **53**, 185-195 (1954).

3) Baker, O., "Multiphase Flow in Pipelines", Pipeline News, June, 23 (1958).

4) Barnea, D., "Flow Pattern Transition for Gas-Liquid Flow in Horizontal And Inclined Pipes", Int. J. Multiphase Flow **6**, 217–225 (1980a).

5) Barnea, D., "Flow Pattern Characterization in Two Phase Flow by Electrical Conductance Probe", Int. J. Multiphase Flow **6**, 387–397 (1980b).

6) Barnea, D., "Flow Pattern Transition for Gas-Liquid Flow in Horizontal And Inclined Pipes", Int. J. Multiphase Flow **6**, 217–225 (1980c).

7) Barnea, D., Shoham, O. and Taitel, Y., "Flow Pattern Transition for Downward Inclined Two Phase Flow: Horizontal to Vertical", Chem. Eng. Sci. **37(5)**, 735–740 (1982).

8) Barnea, D., "Transient-Formulation Modes and Stability of Steady-State Annular Flow", Chem. Eng. Sci. **44(2)**, 325–332, (1989).

9) Cai, Y., Wambsganss, M.W., Jendrzejczyk, J.A., "Application Of Chaos Theory in Identification Of Two-Phase Flow Patterns And Transitions in a Small, Horizontal, Rectangular Channel", J. Fluids Eng. **118**, 383–390 (1996).

10) Carter, P. H., "Transient Detection Using Wavelets", Proceedings of 3rd Annual ONR Full Spectrum Conference (1993).

11) Chui, C. K., "An Introduction to Wavelets", Wavelet Analysis and its Applications **1**, New York, (1992).

12) Clarke, N.N and Rezkallah, K.S., "Void Fraction Measurements in Gas-Liquid Flows Using Image Processing", J. Flow Visual. Image Proc. **3**, 1–11 (1996).

13) Daubechies, I., "Ten Lectures on Wavelets", Society of Industrial and Applied Mathematics, 167-287 (1992).

14) DeGance, A. E. and Atherton, R.W., "Chemical Engineering Aspects of Two-Phase Flow", Chem. Eng., Apr 20, 95-103, 151-157 (1970).

15) Dukler, A. E. and Taitel, Y., "Flow Pattern Transitions in Gas-Liquid Systems: Measurement and Modeling", Multiphase Sci. Technol. **2**, 1–94 (1986).

16) Govier, G. W., and Aziz, K., "The Flow of Complex Mixtures", 503-520 (1972).

17) Graps, A., "An Introduction to Wavelets", IEEE Computational Science and Engineering **2** (1995).

18) Hagelberg, C. R., and Gamage, N., "Applications of Structure Preserving Wavelet Decompositions to Intermittent Turbulence:-A Study,", Wavelet Analysis and its Applications **4**, 45-80 (1994).

19) Hosler, E. R., "Flow Patterns in High Pressure Two-Phase Flow with Heat Addition" AICHE Symp. Ser. **64**, 54-66 (1968).

20) Hsieh, C. C., Wang, S.B. and Pan, C., "Dynamic Visualization of Two-Phase Flow Patterns in a Natural Circulation Loop", Int. J. Multiphase Flow **23(6),** 1147–1170 (1997).

21) Hubbard, M. G. and Dukler, A. E., "The Characterization of Flow Regimes for Horizontal Two-Phase Flow: 1-Statistical Analysis of Wall Pressure Fluctuations", Proc. Heat Trans & Fluid Mech., Saad, M.A. and Moller, A., Eds, 7–121 (1966).

22) Jayanti, S., "Turbulent Flow in a Pipe With Intermittent Rough Patches: an Analogue of Annular Two-Phase Flow", Chem. Eng. Comm. **141–142**, 237–259 (1996).

23) Jones, O. C. Jr. and Zuber, N., "The Interrelation between Void Fraction Fluctuations and Flow Pattern in Two-Phase Flow", Int. J. Multiphase Flow **2**, 273-306 (1976).

24) Kirpalani, D., McCracken, T and Bennett, A, "Characterization of Instability in the Disintegration of Liquid Jets from Twin Fluid Atomizers", ILASS Americas 11th Ann. Conf. Liq. Atom. Spray Sys., 204-208 (1998).

25) Kumar, P. and Foufoula-Georgiou, E., "Wavelets in Geophysics: an Introduction", Wavelet Analysis and its Applications **4**, 1-43 (1994).

26) Lewalle, J., "Wavelet Analysis of Experimental Data:-Some Methods and the Underlying Physics", AIAA Fluid Dyn. Conf., 1-10 (1994).

27) Lewalle, J., "Demonstration of Wavelet Techniques in the Spectral Analysis of Bypass Transition Data", NASA Technical Paper # 3555 (1997).

28) Lewalle, J.," Three Lectures on the Application of Wavelets to Experimental Data Analysis", Von Karman Institute Lecture Series on Adv. Meas. Tech. **2,** 1-24 (1998).

29) Maciejewski, P. K., "Element of an Approach to the Assessment of Random Uncertainty in Transient Measurements", Trans. ASME **118**, 90–95 (1996).

30) Perspff, P. and Pruess, K., "Two-Phase Flow Visualization and Relative Permeability Measurement in Natural Rough-Walled Rock Fractures", Water Resource. Res. **31(5)**, 1175–1186 (1995).

31) Mandhane, J. M., Gregory, G.A. and Aziz, K., "A Flow Pattern Map for Gas-Liquid Flow in Horizontal Pipes", Int. J. Multiphase Flow **1**, 537–553 (1974).

32) Merzkirch, W., "Techniques of Flow Visualization", AGARD-AG-302, North Atlantic Treaty Organization (1987).

33) Mishima, K., Nishihara, T and Hibiki, A.H., "Visualization and Measurement of Two-Phase Flow by Using Neutron Radiography", Nuclear Eng. Des. **175**, 25–35 (1997).

34) Mossa, M. and Tolve, U., "Flow Visualization in Bubbly Two-Phase Hydraulic Jump", Trans ASME **120**, 160–165 (1998).

35) Sato, Y. and Sekoguchi, K., "Liquid Velocity Distribution in Two-Phase Bubble Flow", Int. J. Multiphase Flow **2**, 79–95 (1975).

36) Samways, A. L., Bradbury, L.J.S. and Bruun, H.H., "Pressure Measurements and Convection Velocity Evaluations in Two-Phase Flow", Int. J. Multiphase Flow **23(6)**, 1007–1029 (1997).

37) Taitel, Y., "Flow Pattern Transition in Rough Pipes", Int. J. Multiphase Flow **3**, 597 – 601 (1977a).

38) Taitel, Y., "A Model for Slug Frequency during Gas-Liquid Flow in Horizontal and Near Horizontal Pipes", Int. J. Multiphase Flow **3**, 585–596 (1977b).

39) Taitel, Y., Lee, N. and Dukler, A. E., "Transient Gas-Liquid Flow in Horizontal Pipes: Modeling the Flow Pattern Transitions", AIChE J. **24(5)**, 920–934 (1978).

40) Taitel, Y., "Stability of Severe Slugging", Int. J. Multiphase Flow **12(2)**, 203–217 (1986).

41) Taitel, Y., "Severe Slugging in a Riser System: Experiments and Modeling", Int. J. Multiphase Flow **16(1)**, 57–68 (1990a).

42) Taitel, Y., "Two-Phase Slug Flow", Ad. Heat Trans. **20**, 83–132 (1990b).

43) Torrence, C., and Compo, G. P., " A Practical Guide to Wavelet Analysis". Bull. Amer. Meteor. Soc. **79**, 61-78 (1997).

44) Tutu, N. K., "Pressure Fluctuations and Flow Pattern Recognition in Vertical Two-Phase Flows", Int. J. Multiphase Flow **8**, 443-447 (1982).

45) Wambsganss, M. W., Jendrzejczyk, J.A. and France, D.M., "Two-Phase Flow Patterns and Transitions in a Small, Horizontal, Rectangular Channel", Int. J. Multiphase Flow **17(3)**, 327–342 (1991).

46) Wambsganss, M. W., Jendrzejczyk, J.A. and France, D.M., "Determination and Characteristics of the Transition to Two-Phase Slug Flow in Small Horizontal Channels", Trans. ASME **116**, 140–146 (1994).

Appendix A

A.1 Operating Conditions with Calculated Baker's Map Co-ordinates (in FPS units)

Flow Pattern	Water Flow Rate GPM (US)	Air Flow rate cfm (std.)	$L\lambda/\psi G$	G/λ (lb/ft^2-h^{-1})
Annular Flow	12.2	10.6	128.18	9542.98
	3	14.5	23.04	13054.08
Dispersed Flow	16.8	211	8.87	189959.36
	35	57.5	67.79	51766.18
Slug Flow	3	1.2	278.42	1080.34

Table A.1: Recorded operating conditions for water and air.with calculated Baker's co-ordinates.

A.2 Sample Calculation for Baker's Two-Phase Flow Map

A sample calculation has been provided here for modeling experimental conditions on Baker's two-phase flow maps. The condition selected for modeling the Baker's flow pattern is Condition 1 of the annular flow pattern. Although, the instruments are calibrated in FPS units, all calculations are in SI units.

Water Flow rate L' = 12.2 GPM (US) = 0.000769 m^3/s

Air Flow rate G' = 10.6 ft^3/min (STP) = 0.005002643 m^3/s (STP)

Where STP is at atmospheric pressure and 25°C

Diameter of the pipe = 0.1957" = 0.0243078 m

ρ_g = Density of the gas phase, kg/m^3 =1.202 kg/m^3

ρ_L = Density of the liquid phase, kg/m^3 = 1000kg/m^3

μ_L = Viscosity of liquid phase, Pa-s = $1 \bullet 10^{-3}$ Pa-s

σ = Surface tension, N/m. = 0.073 N/m

G = Mass velocity of gas, $\frac{kg}{m^2 s}$

$$G = \frac{0.005002643 \bullet 1.202}{\frac{\pi}{4} \bullet (0.0243078)^2} = 13.026 \frac{kg}{m^2 s}$$

L = Mass velocity of liquid, $\frac{kg}{m^2 s}$

$$L = \frac{0.000769 \bullet 1000}{\frac{\pi}{4} \bullet (0.0243078)^2} = 1657.941 \frac{kg}{m^2 s}$$

$$\lambda = \left(\frac{\rho_g \quad \rho_L}{(1.202) \quad (1000)}\right)^{\frac{1}{2}}$$ From equation (2.3)

$$\psi = \frac{0.073}{\sigma}\left[\frac{\mu_L}{0.001} \quad \left(\frac{1000}{\rho_L}\right)^2\right]^{\frac{1}{3}}$$ From equation (2.4)

Because air flow rate is measured at standard conditions by the mass flow meter and air-water mixtures are examined;

$\lambda = 1$; $\psi = 1$

The coordinates for the map are given by:

$$X = \frac{L\lambda}{G\psi}$$ From equation (2.7)

$$Y = \frac{cG}{\lambda}$$ From equation (2.9)

c = 737.0984, conversion factor for plotting fluid conditions in SI system

Therefore the coordinates for Baker's flow map for condition 1 of annular flow are:

$$X = \frac{1657.941 \bullet 1}{12.9425 \bullet 1} = 128.1$$

$$Y = \frac{737.10 \bullet 12.95}{1} = 9542.98, \frac{kg}{m^2 s}$$

Appendix B

B.1 Software program for Controlling Flash during Collection of Flow Pattern Photographs

The flash is a small, portable light source for fast stop-motion photography. It has a high peak light output for a very short duration of time. Two flashes of light are included in each flash and are controlled with one digital counter in LabVIEW. This program provides a digital counter for the flash at the rate of 1Hz. A total of 100 flashes are set. The LabVIEW front panel and source code are shown on **Figures B1 and B2** respectively:

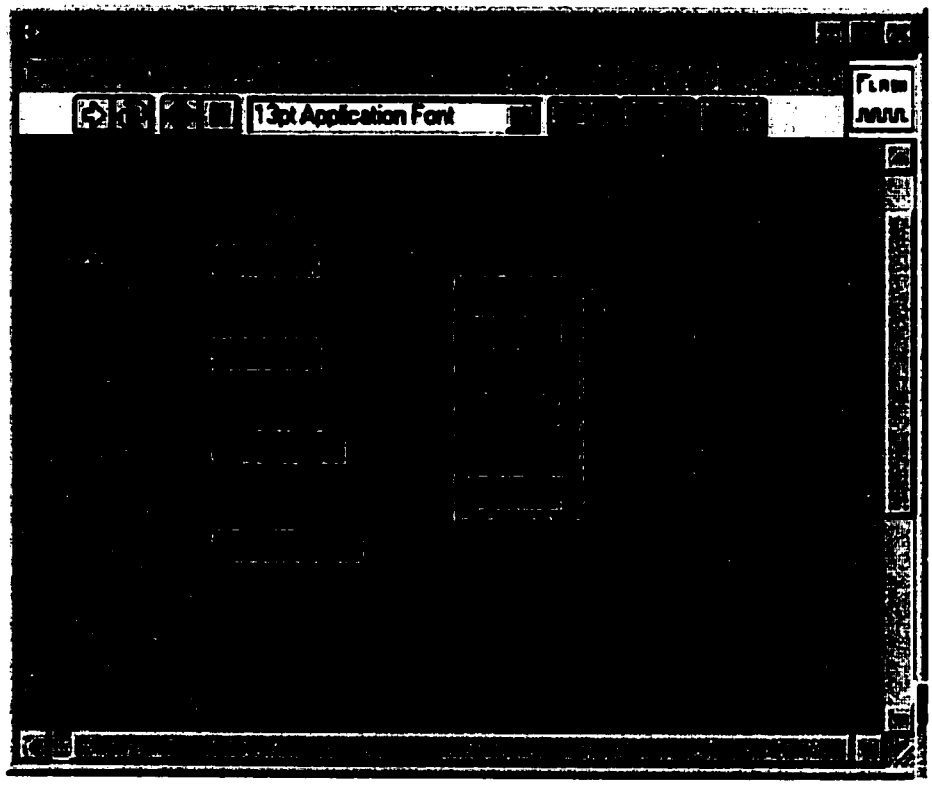

Figure B.1: Front panel for flash control with digital counters.

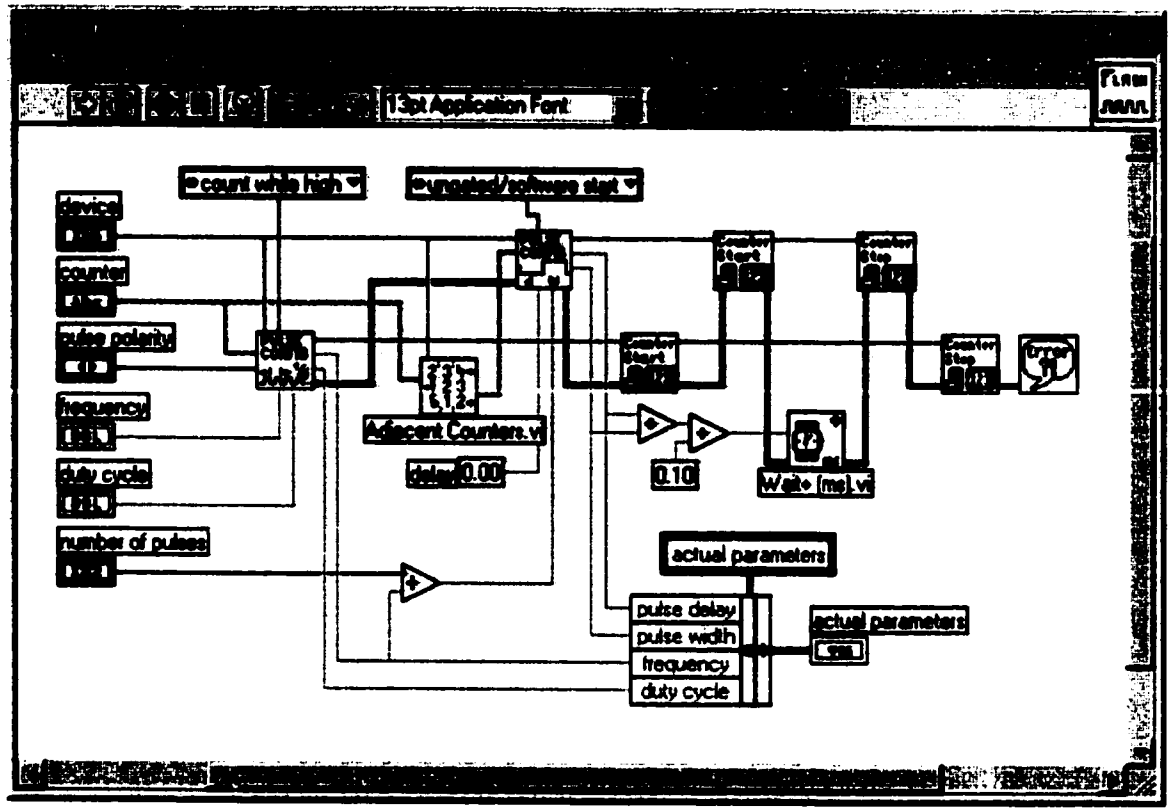

Figure B.2: Block diagram (source code) for controlling flash system.

B.2 Signal Processing Programs developed in MATLAB

Signal processing programs include advanced wavelet-based processing and conventional Fourier power spectra calculations. Using these programs, the plots shown in this thesis can be generated. The basis functions used for wavelet processing are the Morlet basis function and the Daubechies wavelet function. The wavelet toolbox by MATLAB® is required for generating the scalogram plot for self-similarity analysis. The wavelet algorithms are enhanced further with spectral analysis based on the recommendations of other researchers (Torrence and Compo, 1997 and Lewalle, 1998) to design an advanced intermittency detection method as described in chapter five. Using this specialized approach a flow pattern recognition system has been developed.

The design of software programs is classified on the basis of the experimental approach adopted into three types

1) Model Data Software: Programmatically generated data is examined for evaluation of the developed methods using model data software

2) Baseline Experimental Software: Baseline tests for self-similarity of fluctuations and regularity of pulsation are examined using both Daubechies and Morlet's wavelets. These methods are necessary for evaluating the data acquisition and processing system.

3) Pattern Recognition Software: Pattern recognition tests for characterizing the different flow patterns using Morlet's wavelets are conducted using the pattern recognition software. Novel methods in wavelets such as, wavelet spectral analysis and intermittency index estimation for dispersed and annular flow have been introduced in this software.

A 3½ floppy disk containing the collected pressure fluctuations (V) for all experimental conditions has been included in the thesis. The data files are provided in ASCII format

Appendix C

C.1 Wavelet Spectra for 30-second Time Intervals

The five different operating conditions in this thesis are examined for multiple 10-second time intervals. A longer 30-second, time interval result for the scale-averaged wavelet values is shown for each condition. This plot shows a comparison of the scale-averaged power for the different regimes.

C.2 Comparative Plots for Annular, Dispersed and Slug Flow

Scale-averaged plots and their relevant global spectra are presented for each condition for comparison purposes. Because the time period of sampling is large, the differences between the regimes are observed more clearly.

C.2.1 Condition 1

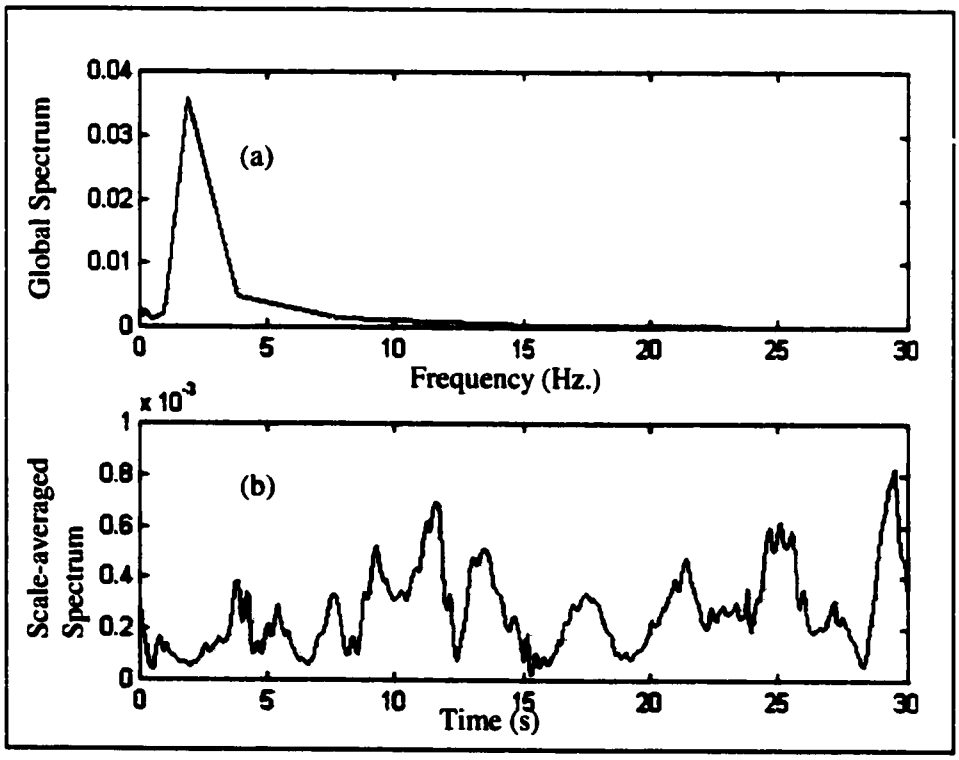

Figure C.1: Global spectra and scale-averaged wavelet spectra for condition 1 of annular flow for 30-second time interval.

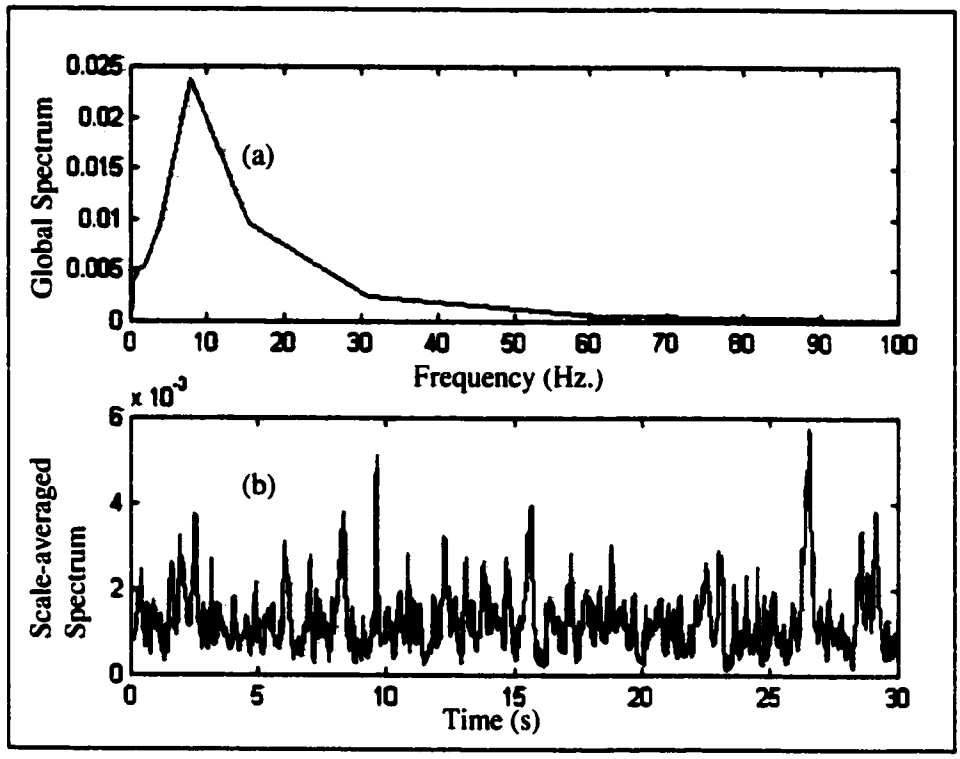

Figure C.2: Global spectra and scale-averaged wavelet spectra for condition 1 of dispersed flow for 30-second time interval.

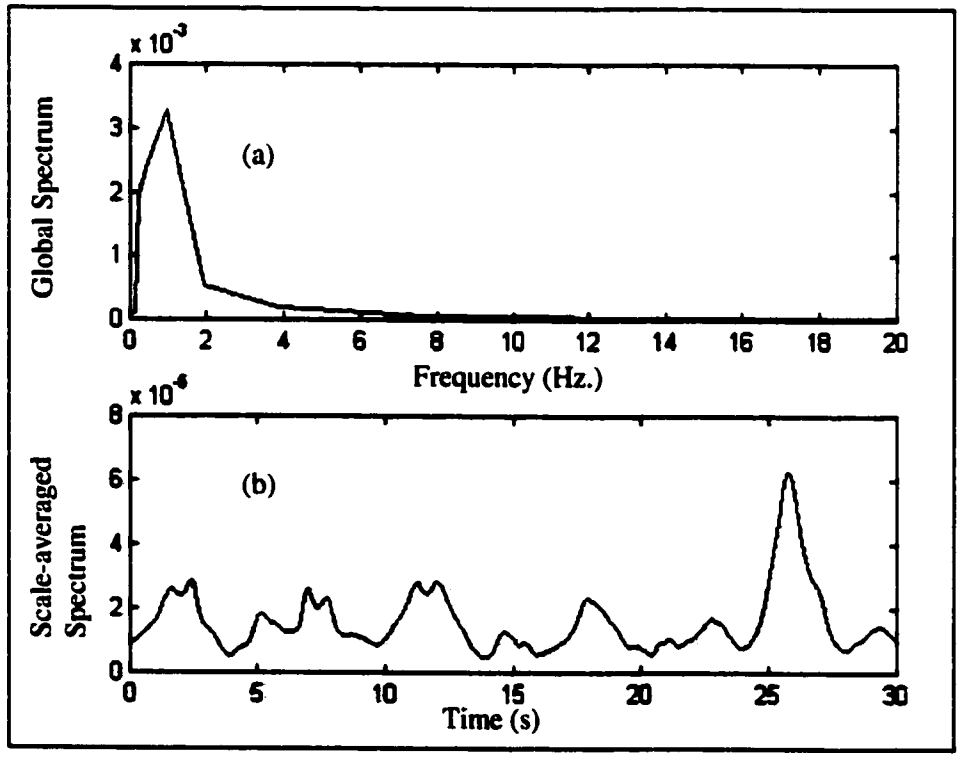

Figure C.3: Global spectra and scale-averaged wavelet spectra for condition 1 of slug flow for 30-second time interval.

C 2.2 Condition 2

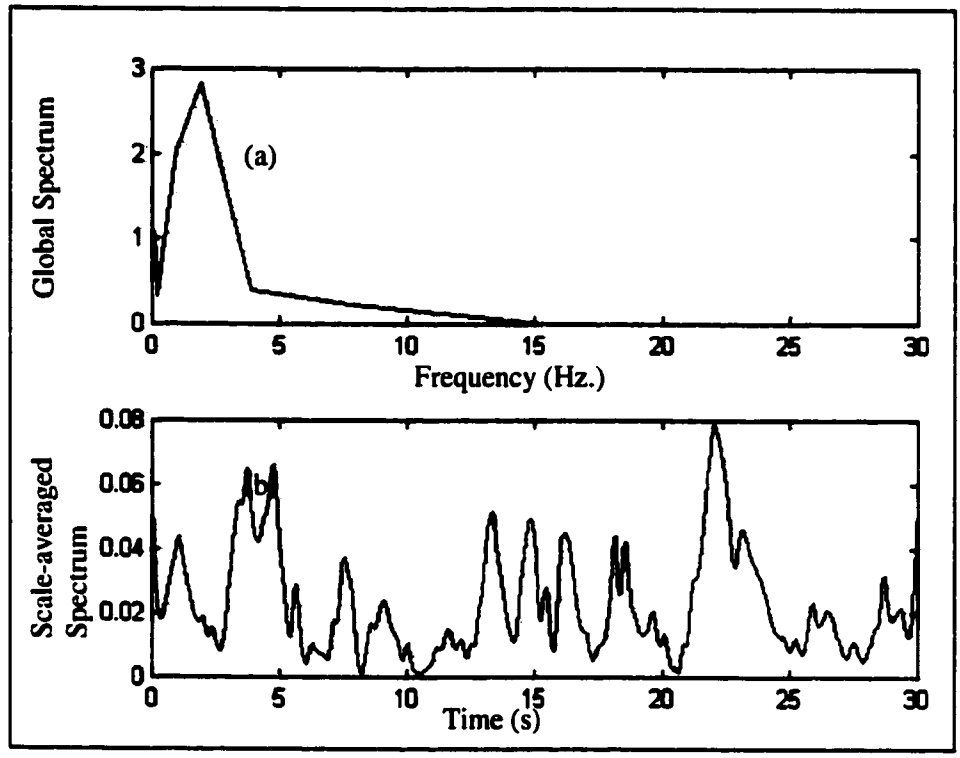

Figure C.4: Global spectra and scale-averaged wavelet spectra for condition 2 of annular flow for 30-second time interval.

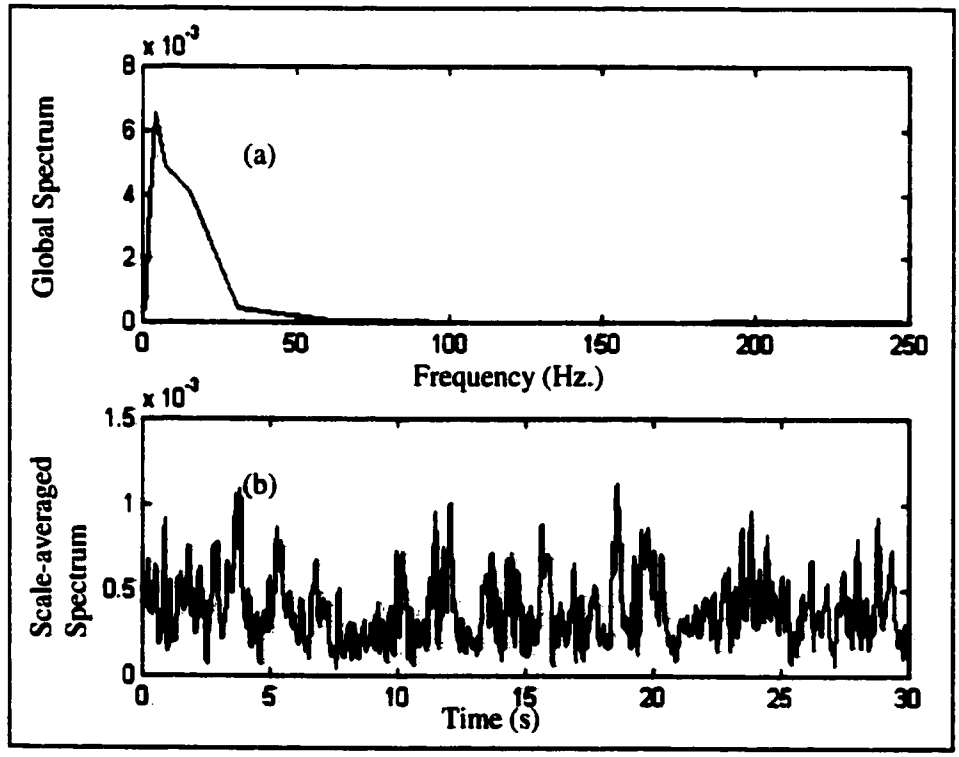

Figure C.5: Global spectra and scale-averaged wavelet spectra for condition 2 of dispersed flow for 30-second time interval.

C 3: Comparison of Fourier Power Spectrum and Global Wavelet Spectrum

Comparative plots between Fourier power spectra and global wavelet spectra for all the conditions analyzed other than those shown in chapter five are plotted here. The global wavelet spectra represent time-averaged peaks in the spectra occuring in frequency bands similar to the Fourier power spectra. This comparison confirms the detection of peaks by wavelet energy plots in the frequency domain.

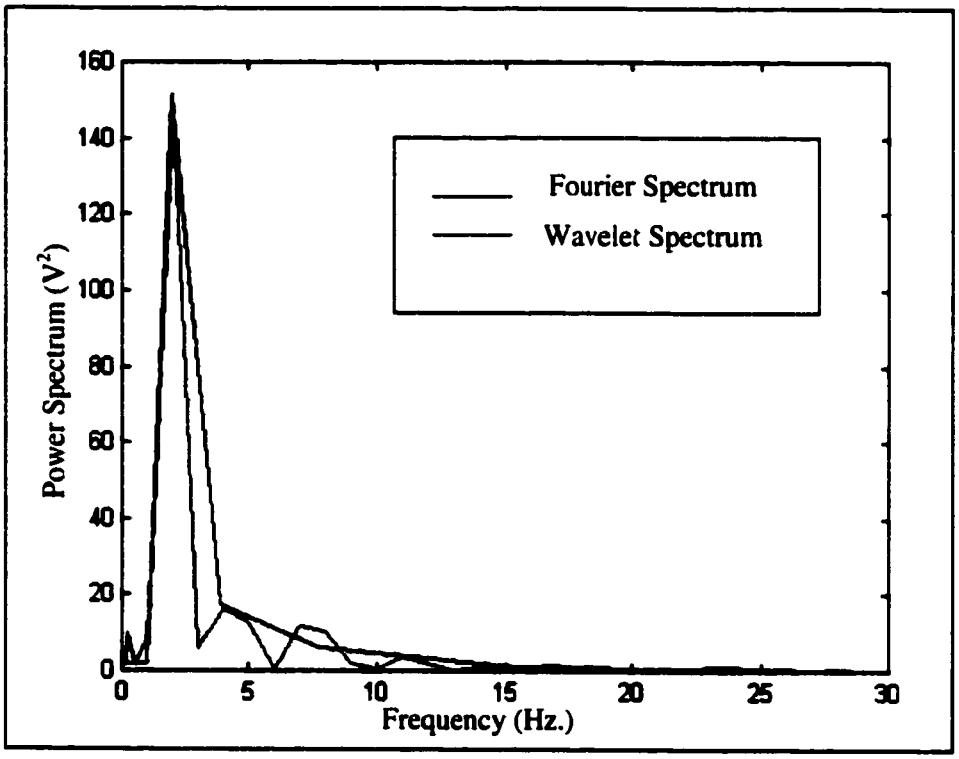

Figure C.6: Comparison of wavelet spectra and power spectral analysis (Fourier) for condition 1 of annular flow during the time interval from 10 to 20 sec.

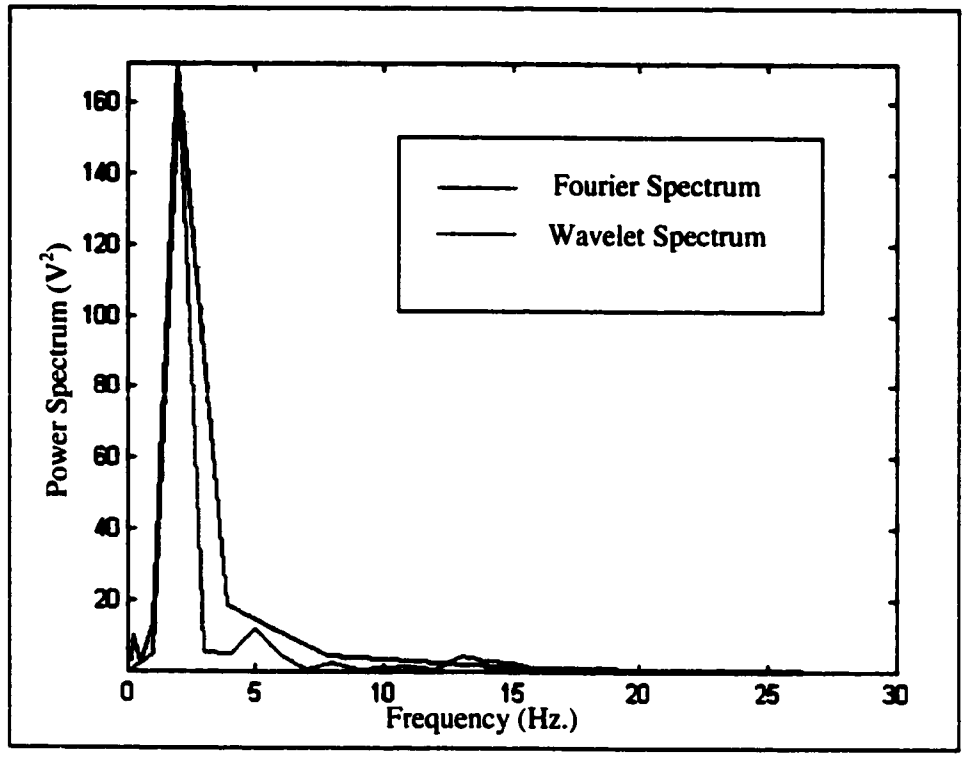

Figure C.7: Comparison of wavelet spectra and power spectral analysis (Fourier) for condition 1 of annular flow during the time interval from 20 to 30 sec.

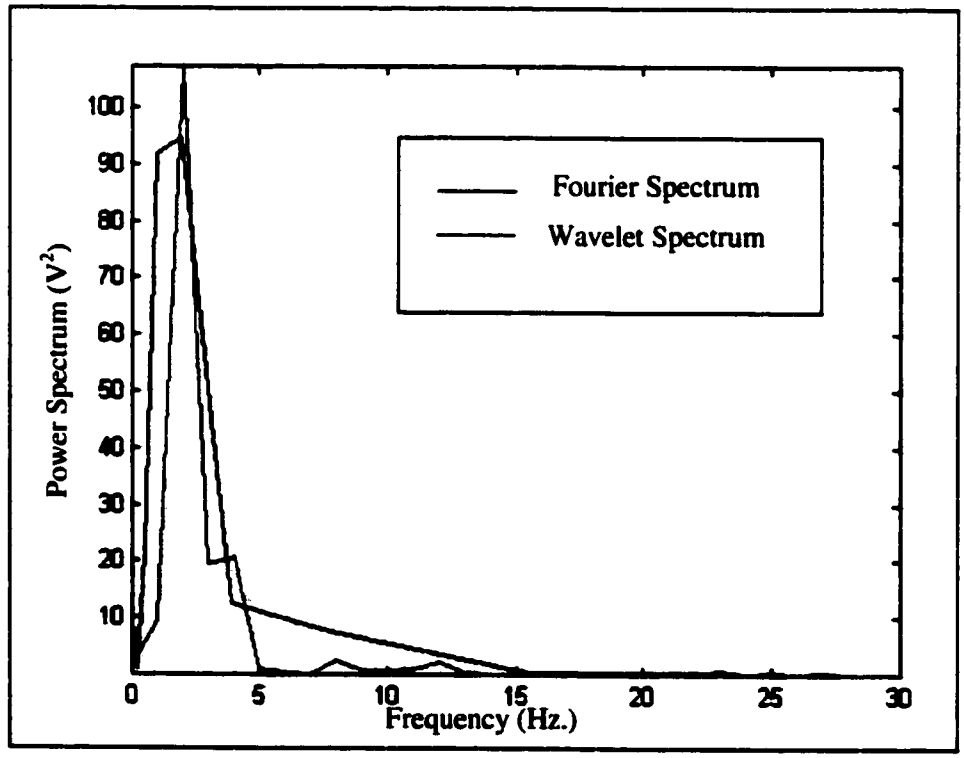

Figure C.8: Comparison of wavelet spectra and power spectral analysis (Fourier) for condition 2 of annular flow during the time interval from 0 to 10 sec.

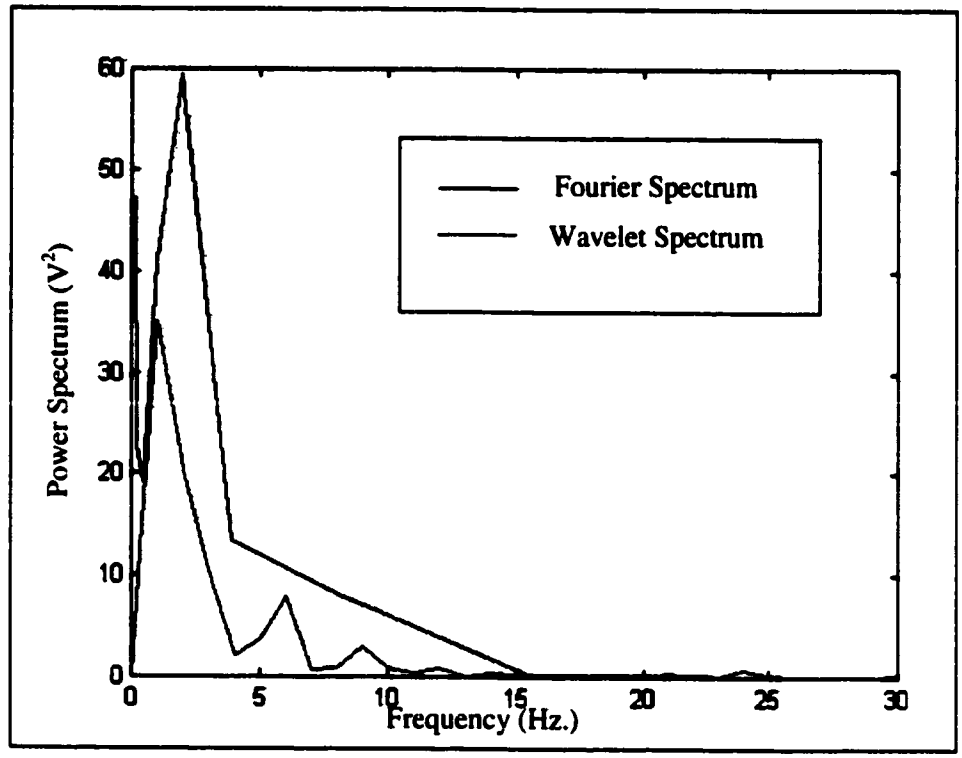

Figure C.9: Comparison of wavelet spectra and power spectral analysis (Fourier) for condition 2 of annular flow during the time interval from 10 to 20 sec.

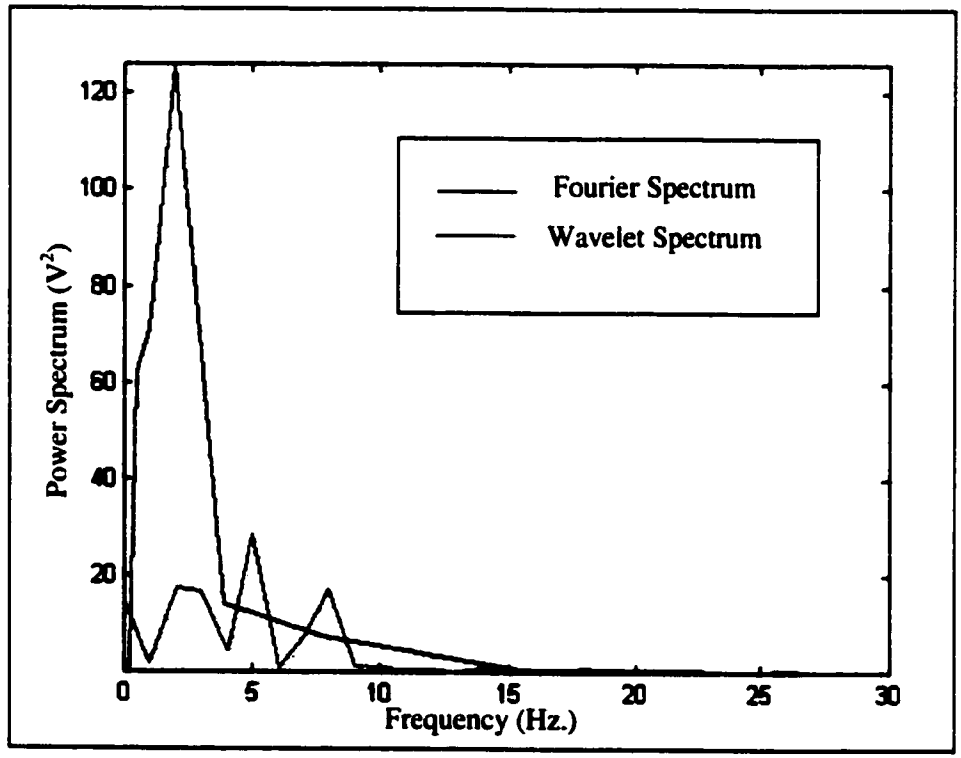

Figure C.10: Comparison of wavelet spectra and power spectral analysis (Fourier) for condition 2 of annular flow during the time interval from 20 to 30 sec.

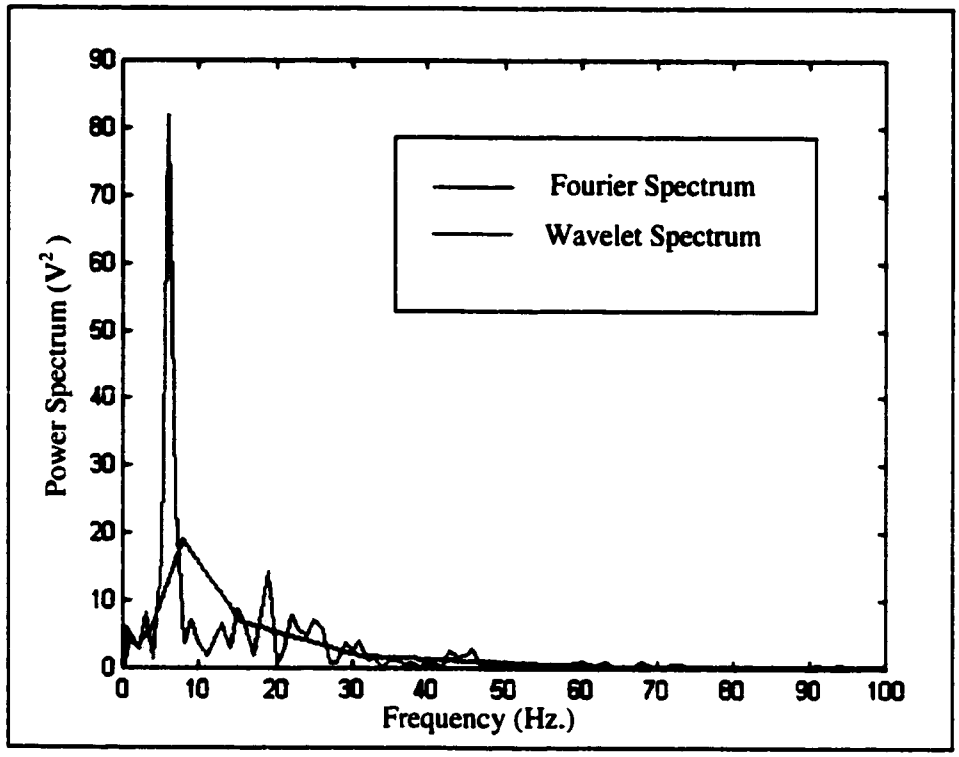

Figure C.11: Comparison of wavelet spectra and power spectral analysis (Fourier) for condition 1 of dispersed flow during the time interval from 10 to 20 sec.

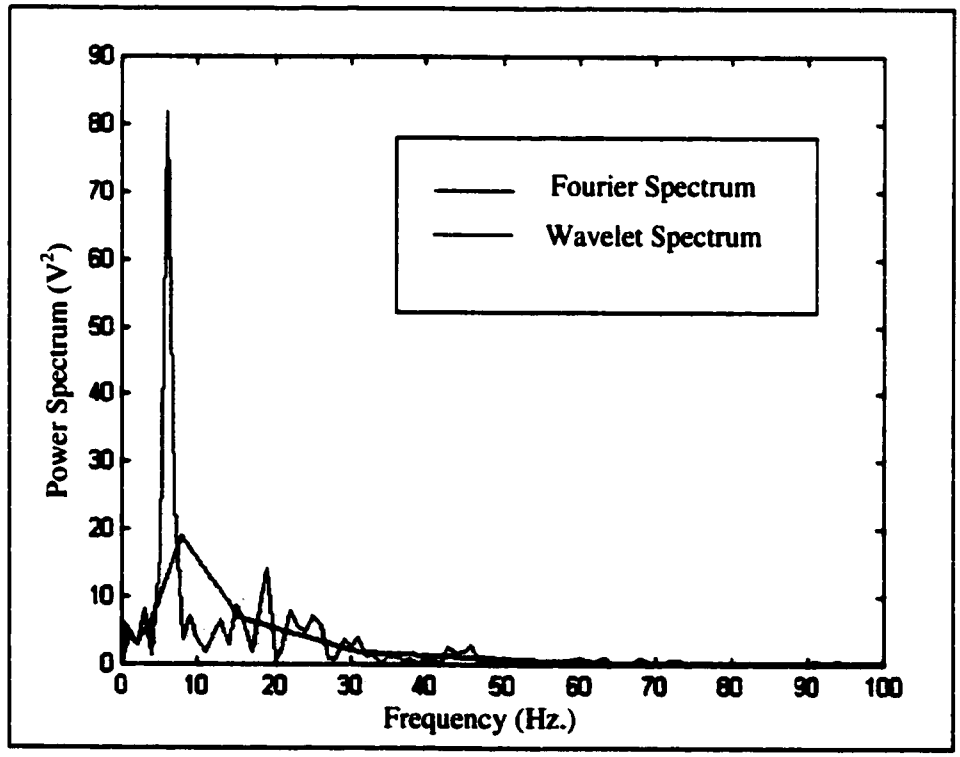

Figure C.12: Comparison of wavelet spectra and power spectral analysis (Fourier) for condition 1 of dispersed flow during the time interval from 20 to 30 sec.

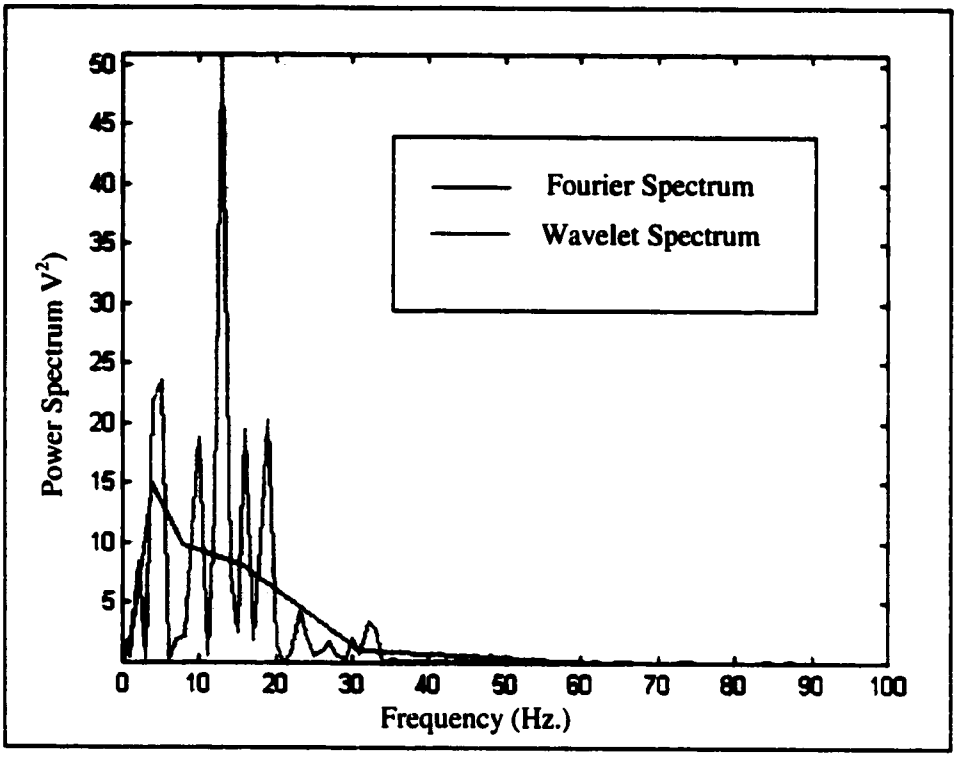

Figure C.13: Comparison of wavelet spectra and power spectral analysis (Fourier) for condition 2 of dispersed flow during the time interval from 0 to 10 sec.

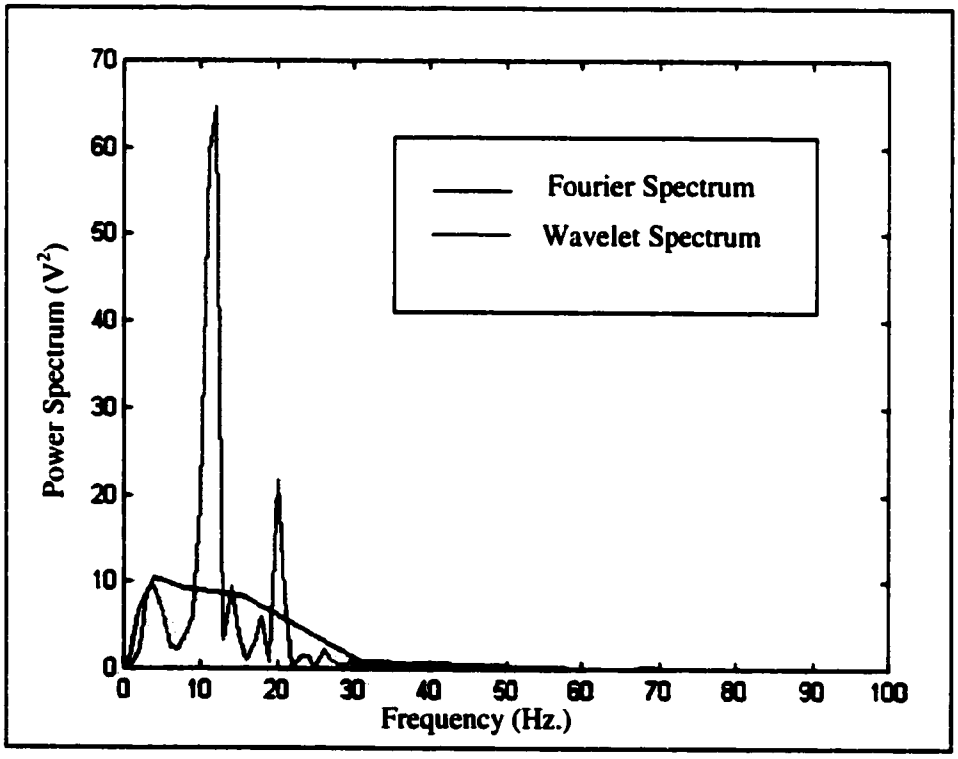

Figure C.14: Comparison of wavelet spectra and power spectral analysis (Fourier) for condition 2 of dispersed flow during the time interval from 10 to 20 sec.

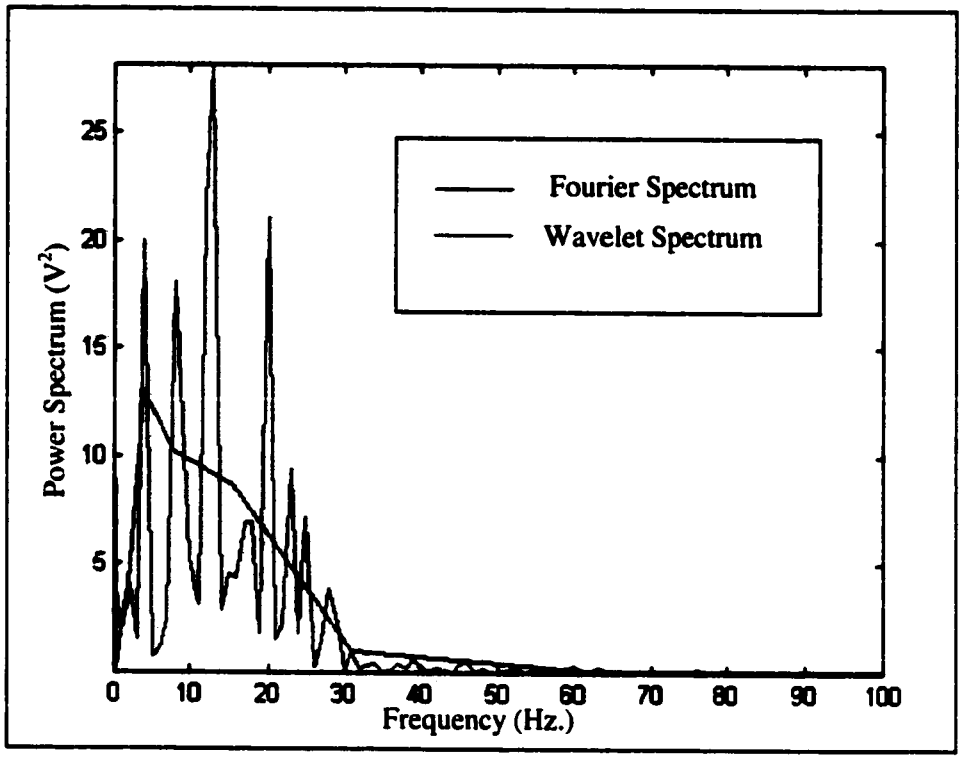

Figure C.15: Comparison of wavelet spectra and power spectral analysis (Fourier) for condition 2 of dispersed flow during the time interval from 20 to 30 sec.

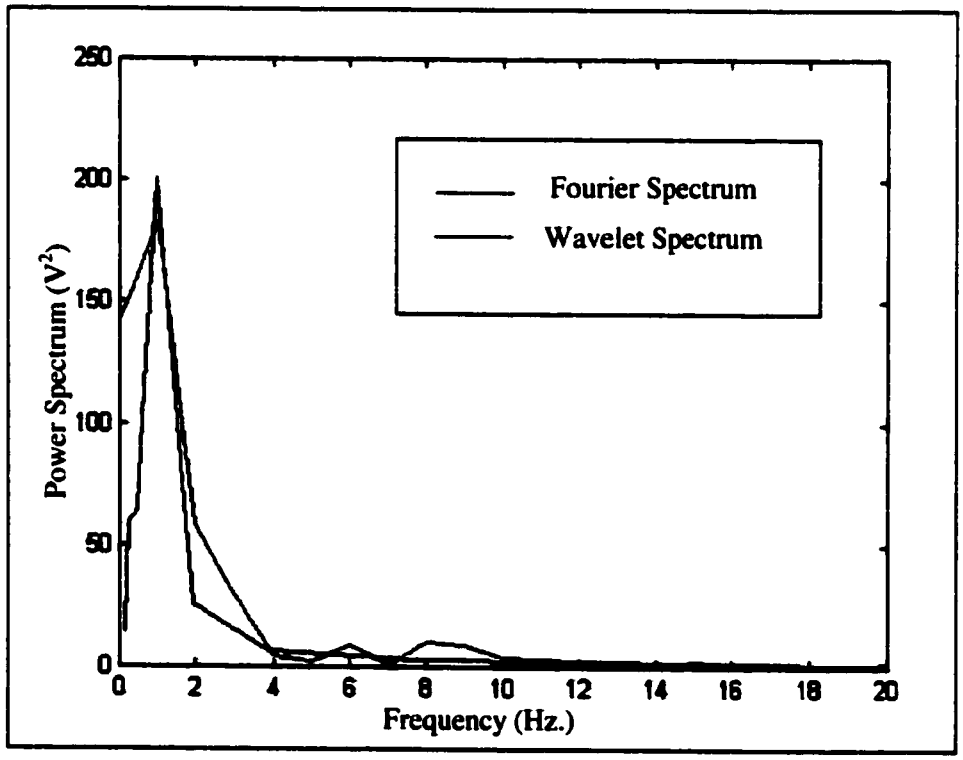

Figure C.16: Comparison of wavelet spectra and power spectral analysis (Fourier) for condition 1 of slug flow during the time interval from 10 to 20 sec.

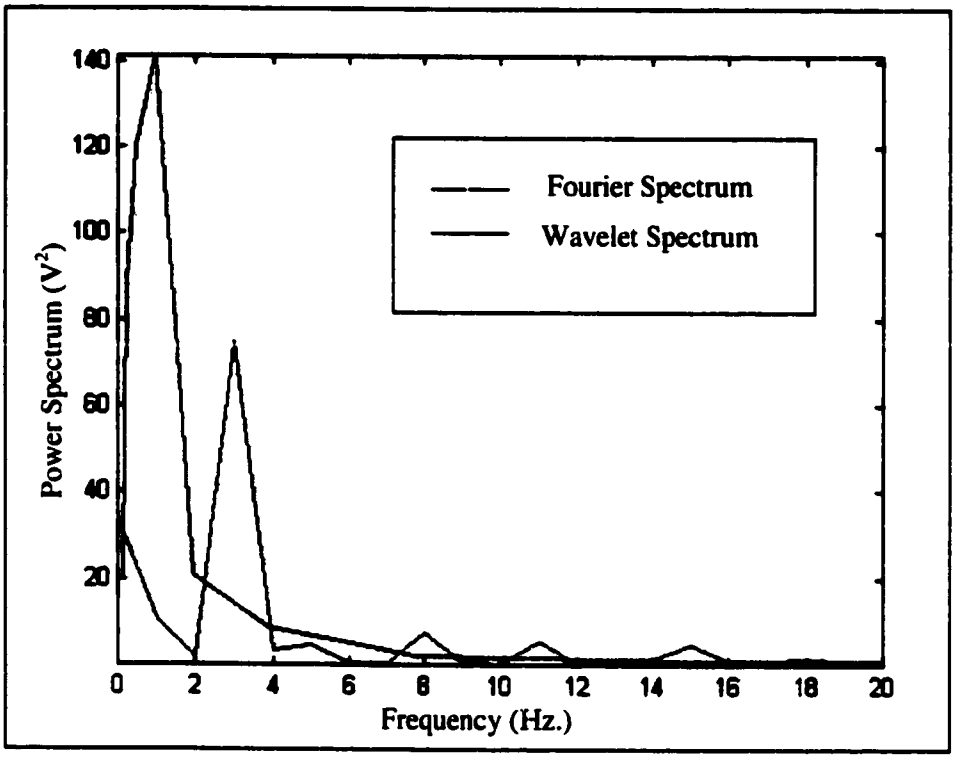

Figure C.17: Comparison of wavelet spectra and power spectral analysis (Fourier) for condition 1 of slug flow during the time interval from 20 to 30 sec.

Note: Units in comparative plots apply only to the Fourier spectrum.

C.4 Discussion

The spectral plots have been categorized according to the flow patterns examined. Spectra for all conditions and time intervals not included in chapter five have been plotted here. The spectral plots show that calculation of the global wavelet spectrum can be used to identify the peak frequency band.

For the slug flow regime, the amount of redundant information using Morlet's wavelet is very high because the frequency is near zero. It is recommended that data be collected at lower rates or sub-sampled for this regime to avoid redundant information using wavelet analysis.